INFRARED SPECTROSCOPY OF ION-HYDROCARBON CLUSTERS

BY

OSCAR RODRIGUEZ JR.

DISSERTATION

Submitted in partial fulfillment of the requirements
for the degree of Doctor of Philosophy in Chemistry
in the Graduate College of the
University of Illinois at Urbana-Champaign, 2011

Urbana, Illinois

Doctoral Committee:

Professor James M. Lisy, Chair
Professor Zaida Luthey-Schulten
Professor Andrew Gewirth
Assistant Professor Benjamin J. McCall

Abstract

Many biological and environmental systems contain ion, water, and hydrophobic components; and it is the balance between these competing interactions which governs their chemistry. This Thesis aims at exploring ion•••hydrocarbon interactions, then ion•••water•••alkane interactions. To accomplish this, a combination of gas phase infrared predissociation spectroscopy (IRPD) and tandem mass spectrometry is utilized.

The solvation of alkali metal ions by methane is discussed first, beginning with the effects of multiple argon atoms on Li^+•••CH_4 dimer clusters followed by a study of $M^+(CH_4)_n$ clusters where it is revealed that ions have a weak electrostatic effect beyond the first solvent shell.

Next, the argon tagging and monitoring unique fragmentation channels are used to selectively probe for high energy $Li^+(H_2O)_{3\text{-}4}Ar_1$ conformers which contain extensive water hydrogen bonding.

Finally, ion•••water•••alkane interactions are probed in $Li^+(H_2O)_n$ clusters containing CH_4 or C_6H_{12} molecules. Some spectra contain hydrogen bonded peaks correlating to weak water•••alkane interactions. Furthermore, there is strong evidence that high energy conformers containing water hydrogen bonding are present in the cluster ion beam. This analysis is expanded to anionic $Cl^-(Water)_m(CH_4)_n$ clusters to compare with cations.

Density functional theory or MP2 level calculations were used to support and help characterize experimental data.

Acknowledgements

I would like to thank my parents, Oscar and Gilda Rodriguez, for their unwavering, complete support and encouragement prior to, and throughout, my graduate career. Without their prayers my accomplishment would only be an unfulfilled dream. My sister Gloria Isela Rodriguez, always keeping me grounded and shared humor when I needed it. My grandparents Blas and Hortencia P. Rodriguez and Daniel and Guadalupe S. Hernandez provided an unyielding foundation on which their grandchildren were able to succeed. I appreciate all my family and classmates from Texas who are too many to name, but all deserve my gratitude.

There are several world-class scientists at the University of Illinois, but I'm certain that Professor James M. Lisy is the finest any graduate student could work for. I am grateful to him for the support, expertise, and, above all, the patience he provided that allowed me to succeed.

My graduate career, like any other, would never have blossomed without the help of my research group members, Dorothy J. Miller, Amy L. Nicely, and Jordan P. Beck. I owe a special thanks to Jason D. Rodriguez who took the time to teach me the laboratory methods and patiently answered all of my questions. I consider myself fortunate to have worked with such professionals. Also, I'd like to thank Mitchell Ong, Krish Sarkar, and Jeb Kegerris for their camaraderie.

I would also like to thank the members of my committee, Professors Zaida Luthey-Schulten, Andrew Gewirth, and Benjamin J. McCall for their availability and quick responses to my messages. I must also thank my undergraduate Physical Chemistry

professor Dr. Philip “Dr. D” DeLaussus who was the first to encourage me to attend graduate school.

The work of the SCS staff, in particular, Jim Wentz and Mike Hallock, and our Chemistry secretaries, Vicki, Beth, Connie, Theresa, and Sandy, is greatly appreciated. Without them, my graduate career would have lasted much longer.

Above all, none of my personal accomplishments wound have taken place without the support of my wife, and best friend, Lorena Janeth Rodriguez. Any success I have had, or will have, is directly the result of her patience and love. And, my graduate career was made much easier thanks to the company of our son, Nicolás Rodriguez. His joy is very contagious, and helpful for all our family.

To Lorena and Nicolás

Table of Contents

Chapter 1

Introduction

1.1 Background

Many processes like protein function [1], clathrate formation [2,3], and solvation and condensation [4], are governed by competing, non-covalent interactions which can be fundamentally changed by the presence of ions. [5]

One way to study these interactions at the molecular level is to generate gas phase cluster ions. [6-11] In this environment, ions can draw electron density from neighboring solvent molecules, which in turn, changes the nature of the vibrational modes within the solvating molecule.[7,8,11] These perturbations can be probed using infrared spectroscopy. Shifts of bands in the IR spectrum can provide valuable information such as ion•••ligand strength [12], while the presence or absence of IR bands can indicate gas phase ion solvent shell size and cluster structure. [4,8,11,13-17]

The method of choice for work presented in this Thesis is infrared predissociation spectroscopy (IRPD), or action spectroscopy, used together with a tandem mass spectrometer. In this technique a desired cluster ion can be mass selected and probed with an IR laser. Next, a vibrational mode in the cluster ion can absorb energy of a resonate IR photon (~25 – 40 kJ/mol) which is distributed throughout the cluster. The most labile ligand can fragment if the internal energy after photon absorbed exceeds the binding energy of that ligand.[11] The fragment ion can then pass through another mass filter and be detected.

In some instances, the imparted energy from a resonate IR photon is insufficient to cause fragmentation of the most labile ligand. In these cases rare gas (or molecule) tagging can be employed. This technique takes advantage of the fact that rare gas atoms (or small "messenger" molecules, i.e. H_2) can participate in ion solvation, yet minimally disturb the cluster ion and have binding energies (~5-20 kJ/mol) less than the energy imparted by an IR photon. [18-21] Therefore fragmentation of the "tagging" atom (or molecule) can readily occur after photon absorption.

An interesting result of utilizing the rare gas tagging method is colder cluster temperatures (50 – 150 K), compared to non-tagged clusters (200 – 500 K) [15], which can significantly affect the ion solvation process. If the internal energies (effective temperatures) of nascent cluster ions are insufficient to overcome barriers to rearrangement into the global minimum energy structure, then different structural conformers are "trapped" and can exhibit unique spectroscopic features.[15,22-25]

1.2 Lithium Ion

The majority of work reported in this Thesis contains Li^+ as the ion of interest. Li^+ is intriguing because it is the smallest alkali metal ion, therefore carries the highest charge density.[26] As a result, alkali metal ion•••ligand electrostatic interaction strengths are strongest for Li^+ and trend as $Li^+ > Na^+ > K^+ > Rb^+ > Cs^+ >$.[10]

There are several practical reasons for studying Li^+. For example, lithium ion battery technology has been of great economic and environmental interest as the demand and need for alternative energy grows.[27] Recently, the safer Li^+ battery technology has become the power source of choice over the more expensive hydrogen fuel cells in energy efficient car development.[28]

In the biological field, Li^+ has been used since the 1950s to treat manic depression and bipolar disorder.[29,30] New evidence suggests that Li^+ treatment may be applied to acute brain injuries and chronic neurodegenerative diseases.[31] Despite the well documented effectiveness of Li^+ therapy, the exact chemical mechanisms behind the treatments are still uncertain.[30,32]

1.3 Hydrocarbon and Water Studies

CH_4 is a spherical top molecule with no permanent dipole moment.[33] As the smallest organic molecule, CH_4 has been attractive to investigate weak non-covalent interactions experimentally and computationally.[34-41] Also, weak CH_4•••CH_4 interactions, ~1 - 2 kJ/mol [42,43], make CH_4 an ideal solvent where first- and second-shell ligands minimally interact with each other in clusters. Thus, an ion's electrostatic effect beyond the first solvent shell can be studied, which is one of the goals of this Thesis.

Until recently, an ion's long range effects, especially in hydrated systems, has not been fully understood. For ions in solution, Saykally and co-workers proposed that the perturbation on hydrogen bonded networks beyond the first solvent shell was a result of an ions' electric field exerted on first shell molecules.[44] In more straightforward $M^+(CO_2)_n$ gas phase experiments, Duncan and co-workers found that several transition metal ions had virtually no electrostatic effect on second shell CO_2 molecules.[45-50]

Another aim of this Thesis is to probe water-alkane interactions in cluster ions. Extensive research on the water-hydrophobic interface in the condensed phase has been reported by Richmond and co-workers using the interface specific technique vibrational sum frequency spectroscopy (VSFS).[51-58] A very weak interaction was found between

water and the alkane at their interface based on a shift of the free O-H modes in the IR-VSF spectra, and, interestingly, changing the alkane had no effect on the spectra.[51,55] Theoretical work has been carried out to better understand the water-alkane interaction and recently the alkane has been proposed as the proton accepting component in a water-alkane hydrogen bonded motif.[59-62]

1.4 Overview

The goal of this Thesis is to investigate the solvation of alkali metal ions by methane including an ion's electrostatic effect beyond the first solvent shell, then include water in the cluster ions to probe electrostatic interactions in ion•••water•••alkane complexes. The work done can be described in three phases.

First, the ion•••CH_4 electrostatic interaction will be studied starting by investigating the argon tagged Li^+•••CH_4 dimer in chapter 3. Chapters 4 and 5 are dedicated to fully analyze the solvation of the alkali metal ions by methane.

In the second phase, previous $Li^+(H_2O)_{3-4}Ar_1$ studies are extended in chapter 6 to check for high energy conformers. This work was undertaken in response to prior studies which showed that argon tagging can result in trapping and probing of high energy conformers using unique fragmentation channels. This is important to gain a better understanding of different structural water motifs that can be present conformers.

In the third phase, ion•••water•••alkane clusters are studied in a three part chapter series. $Li^+(H_2O)_{1-4}(CH_4)_n$ clusters will be studied in chapter 7 to probe the effects of the small alkane on the hydrated Li^+ clusters. In chapter 8, the alkane is changed to cyclohexane. This is done to compare the effects of different alkanes on $Li^+(H_2O)_n$ clusters. Finally, $Cl^-(Water)_{1-3}(CH_4)_n$ clusters are probed in chapter 9 in order to compare

the solvation of the anion with that of the cation by water and methane reported in chapter 7.

1.5 References

[1] D. L. Nelson, M. M. Cox, *Lehninger Principles of Biochemistry*, Worth Publishers, New York, 2000.
[2] M. V. Kirov, G. S. Fanourgakis, S. S. Xantheas. *Chem. Phys. Lett.* 461 (2008) 180.
[3] E. D. Sloan, Jr, *Clathrate Hydrates of Natural Gases*, Marcel Dekker, New York, 1998.
[4] K. Muller-Dethlefs, P. Hobza. *Chem. Rev.* 100 (1999) 143.
[5] J. M. Lisy, in *Cluster Ions*, C.-Y. Ng, T. Baer, I. Powis, Wiley and Sons, New York, 1993, 217.
[6] A. W. Castleman Jr, R. G. Keesee. *Chem. Rev.* 86 (1986) 589.
[7] M. A. Duncan. *Annu. Rev. Phys. Chem.* 48 (1997) 69.
[8] M. A. Duncan. *Int. Rev. Phys. Chem.* 22 (2003) 407.
[9] P. Kebarle. *Annu. Rev. Phys. Chem.* 28 (1977) 445.
[10] R. G. Keesee, A. W. Castleman Jr. *J. Phys. Chem. Ref. Data* 15 (1986) 1011.
[11] J. M. Lisy. *Int. Rev. Phys. Chem.* 16 (1997) 267.
[12] T. D. Vaden, C. J. Weinheimer, J. M. Lisy. *J. Chem. Phys.* 121 (2004) 3102.
[13] O. M. Cabarcos, C. J. Weinheimer, T. J. Martinez, J. M. Lisy. *J. Chem. Phys.* 110 (1999) 9516.
[14] D. J. Miller, J. M. Lisy. *J. Am. Chem. Soc.* 130 (2008) 15393.
[15] D. J. Miller, J. M. Lisy. *J. Am. Chem. Soc.* 130 (2008) 15381.
[16] C. J. Weinheimer, J. M. Lisy. *J. Chem. Phys.* 105 (1996) 2938.
[17] C. J. Weinheimer, J. M. Lisy. *J. Phys. Chem.* 100 (1996) 15305.
[18] D. W. Boo, Y. T. Lee. *Int. J. Mass Spectrom. Ion Processes* 159 (1996) 209.
[19] J. M. Headrick, J. C. Bopp, M. A. Johnson. *J. Chem. Phys.* 121 (2004) 11523.
[20] J. M. Lisy. *J. Chem. Phys.* 125 (2006)
[21] M. Okumura, L. I. Yeh, J. D. Myers, Y. T. Lee. *J. Chem. Phys.* 85 (1986) 2328.
[22] J. P. Beck, J. M. Lisy. *J. Phys. Chem. A* 114 (2010) 10011.
[23] A. L. Nicely, D. J. Miller, J. M. Lisy. *J. Mol. Spectrosc.* 257 (2009) 157.
[24] J. D. Rodriguez, J. M. Lisy. *Int. J. Mass Spectrom.* 283 (2009) 135.
[25] O. Rodriguez Jr, J. M. Lisy. *J. Phys. Chem. A* 115 (2011) 1228.
[26] S. K. Shukla. *Chromatographia* 6 (1973) 371.
[27] H. Li, Z. Wang, L. Chen, X. Huang. *Adv. Mater.* 21 (2009) 4593.
[28] J. Tollefson. *Nature* 456 (2008) 436.
[29] C. I. Ragan. *Met.-Based Drugs* 4 (1997) 125.
[30] N. Riadh, M. Allagui, E. Bourogaa, C. Vincent, F. Croute, A. Elfeki. *BioMetals* (2011) *In Press*.
[31] A. Wada, H. Yokoo, T. Yanagita, H. Kobayashi. *J. Pharmacol. Sci.* 99 (2005) 307.
[32] R. Williams, W. J. Ryves, E. C. Dalton, B. Eickholt, G. Shaltiel, G. Agam, A. J. Harwood. *Biochem. Soc. Trans.* 32 (2004) 799.
[33] G. Herzberg, *Molecular Spectra and Molecular Structure II. Infrared and Raman Spectra of Polyatomic Molecules,* Van Nostrand, New York, 1945.

[34] G. Calderoni, F. Cargnoni, R. Martinazzo, M. Raimondi. *J. Chem. Phys.* 121 (2004) 8261.
[35] M. Geleijns, N. Halberstadt, J. Millan, P. E. S. Wormer, A. Van der Avoird. *Faraday Discuss.* 118 (2001) 143.
[36] M. Geleijns, A. Van Der Avoird, P. E. S. Wormer, N. Halberstadt. *J. Chem. Phys.* 117 (2002) 7562.
[37] T. G. A. Heijmen, P. E. S. Wormer, A. Van Der Avoird, R. E. Miller, R. Moszynski. *J. Chem. Phys.* 110 (1999) 5639.
[38] V. D. Makhaev. *Russ. Chem. Rev.* 72 (2003) 257.
[39] R. E. Miller, T. G. A. Heijmen, P. E. S. Wormer, A. Van Der Avoird, R. Moszynski. *J. Chem. Phys.* 110 (1999) 5651.
[40] M. Wangler, D. A. Roth, I. Pak, G. Winnewisser, P. E. S. Wormer, A. Van der Avoird. *J. Mol. Spectrosc.* 222 (2003) 109.
[41] N. Zvereva-Loete, Y. N. Kalugina, V. Boudon, M. A. Buldakov, V. N. Cherepanov. *J. Chem. Phys.* 133 (2010) 184302.
[42] L. Ferrighi, G. K. H. Madsen, B. Hammer. *Chem. Phys. Lett.* 492 (2010) 183.
[43] J. B. L. Martins, J. R. S. Politi, E. Garcia, A. F. A. Vilela, R. Gargano. *J. Phys. Chem. A* 113 (2009) 14818.
[44] J. D. Smith, R. J. Saykally, P. L. Geissler. *J. Am. Chem. Soc.* 129 (2007) 13847.
[45] G. Gregoire, N. R. Brinkmann, D. van Heijnsbergen, H. F. Schaefer, M. A. Duncan. *J. Phys. Chem. A* 107 (2003) 218.
[46] G. Gregoire, M. A. Duncan. *J. Chem. Phys.* 117 (2002) 2120.
[47] N. R. Walker, G. A. Grieves, R. S. Walters, M. A. Duncan. *Chem. Phys. Lett.* 380 (2003) 230.
[48] N. R. Walker, R. S. Walters, M. A. Duncan. *J. Chem. Phys.* 120 (2004) 10037.
[49] N. R. Walker, R. S. Walters, G. A. Grieves, M. A. Duncan. *J. Chem. Phys.* 121 (2004) 10498.
[50] R. S. Walters, N. R. Brinkmann, H. F. Schaefer, M. A. Duncan. *J. Phys. Chem. A* 107 (2003) 7396.
[51] M. G. Brown, D. S. Walker, E. A. Raymond, G. L. Richmond. *J. Phys. Chem. B* 107 (2003) 237.
[52] D. K. Hore, D. S. Walker, G. L. Richmond. *J. Am. Chem. Soc.* 130 (2008) 1800.
[53] C. L. McFearin, G. L. Richmond. *J. Mol. Liq.* 136 (2007) 221.
[54] C. L. McFearin, G. L. Richmond. *Appl. Spectrosc.* 64 (2010) 986.
[55] F. G. Moore, G. L. Richmond. *Acc. Chem. Res.* 41 (2008) 739.
[56] G. L. Richmond. *Annu. Rev. Phys. Chem.* 52 (2001) 357.
[57] L. F. Scatena, M. G. Brown, G. L. Richmond. *Science* 292 (2001) 908.
[58] L. F. Scatena, G. L. Richmond. *J. Phys. Chem. B* 105 (2001) 11240.
[59] S. G. Olesen, T. L. Gausco, G. H. Weddle, S. Hammerum, M. A. Johnson. *Mol. Phys.* 108 (2010) 1191.
[60] S. G. Olesen, S. Hammerum. *J. Phys. Chem. A* 113 (2009) 7940.
[61] S. G. Olesen, S. Hammerum. *Eur. J. Mass Spectrom.* 15 (2009) 239.
[62] B. Raghavendra, E. Arunan. *Chem. Phys. Lett.* 467 (2008) 37.

Chapter 2

Experimental Details

The method used in experiments for this Thesis is a combination of tandem mass spectrometry and infrared predissociation (IRPD) spectroscopy. Density functional theory or MP2 level calculations are used to support experimental results. Specific experimental and computational details accompany the ensuing chapters of this Thesis, so an overview of cluster generation, the triple quadrupole apparatus, IRPD spectroscopy, and calculations are presented here.

2.1 Cluster Generation

Gas phase cluster ions are generated in a source chamber seen in Figure 2.1 with the triple quadrupole apparatus.[1-3] MKS (model 1159) flow controllers are used to specify the flow rate of the gas solvent of interest and argon gas. Solvent gas flows are typically ~0.5-30 sccm (standard cubic centimeters/minute) while argon gas flow is ~110-140 sccm; making argon the primary gas in the experiments. After passing through the flow controllers, the gases mix in a single gas line where the backing pressure, usually between 400-600 torr, is measured. The gases are then forced through a 30° conical nozzle with a 180 μm diameter orifice into the source chamber which is pumped by a Varian 10-inch, 3650 L/s diffusion pump backed in series by a 60 L/s roots pump and duel-stage 10 L/s rotary vane pump. Under gas load the source chamber pressure is measured at ~1.0 x 10^{-4} torr. Because the source chamber:backing nozzle pressure ratio far exceeds a critical ratio of 2.1, a supersonic expansion is achieved and neutral clusters

are formed.[4] About 100 nozzle diameters down stream of the nozzle exit, neutral clusters are intercepted with alkali metal ions ejected from a homemade ion gun.

The ion gun consists of a 0.008 inch diameter coiled tungsten wire which is thoroughly coated with an alkali halide/molecular sieve paste containing the ion of interest. A current between 2.5-3.2 A is applied to the filament coil ejecting ions by thermionic emission. In addition, a bias of ~ +23-27 V relative to chamber ground is applied to the ions. Voltages are applied to electrostatic lenses which are used to collimate the ions toward the neutral cluster beam. The bias and electrostatic voltage polarities can be switched to optimize for anions.

Ion collisions with fully expanded neutral clusters generates hot, unstable cluster ions containing ~1000 kJ/mol of excess energy from the collision and subsequent solvation.[2,5] This energy is dissipated via evaporative cooling.[2,5,6] Should weakly interacting argon atoms be the primary evaporating ligand, then more evaporative events can occur compared to stronger interacting ligands, in turn resulting in more energy lost through argon evaporation. Thus, clusters formed mainly through argon evaporation have temperatures ~50-150 K [2] while clusters formed by evaporating water ligands, for example, have temperatures ~250-500 K.[2] Evaporation of ligands continues until a quasi-stable state is reached, or until the lifetime of the cluster ion of interest is longer than the time to transverse the one meter detector chamber (vide infra). Once a quasi-stable state is reached, the cluster ions pass through a 1 mm skimmer into a differentially pumped chamber pumped by 200 L/s turbomolecular pump backed by a duel-stage 3 L/s rotary vane pump. This differential pumping chamber serves as an ion guiding,

intermediate chamber also adds the benefit of reducing the detector chamber gas load. This chamber contains a 9.5 cm octopole ion guide and electrostatic lenses to facilitate ion guiding. The octopole operates at 1.2 MHz (peak to peak voltage ~730 V) A DC voltage, typically between -100 and -400 V is applied to the octopole. Furthermore, a pyroelectric detector is placed in the differential pumping chamber, after the octopole ion guide assembly, and be adjusted externally to help align the output of a counter propagating (relative to the direction of the cluster ion beam) laser beam through the apparatus.

Cluster ions exit the differentially pumped chamber and enter the detection chamber through a 0.25" aperture. The detection chamber is pumped by a Varian 6 inch 1200 L/s diffusion pump backed by a duel-stage 3 L/s rotary vane pump. Depending on gas load, pressures in the detection chamber are typically between ~5 $x10^{-8}$ – 1 $x10^{-7}$ torr making the chamber essentially a collision-free environment as the mean free path is greater than the length of the detector chamber, ~1 meter (*vide infra*).

2.2 Triple Quadrupole Apparatus

The detector chamber houses three quadrupoles; all powered by Extrel power supplies. Each quadrupole consists of 9.5 mm diameter rods. The first and third quadrupoles are 20 cm in length and act a mass filters. The second quadrupole in fact consists of three closely spaced 20 cm quadrupoles which essentially act as one, r.f. (radio frequency) only mode, 60 cm quadrupole. Thus the length of the detector chamber is ~1 m. All quadrupoles operate at 1.2 MHz (peak to peak voltage of 7200 V). A DC component of ±200 V to ±800 V is applied to the first and third quadrupoles for mass

selecting. Electrostatic lenses are positioned at the entrance and exit of each quadrupole to aid in ion guiding.

Cluster ions exiting the third, and final, quadrupole are detected by a combination conversion dynode (CD) and channeltron electron multiplier (CEM). A -4 kV voltage is applied to the CD. Positive cluster ions strike the CD causing ejection of ~4 electrons [7] that are attracted to, and enter, the CEM which is biased between +1.8 and 3 kV.

Electrons cascade through the CEM with a final gain of ~10^7-10^8 electrons per initial electron. CEM pulse widths are 10 ns and are 1 mV in amplitude. The pulses pass through a 1.2 MHz notch filter to eliminate any noise originating from the quadrupoles and octopole ion guide of the same frequency. Next, the pulses pass through a pre-amplifier. Over three stages, the pulses are amplified 125x then go through a discrimination phase. Here, a discriminator eliminates pulses which are less than 30 mV, or noise generated from stray electrons. Pulses greater than 30 mV originate from true signal. In addition, the discriminator acts to convert passing pulses into 50 ns pulse width, 2.5 V amplitude TTL pulses. These TTL pulses are considered as “ion counts” and kept below 1 x10^6 counts/sec. This assures pulses are not overlapping and that each is counted. The signal is split to a rate meter and multi-channel scalar (MCS) card which is used for data acquisition.[8]

2.3 Infrared Predissociation Spectroscopy

The infrared light used in the experiments originate from a Nd:YAG (Continuum Surelite-II 10 Hz) pumped Laservision optical parametric oscillator/optical parametric amplifier system;[9] referred to as OPO/OPA herein. First steering mirrors guide the

1064 nm output of the Nd:YAG laser (~520-530 mJ/pulse) into the OPO/OPA housing. The beam passes a telescope then is split by a beam splitter.

30% of the 1064 nm beam will be directed into the OPO stage. The beam passes through a potassium titanyl phosphate (KTP) crystal which acts as a frequency doubler, generating a single 532 nm photon from two 1064 nm photons. The 532 nm beam proceeds to pump another KTP crystal acting as the OPO. Through computer-controlled fine angle tuning, a range of mid-IR frequencies can be obtained with a bandwidth of 3 cm^{-1}.

The mid-IR output beam from the OPO is then combined with the 1064 nm, undoubled frequency portion of the initial beam entering the OPO/OPA housing. A different frequency generation is utilized to amplify the mid-IR component which then exits the OPO/OPA housing. Typical pulse energies are ~2 – 15 mJ/pulse in the mid-IR range of 2600 – 3800 cm^{-1}. A series of lenses and mirrors are used to direct the mid-IR beam into the triple quadrupole apparatus, counter-propagating the cluster ion beam. Using the internal pyroelectric detector mention earlier, the IR beam is gently focused such that the beam waist spans the second quadrupole.

In infrared predissosication (IRPD) spectroscopy, or action spectroscopy, the cluster ion of interest is mass selected in the first quadrupole and allowed to pass to the second quadrupole. Here, the cluster ion may interact with an mid-IR photon from the counter-propagating output of the OPO/OPA. If the photon frequency is on resonance with a cluster ion vibrational mode, absorption of the photon energy can occur. The imparted energy, along with internal energy in the cluster, can lead to the fragmentation of one or more ligands. The third quadrupole mass filter can then be strategically tuned to allow the

subsequent fragment ion to pass through and be detected. The detected signal is collected by a multi-channel scalar (MCS card) [8], mentioned earlier.

During the course of passing though the second quadrupole, some cluster ions might undergo unimolecular fragmentation. This may cause a fragment ion to transverse the third quadrupole, be detected, and counted by the MCS card. To account for signal detection arising from anything else other than photodissociation, we employ a method wherein the MCS card acquires data based on the time required for fragment cluster ions from only the second quadrupole to reach the detector after a laser shot has been fired.

To achieve this, a time of flight (TOF) is obtained by applying a 5V pulse to the lens at the first quadrupole entrance, perturbing the cluster ion beam. After some time, the perturbation can cause a decrease, or increase, in signal at the detector. Flight times are usually between 100 – 300 μs, and can be used to approximate the times for clusters to reach the detector, ranging from the entrance and exit, of the second quadrupole, i.e. all the clusters in the second quadrupole.

Time windows are established such that after a laser shot is fired the MCS card begins collecting data when the first clusters from the second quadrupole exit reach the detector, and stops collecting data when clusters from the second quadrupole entrance (when the laser shot was fired) reaches the detector. This window is called “Laser On”. After a brief delay, the MCS card collects signal in a window called “Laser Off” arising from fragment ions reaching the detector from any other source of fragmentation other than photodissociation, i.e. unimolecular or collision-induced dissociation. The counts from the “Laser Off” window are subtracted from the counts in the “Laser On” window

to obtain true signal. An example of data for $Rb^+(CH_4)_4$ at a frequency on resonance with the totally symmetric vibrational mode of methane is shown in Figure 2.2.

The photodissociation cross sections are obtained by,

$$\sigma(cm^2) = -\frac{\log(1 - \%\text{Depletion}/100)}{\text{Laser Fluence}(cm^{-2})}$$

where,

$$\%\text{Depletion} = \frac{\text{Signal (counts)-Background (counts)}}{\left[I_{\text{Parent Ion}}\left(\frac{\text{counts}}{\text{sec}}\right)\right] * [\text{width of window signal (s)}] * [\#\text{of laser shots}]} x100$$

$$\text{Laser Fluence}(cm^{-2}) = \frac{\#\text{photons}}{\pi r^2}$$

$$\#\text{photons} = \frac{\text{Laser power at TQ entrance (mJ/pulse)}/1000}{\text{Photon energy (J/photon)}}$$

The photodissociation cross section can be plotted as a function of laser frequency to generate an IRPD spectrum. Absolute frequency calibration is achieved by simultaneously recording a photoacoustic spectrum of atmospheric water vapor for the O-H stretching region (3200 – 3900 cm^{-1}) and recording a reference spectrum of CH_4 or HCl gas for the O-D or C-H stretching regions (2600 – 3200 cm^{-1}).

2.4 Computational Details

Density functional theory or MP2 level calculations were used to help characterize experimental data presented in this Thesis. Specific levels of theory and methods are discussed in the ensuing chapters. Briefly, reasonable initial geometries were generated using Spartan 02.[10] Geometry optimizations and harmonic vibrational frequencies were carried out using Gaussian 03 suite.[11] Generally, density functional

theory (DFT) using the B3LYP functional and 6-31+G* basis set is used for geometry optimization and obtaining harmonic vibrational frequencies.

When time allows, second-order Møller-Plesset (MP2) level theory is employed to obtain relative energies of different structural conformers, ligand binding energies, and harmonic vibrational frequencies.

Simulated spectra are generated using the SWizard [12] program while calculated structures reported in this Thesis are generated using Molden.[13]

2.5 Figures

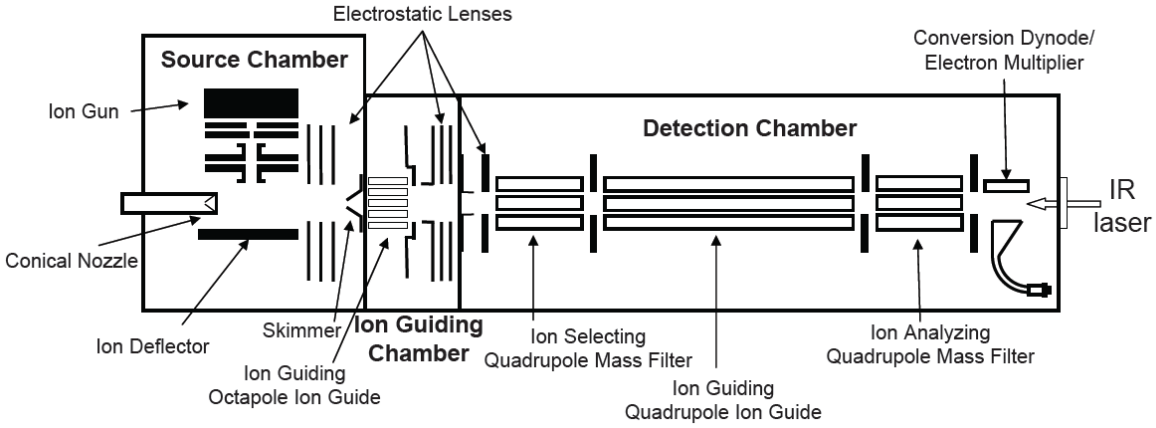

Figure 2.1: Triple quadrupole apparatus.

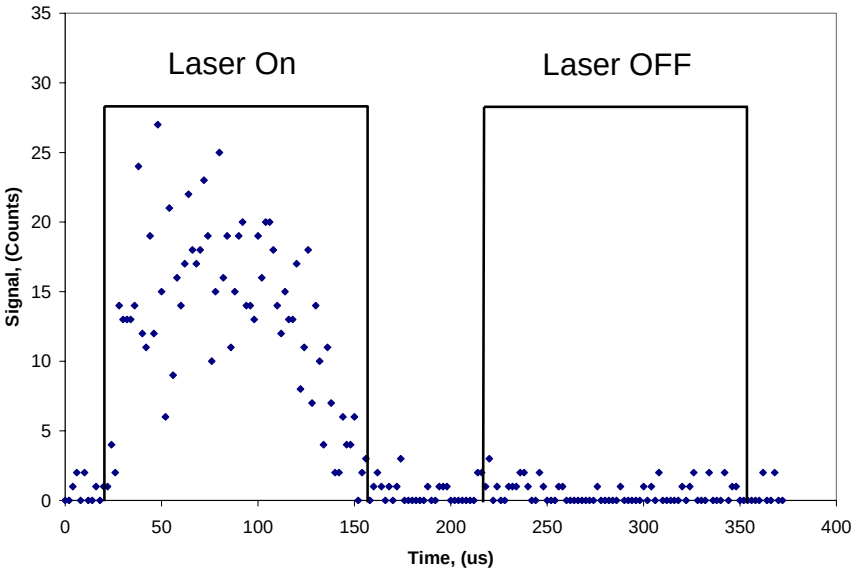

Figure 2.2. MCS output obtain at a frequency on resonance with the totally symmetric mode of methane in $Rb^{+}(CH_4)_4$. The MCS card registers signal in the "Laser On" and "Laser Off" windows.

2.6 References

[1] D. J. Miller, J. M. Lisy. *J. Am. Chem. Soc.* 130 (2008) 15393.
[2] D. J. Miller, J. M. Lisy. *J. Am. Chem. Soc.* 130 (2008) 15381.
[3] C. J. Weinheimer: The Role of Hydrogen Bonding in Alkali Metal Ion Solvation, University of Illinois at Urbana-Champaign, 1998.
[4] D. R. Miller, in *Atomic and Molecular Beam Methods*, G. Scoles, Oxford University Press, 1988, 380.
[5] O. M. Cabarcos, C. J. Weinheimer, J. M. Lisy. *J. Phys. Chem. A* 103 (1999) 8777.
[6] C. E. Klots. *J. Chem. Phys.* 83 (1985) 5854.
[7] J. D. Rodriguez: Modeling Ionophore Selectivity in the Gas Pgase: IR Spectroscopy of Solvated Metal Ion-Crown Ether Complexes, University of Illinois, Urbana, IL, 2009.
[8] C. A. Corbett: Study of the Interplay Among Non-Covalent Interactions in Structural Determination of Gas Phase Cluster Ions, University of Illinois, Urbana, IL, 2001.
[9] D. Guyer: LaserVision Manual, 2006.
[10] J. Kong, C. A. White, A. I. Krylov, C. D. Sherrill, R. D. Adamson, T. R. Furlani, M. S. Lee, A. M. Lee, S. R. Gwaltney, T. R. Adams et al., SPARTAN'02, Wavefunction, Inc., Irvine CA, 2002.
[11] M. J. Frisch, G. W. Trucks, H. B. Schlegel, G. E. Scuseria, M. A. Robb, J. R. Cheeseman, J. A. Montgomery Jr., T. Vreven, K. N. Kudin, J. C. Burant et al., Gaussian 03, Revision B.04, Gaussian, Inc., Pittsburgh, PA, 2003.
[12] S. I. Gorelsky, *SWizard program*, 4.1, University of Ottawa, Canada, 2005.
[13] G. Schaftenaar, J. H. Noordik. *J. Comput.-Aided Mol. Des.* 14 (2000) 123.

Chapter 3

IRPD Spectroscopy of $Li^+(CH_4)_1Ar_n$, n=1-6, Clusters[1]

3.1 Introduction

Methane, CH_4, is the simplest of the organic hydrocarbons and thus serves as a useful model for when trying to understand simple ion•••hydrocarbon systems. Characterizing these non-covalent interactions may prove useful in understanding the role of these complexes in nature, ranging from fuels [1] to clathrates.[2,3]

Ion•••CH_4 complexes have been studied extensively with many of the first- [4-11], second- [12-17], and third-row [18-22] transition metal ions. These experiments can provide thermodynamic and dissociation pathway information based on the reactions and subsequent activation of CH_4. Our interests however lay in the weaker electrostatic ion•••ligand interactions of alkali metal cluster ions.

While CH_4 is a nonpolar spherical top molecule, its strong affinity for clustering has been studied. In the cases of halide anion complexes, $X^-(CH_4)_n$, X=F [23-25], Cl [23,26,27], and Br [25], CH_4 was shown to interact via ionic hydrogen bonding with a single C-H, i.e. η_1 configuration, which lowers the CH_4 symmetry from T_d to C_{3v}. Spectra indicate an intense infrared active ν_1 band emerging from the ionic hydrogen bond. A doubly degenerate mode of the new symmetry, ν_3(e), was observed along with well resolved rotational subbands. All of the observed features were shifted to lower

[1] This Chapter is reproduced in part and reprinted with permission from Oscar Rodriguez Jr. and James M. Lisy. *The Journal of Physical Chemistry A*. 2011, 115 (7), pp. 1228-1233. © American Chemical Society.

frequency. The magnitude of the shifts reflected the strength of the electrostatic interaction and followed the trend $F^- > Cl^- > Br^-$.

More closely related to our current study were the reported $M^+(CH_4)_n$, M=Al [28] and Mn [29], complexes by Bieske and co-workers. In cation complexes, CH_4 was reported to bind in an η_3 configuration. This would also lower the CH_4 symmetry from T_d to C_{3v}. For both Al^+ and Mn^+, the ν_1 totally symmetric mode was rendered infrared active and shifted to lower frequency, while the doubly degenerate and symmetric modes, $\nu_3(e)$ and $\nu_3(a_1)$, of the new C_{3v} symmetry and rotational subbands were too weak to be observed.

We recently completed an IRPD study of $Li^+(CH_4)_n$, n=1-9, clusters measuring the ν_1 band, now IR active, and the $\nu_3(e)$ band as a function of cluster size.[30] At n=5, the filling of the second solvent shell was noted with CH_4 ligands that gave rise to new ν_1 and $\nu_3(e)$ bands near the neutral CH_4 gas phase values. This indicated that the electrostatic perturbation by the ion is small beyond the first solvent shell.[30]

In general, ion•••CH_4 interactions are understood to be relatively weak. This can result in conformational changes (as noted above with η_1 and η_3 configurations) of CH_4 in clusters. For example, photodissociation spectroscopy of $MgCH_4^+$ while scanning in the 3p←3s region of Mg^+ revealed an absorption band assigned to an η_3 configuration in the ground electronic state.[31] After excitation, relaxation to an η_2 configuration was reported prior to insertion of Mg^+ into CH_4 leading to a $MgCH_3^+$ fragment. A similar conformational change upon relaxation was observed for the $ZnCH_4^+$ complex.[6] A related experiment of the $CaCH_4^+$ complex also revealed an η_3 configuration [32],

however no change in complex conformation was observed after excitation in the 4p←4s region of Ca^+.

Li^+ is an intriguing ion for use in our experiments. A small ionic radius [33], high charge density [34], and closed shell configuration enable Li^+ to induce substantial perturbations on adjacent molecules in small cluster ions. Previous theoretical studies of the Li^+•••CH_4 dimer have shown that an η_3 coordinated CH_4 is the minimum energy structure as Li^+ will tend to interact with the electron dense carbon.[35,36] The vibrational modes can be significantly impacted by these non-covalent electrostatic interactions [37,38] and monitored via infrared predissociation spectroscopy.[30]

In our experiments, cluster ion photofragmentation is essential for detecting the absorption of an infrared photon. However, Li^+•••ligand interactions can readily generate binding energies that exceed the energy provided by a mid-infrared photon, ~35 kJ/mol.[39] Toennies and co-workers were able to determine a Li^+•••CH_4 interaction potential of 0.38 eV, or 36.66 kJ/mol [40] based on ion scattering experiments. To circumvent this issue, we employ argon tagging because the low ion•••Ar binding energy in cluster ions of ~ 5-20 kJ/mol [41,42] is easily exceeded by the IR photon. The lower binding energy of argon provides a second benefit; a lower internal energy or effective temperature (~ 50-150 K) [43], leading to narrower, better-resolved spectral features. In contrast, non-argonated cluster temperatures can range from ~250-500 K [39] and exhibit spectral broadening.

3.2 Experimental Methods

The infrared predissociation spectra of $Li^+(CH_4)Ar_{1-6}$ cluster ions were obtained studied by combining mass spectrometry using a triple quadrupole apparatus with a tunable infrared laser. A more detailed account of the experimental apparatus can be found elsewhere [39] so only a brief summary is presented here. First, a small amount of CH_4 gas seeded in argon gas (~0.25 - 0.5%) is expanded though a 30º conical nozzle (180 μm diameter) at backing pressures on the order of 450 torr into the source vacuum chamber to generate a beam of neutral CH_4/Ar clusters. About 100 nozzle diameters downstream, lithium ions, generated via thermionic emission from a tungsten filament coated with a LiCl paste, perpendicularly collide with neutral clusters to form nascent cluster ions. Excess energy, arising from the collisional and solvation processes, is dissipated by evaporative cooling [44] which lowers the internal energy (effective temperature) of the cluster ions to a point where they are sufficiently stable to traverse the length of the apparatus. A skimmed beam of quasi-stable cluster ions is guided through an octapole ion guide, into a second differentially pumped vacuum chamber, then into the detector chamber with the triple quadrupole. The cluster ions of interest are mass selected in the first of three quadrupoles. These mass selected cluster ions enter the second, r.f. only, quadrupole where they can interact with photons from a pulsed tunable infrared laser (Laservision OPO/OPA pumped by a 1064 nm output of a Surelite II 10 Hz Continuum Nd:YAG laser). Absorption of a resonant photon in the C-H stretching region imparts ~33 - 37 kJ/mol of energy into the cluster ion which can lead to fragmentation. The fragment ions are subsequently mass detected by a third quadrupole and then monitored using a conversion dynode/channeltron electron multiplier combination.

Infrared spectra are obtained by monitoring the extent of photofragmentation, corrected by the laser fluence to yield photodissociation cross sections as a function of frequency in the C-H stretching region (2800 cm^{-1} - 3100 cm^{-1}). Different fragmentation channels were initially monitored to determine the channel with the optimal signal to noise. That channel and possibly one or two others are then used to determine the spectrum for that cluster ion and to check for possible structural conformers. Absolute frequency calibration (±3 cm^{-1} resolution) was carried out by simultaneously scanning the IR spectrum of CH_4 in a gas reference cell. Experimental spectra were smoothed via three-point-adjacent averaging while reported frequencies are obtained from fitting experimental data to Gaussian lineshapes using the OriginLab 7.5 program.[45]

3.3 Computational Methods

Density functional theory calculations were carried out at the B3LYP/6-31+G* level to obtain vibrational frequencies. First, initial geometries were obtained using SPARTAN 02.[46] Minimum energy geometries and harmonic vibrational frequencies were obtained using GUASSIAN 03.[47] The vibrational frequencies were then scaled to fit experimental neutral CH_4 values (0.9575 for B3LYP/6-31+G* calculations). MP2/aug-cc-pVDZ calculations were used to obtain relative energies for optimized $Li^+(CH_4)_1Ar_6$ structures and determine single point binding energies of CH_4 and Ar.

3.4 Results and Discussion

As reported previously, interaction with the cation lowers the T_d symmetry of CH_4 to C_{3v} symmetry [28], reflecting the η_3 configuration with three C-H oscillators

facing the ion and one lone C-H oscillator pointing away. This configuration lends IR activity to the normally IR inactive totally symmetric ν_1 mode with a vibrational transition moment parallel to the symmetry axis and causes a shift to lower frequency from the neutral gas phase value (2917 cm^{-1}).[48] Meanwhile, the triply degenerate, IR active, ν_3 mode (neutral gas phase value of 3019 cm^{-1}) [48] is split into a doubly degenerate C-H stretch mode, $\nu_3(e)$, with a transition moment perpendicular to the symmetry axis, which also shifts to lower frequency. The other component, a weak symmetric mode of the C-H oscillator stretching away from the ion, $\nu_3(a_1)$, is shifted to higher frequency. We attempted to locate minima for $Li^+(CH_4)_1Ar_n$ using η_1 and η_2 coordinated CH_4 in the initial geometries. However, in each case the computations converged to an η_3 configuration for CH_4.

The spectrum for n=1 is shown in Figure 3.1 along with the calculated B3LYP/6-31+G* spectrum. The experimental spectrum is dominated by the ν_1 band at 2859 cm^{-1}, shifted 58 cm^{-1} from the ν_1 Raman active band in gas phase CH_4. The weak feature near 2965 cm^{-1} represents the $\nu_3(e)$ doubly degenerate mode while $\nu_3(a_1)$ mode is only faintly observed above background. Rotational structure was not observed, most likely due to spectral broadening, but the calculated spectrum is consistent with the experimental spectrum.

A full spectral summary for $Li^+(CH_4)_1Ar_n$, n=1-6, clusters is shown in Figure 3.2. As additional argon atoms are added to the cluster ion, the dominant ν_1 band shifts to higher frequencies. This reflects the weakening of the Li^+•••CH_4 interaction as the Ar solvent shell expands, and is also indicated by the CH_4 binding energy trend (see Table 3.1), which decreases slightly with increasing numbers of argon

The analysis of the ν_3(e) bands is more problematic due to the width of the bands. With the exception of the n=3 and 6 cluster ions, the ν_3(e) bands are 30-40 cm^{-1} in width. We suspect that thermal effects for n=1 and 2, and multiple isomers for n=4 and 5 might be responsible. Calculations for n=3 indicate a single minimum energy structure with a tetrahedral configuration of the four ligands. For n=4, a pyramidal configuration with C_{4v} symmetry is preferred, but a trigonal bipyramidal conformer with C_{3v} symmetry is calculated to be only ~2 kJ/mol higher in energy at the B3LYP/6-31+G* level. There is a lengthening of the Li^+•••CH_4 distance in this conformer to 2.29 Å from the distance in the C_{4v} structure of 2.26 Å. The calculated vibrational frequencies for both conformers are reported in Table 3.1. A similar scenario arises for the n=5 case. The preferred structure is a slightly distorted octahedral structure, but a second trigonal bipyramid structure, again ~2 kJ/mol higher in energy at the B3LYP/6-31+G* level, has CH_4 situated in the first solvent shell along with four other argon atoms and the fifth argon atom in the second solvent shell. The calculated vibrational frequencies for both conformers are reported in Table 3.1 with the frequencies for the octahedral structure more closely resembling the experimental values. The difference in vibrational frequencies for these isomers is small (~2 cm^{-1}) for both the ν_1 and ν_3(e) bands, yet only the ν_3(e) bands are significantly broadened. It is possible that the ν_3(e) vibrational motion due to the perpendicular transition moment may be more sensitive to adjacent argon atoms. The decrease in binding energy of both CH_4 and Ar for n=4 and 5 suggests that the accommodation of more than four ligands comes at the expense of steric hindrance. This would be consistent with the broadening of the ν_3(e) mode. Finally, the weak $\nu_3(a_1)$ bands

could only be modestly observed above background and do not contribute significantly to the spectra. Therefore only calculated $\nu_3(a_1)$ modes are reported in Table 3.1.

The spectrum for n=6 (Figure 3.2) is dominated by a sharp peak at 2887 cm^{-1} that represents the perturbed ν_1 mode while the ν_3(e) mode is observed at 2991 cm^{-1}. These bands occur at approximately the same frequencies as their n=5 counterparts and indicates that the addition of the sixth argon atom is not altering the $Li^+•••CH_4$ interaction. This suggests that the sixth argon is not adjacent to the ion, where it could impact the $Li^+•••CH_4$ interaction, but displaced to a second solvent shell. This conformer is built on the octahedral structure described for $Li^+(CH_4)_1Ar_5$ and is consistent with the coordination shell size of six ligands from Li^+Ar_{1-6} calculations previously reported.[49,50] Calculated frequencies in Table 3.1 for this structure match well with the experimental values. The calculated structure, labeled **(1)**, is shown in Figure 3.3.

The n=6 spectrum from Figure 3.2, reproduced in Figure 3.4 (spectrum **a**) has, in addition, two other features, a small but distinct band at 2914 cm^{-1} and a broad shoulder on the high frequency side of the ν_3(e) feature, centered at about 3017 cm^{-1}. These frequencies essentially correspond to the literature values [48] for the ν_1 and ν_3 modes of neutral gas phase CH_4 and indicates the presence of a second structural conformer containing a minimally perturbed CH_4. A logical assessment would place CH_4 in the second solvent shell making it the most labile ligand and susceptible to IR photofragmentation. The calculated structure confirms this assignment for conformer **(2)** as seen in Figure 3.3. The loss channel dependence was tested by monitoring the [CH_4] fragmentation channel, spectrum **(b)** in Figure 3.4. The infrared signatures from conformer **1** in spectrum **(a)** are completely absent in spectrum **(b)**; only the two features

associated with the weakly perturbed CH_4, conformer **(2)**, are detected at 2914 cm^{-1} and 3017 cm^{-1}.

Note the ratio of intensities between the two features in spectrum **(b)** is also substantially different from n=1-6 series in which CH_4 is in the first shell (see Figure 3.2). The observation of a less intense ν_1 mode compared to the ν_3(e) mode in spectrum **(b)** suggests that while the Li^+•••CH_4 interaction is sufficient to allow the otherwise IR-inactive ν_1 mode to be observed, the IR-active ν_3 mode is dominant. This further supports the structural assignment of CH_4 to the second shell. It is also likely that weakly hindered rotational subbands associated with the minimally perturbed ν_3 modes are responsible for the band broadening.

The spectroscopic observation of conformer **(2)** was somewhat unexpected. First, conformer **(2)** is calculated to be +11.89 kJ/mol higher in energy than conformer **(1)** and thus energetically unfavored. Second, the respective polarizabilities (x10^{-24} cm^3) [48] for CH_4 and Ar are 2.59 and 1.64 suggesting a stronger Li^+•••CH_4 than Li^+•••Ar interaction. This is reflected in calculated dimer binding energies from this work, 48.05 kJ/mol and 23.11 kJ/mol for Li^+•••CH_4 and Li^+•••Ar complexes respectively, and experimental binding energies of 36.66 kJ/mol[40] and 30.2 kJ/mol [51] for Li^+•••CH_4 and Li^+•••Ar based on scattering cross section experiments. The detection of this higher energy conformer must be due to the argon trapping mechanism, observed in other systems where the barrier to rearrangement is greater than the argon binding energy.[43,52-55]

The surprising spectral dependence on photofragmentation channel led us to investigate a total of eleven possible loss channels for n=6 at 2914 cm^{-1}, the ν_1 frequency of the minimally perturbed CH_4, conformer **(2)**. Of those eleven channels, only two, the

3Ar and CH_4 loss channels, displayed any measurable fragmentation. This leaves two questions to answer. Why only these two? What is responsible for the difference in photodissociation dynamics between the two $Li^+(CH_4)_1Ar_6$ conformers?

Clearly from Figure 3.4, loss of CH_4 is sensitive to only conformer **(2)** when the CH_4 is in the second shell. This fragmentation channel can appear to be explained in a straightforward manner. An IR photon (~35 kJ/mol) absorbed by a second shell CH_4 may be able to couple to other CH_4 modes prior to energy redistribution into the Li^+Ar_6 octahedral core such as the $\nu_2+\nu_4$ combination mode near 2845 cm^{-1}.[24] This could explain the rapid fragmentation of CH_4 before energy redistribution can occur. Excess energy would be retained by the CH_4 fragment.

For conformer **(1)**, the optimal dissociation channel is the loss of three argons. In this configuration, the vibrational energy is transferred to the cluster ion and results in the loss of the most labile species, argon atoms. Yet, this three argon loss channel is also associated, albeit more weakly, with conformer **(2)**. One explanation for this minor dissociation pathway involves a reorganization of the cluster ion following excitation of CH_4. In this mechanism, a portion of the energy which caused direct CH_4 fragmentation mentioned previously, is responsible for overcoming an energetic barrier to rearrangement of the first solvent shell allowing CH_4 to bind directly to the ion, i.e. conformer (**1**). As a result, conformer (**1**) would contain < ~46 kJ/mol from ~11 and ~35 kJ/mol of excess and photon energies respectively. Using the Ar binding energies from Table 3.1 we see that fragmentation of successive argons is ~1, 13.82, and 11.90 kJ/mol from n=6, 5, and 4 minimum energy conformers respectively, or ~26.72 kJ/mol total. This leaves <~19.28 kJ/mol of excess energy, not enough required to remove an argon

from n=3, 19.82 kJ/mol (see Table 3.1). Thus only three argons dissociate, leaving $Li^+(CH_4)_1Ar_3$ fragment cluster ion. This structural rearrangement of the cluster ion prior to dissociation has been previously observed in our laboratory and has been used to detect structural isomers via different fragmentation channels.[55]

3.5 Conclusions

$Li^+(CH_4)_1Ar_n$, n=1-6, clusters were studied using vibrational predissociation spectroscopy in the C-H stretching region. For $Li^+(CH_4)_1Ar_n$ clusters the CH_4 ν_1 and ν_3(e) bands for n=1 were shifted to lower frequency by 58 cm^{-1} and 55 cm^{-1} respectively relative to neutral CH_4 values. The shifts were less pronounced as more argon atoms are added indicating additional argon slight weaken the ion•••CH_4 interaction. Analysis of the vibrational frequencies for the n=5 and 6 species indicated a coordination number of six for Li^+ for argon, or argon with one CH_4. This is in contrast to the smaller coordination number of four when CH_4 is the sole ligating species. The weaker interaction between Li^+ and argon allows for a larger coordination number.

Two structurally distinct conformers were observed for n=6 which has six ligands in the first shell, where either an argon or CH_4 can reside in the second shell. While both conformers were observed in the 3 argon loss channel, the higher energy conformer with CH_4 in the second solvent shell was exclusively detected in the CH_4 loss channel. The ν_1 and ν_3(e) bands corresponding to the higher energy conformer appear near the neutral CH_4 values with essentially no shift in the ν_1 and ν_3 vibrational frequencies. This indicates that the electrostatic influence of the ion does not extend significantly beyond the first solvent shell of six argon atoms. Furthermore, this second shell CH_4 conformer is

calculated to be +11.89 kJ/mol higher in energy than the minimum energy conformer. Only the high energy conformer was detected via the $-CH_4$ fragmentation channel, an indication that CH_4 fragmentation occurred prior to complete energy redistribution into the cluster. Since, CH_4 in this conformer was calculated to be bound to the cluster by 5.63 kJ/mol, the excess energy from the photon energy was likely coupled into other CH_4 vibrational modes and retained in the fragmenting CH_4 ligand.

3.6 Figures and Tables

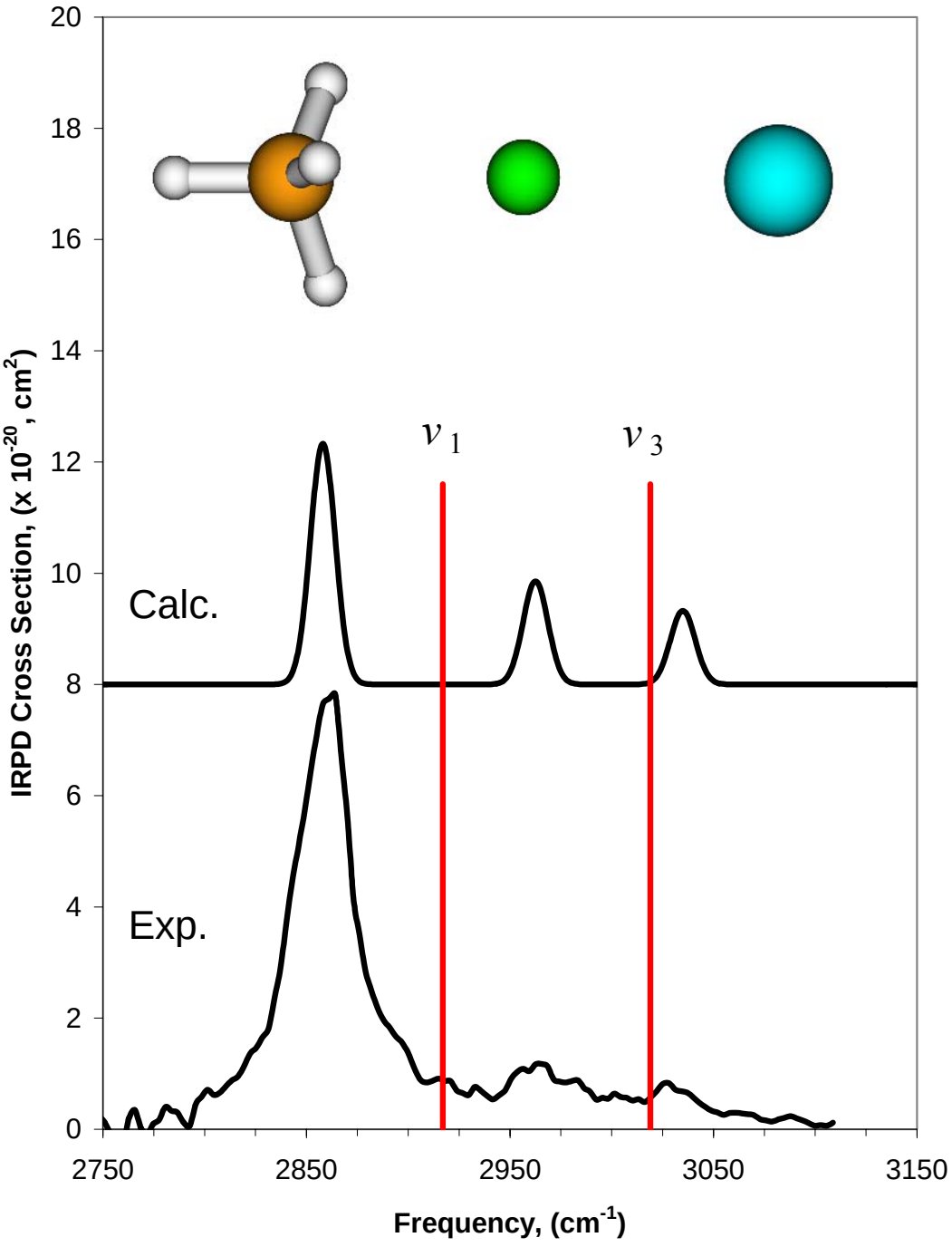

Figure 3.1: Infrared predissociation (IRPD) of $Li^+(CH_4)_1Ar_1$ with the B3LYP/6-31+G* calculated spectrum and structure. The labeled lines represent the totally symmetric, ν_1, and triply degenerate, ν_3, vibrational modes of neutral methane at 2917 cm^{-1} and 3019 cm^{-1} respectively.

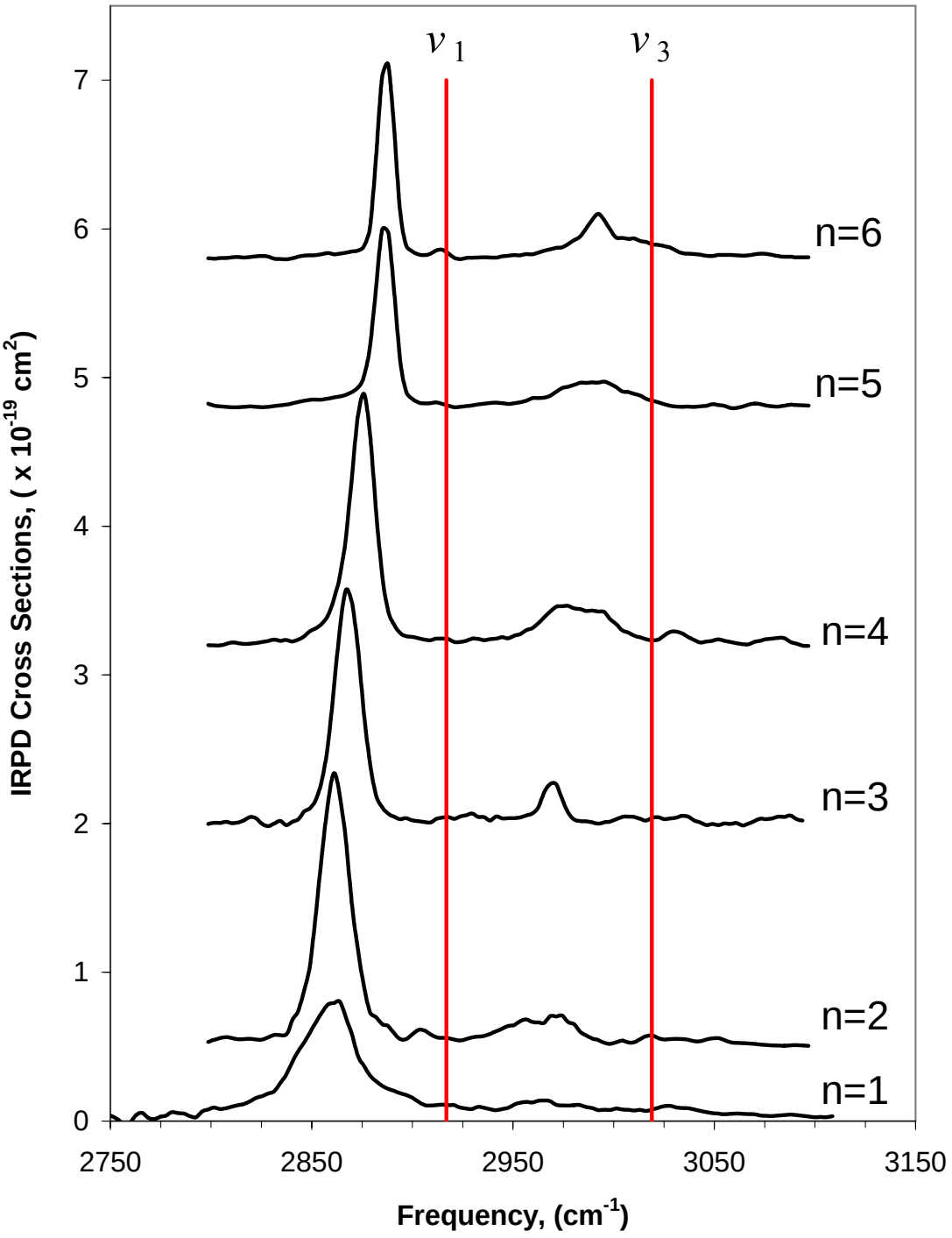

Figure 3.2: Infrared predissociation (IRPD) summary of $Li^+(CH_4)_1Ar_n$, n=1-6. Loss channels monitored varied with cluster size, -Ar for n=1-3, -2 Ar for n=4-5, and -3 Ar for n=6.

Table 3.1. Experimental and calculated B3LYP/6-31+G* vibrational frequencies (cm^{-1}) along with calculated MP2/aug-cc-pVDZ binding energies, D_e (kJ/mol), for both CH_4 and Ar.

	Experimental	Calculated	Experimental	Calculated	Calculated	CH_4	Ar
	ν_1, (cm^{-1})	ν_1, (cm^{-1})	ν_3(e), (cm^{-1})	ν_3(e), (cm^{-1})	$\nu_3(a_1)$, (cm^{-1})	B.E., (kJ/mol)	B.E., (kJ/mol)
$Li^+(CH_4)_1$	-	2855	-	2959	3033	48.05	-
$Li^+(CH_4)_1Ar_1$	2859	2858	2965	2962	3034	47.84	23.49
$Li^+(CH_4)_1Ar_2$	2861	2863	2966	2967	3035	46.02	21.13
$Li^+(CH_4)_1Ar_3$	2868	2869	2969	2973	3035	44.12	19.82
[a]$Li^+(CH_4)_1Ar_4$	2875	2878	2981	2983	3034	35.64	11.90
[b]$Li^+(CH_4)_1Ar_4$	2875	2880	2981	2985	3031	33.03	9.30
[c]$Li^+(CH_4)_1Ar_5$	2886	2888	2989	2993	3032	34.67	13.82
[d]$Li^+(CH_4)_1Ar_5$	2886	2879	2989	2984	3031	[e]33.03	1.52
[f]$Li^+(CH_4)_1Ar_6$	2887	2888	2991	2994	3033	[g]34.67	0.96
[h]$Li^+(CH_4)_1Ar_6$	2914	2914	3017	3011	3026	5.63	[i]18.51

[a]Pyramid conformer
[b]Trigonal bipyramid conformer
[c]Octahedral conformer
[d]Trigonal bipyramid conformer with one argon ligand in the second shell
[e]Calculated binding energy for the first shell CH_4 ligand in the trigonal bipyramid, approximating that the second shell argon atom will not perturb the first shell, thus binding energy
[f] Octahedral conformer with CH_4 in the 1st solvent shell
[g]Calculated binding energy for a first shell CH_4 ligand of the octahedral first shell core, approximating no perturbation by the second shell argon atom
[h]Conformer with CH_4 in the 2nd solvent shell
[i]Calculated binding energy for an argon atom of the Li^+Ar_6 complex approximating that the second shell CH_4 would not significantly perturb the first shell structure, thus binding energy

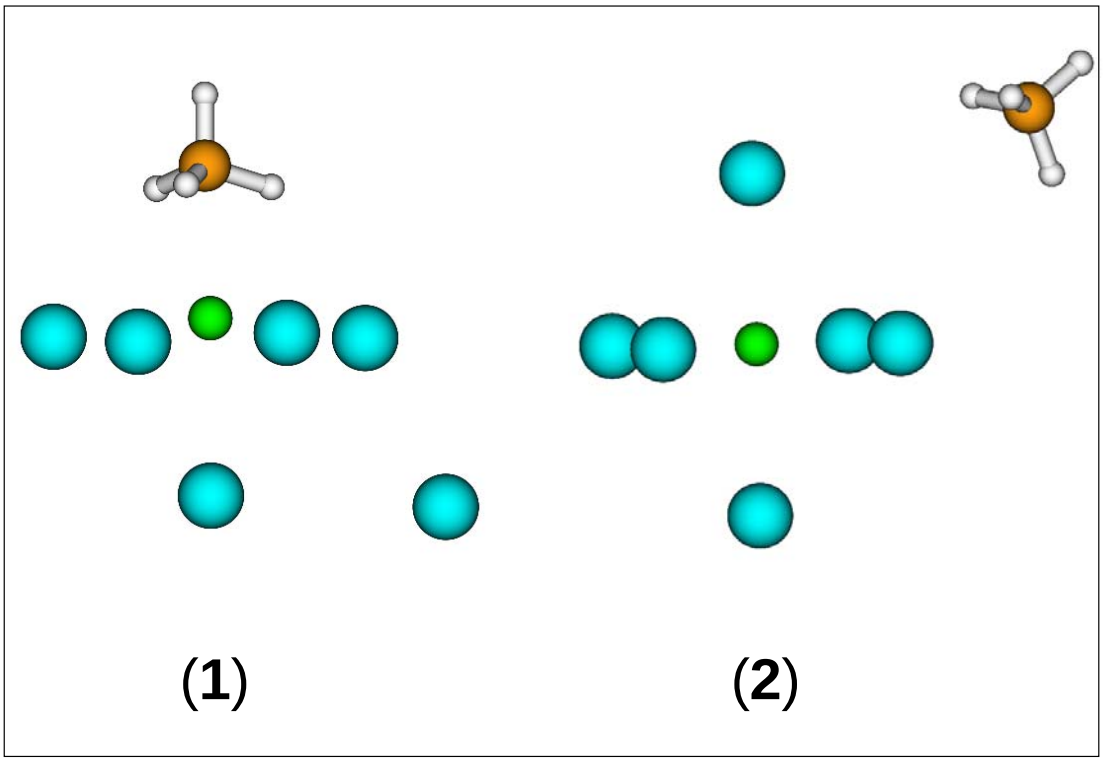

Figure 3.3: Two conformers for $Li^+(CH_4)_1Ar_6$ calculated at the MP2/aug-cc-pVDZ level. CH_4 resides in the first solvent shell in conformer (1) and in the second solvent shell in conformer (2).

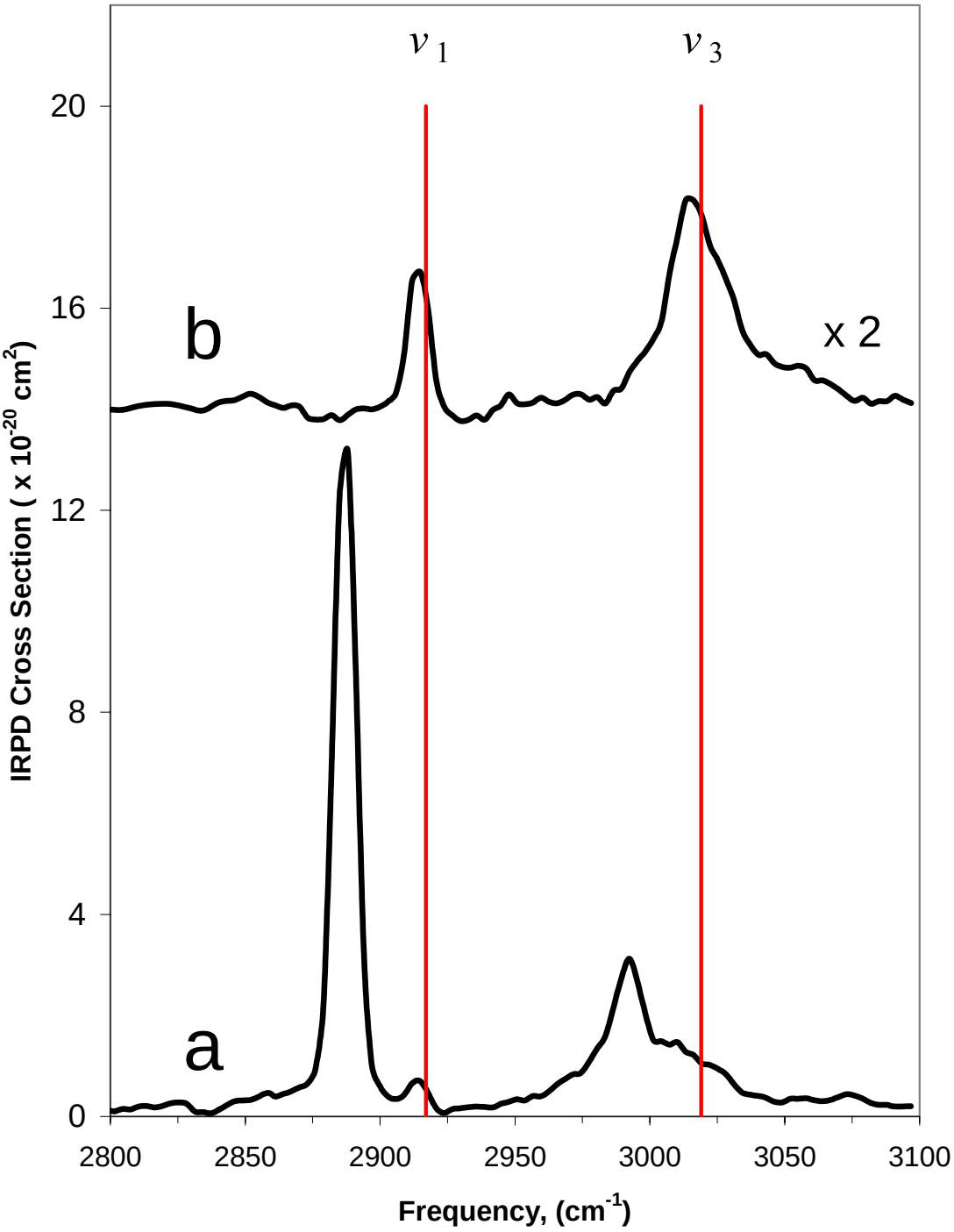

Figure 3.4: Infrared predissociation (IRPD) spectra for $Li^+(CH_4)_1Ar_6$ monitoring the 3 argon loss channel (**a**) and CH_4 loss channel (**b**).

3.7 References

[1] R. A. Kerr. *Science* 303 (2004) 946.
[2] E. D. Sloan, Jr, *Clathrate Hydrates of Natural Gases*, Marcel Dekker, New York, 1998.
[3] E. D. Sloan. *Energy & Fuels* 12 (1998) 191.
[4] N. Aristov, P. B. Armentrout. *J. Phys. Chem.* 91 (1987) 6178.
[5] R. Georgiadis, P. B. Armentrout. *J. Phys. Chem.* 92 (1988) 7067.
[6] W. Y. Lu, T. H. Wong, P. D. Kleiber. *Chem. Phys. Lett.* 347 (2001) 183.
[7] L. S. Sunderlin, P. B. Armentrout. *J. Phys. Chem.* 92 (1988) 1209.
[8] L. S. Sunderlin, P. B. Armentrout. *J. Am. Chem. Soc.* 111 (1989) 3845.
[9] P. A. M. van Koppen, P. R. Kemper, J. E. Bushnell, M. T. Bowers. *J. Am. Chem. Soc.* 117 (1995) 2098.
[10] Q. Zhang, P. R. Kemper, M. T. Bowers. *Int. J. Mass Spectrom.* 210-211 (2001) 265.
[11] Q. Zhang, P. R. Kemper, S. K. Shin, M. T. Bowers. *Int. J. Mass Spectrom.* 204 (2001) 281.
[12] P. B. Armentrout. *J. Phys. Chem. A* 110 (2006) 8327.
[13] P. B. Armentrout, M. R. Sievers. *J. Phys. Chem. A* 107 (2003) 4396.
[14] Y.-M. Chen, P. B. Armentrout. *J. Phys. Chem.* 99 (1995) 10775.
[15] Y.-M. Chen, P. B. Armentrout. *J. Phys. Chem.* 99 (1995) 11424.
[16] Y.-M. Chen, M. R. Sievers, P. B. Armentrout. *Int. J. Mass Spectrom. Ion Processes* 167-168 (1997) 195.
[17] M. R. Sievers, Y. M. Chen, C. L. Haynes, P. B. Armentrout. *Int. J. Mass Spectrom.* 195-196 (2000) 149.
[18] K. K. Irikura, J. L. Beauchamp. *J. Am. Chem. Soc.* 111 (1989) 75.
[19] K. K. Irikura, J. L. Beauchamp. *J. Am. Chem. Soc.* 113 (1991) 2769.
[20] K. K. Irikura, J. L. Beauchamp. *J. Phys. Chem.* 95 (1991) 8344.
[21] F. X. Li, P. B. Armentrout. *J. Chem. Phys.* 125 (2006) 133114.
[22] F.-X. Li, X.-G. Zhang, P. B. Armentrout. *Int. J. Mass Spectrom.* 255-256 (2006) 279.
[23] Z. M. Loh, R. L. Wilson, D. A. Wild, E. J. Bieske, M. S. Gordon. *Aust. J. Chem.* 57 (2004) 1157.
[24] Z. M. Loh, R. L. Wilson, D. A. Wild, E. J. Bieske, J. M. Lisy, B. Njegic, M. S. Gordon. *J. Phys. Chem. A* 110 (2006) 13736.
[25] D. A. Wild, Z. M. Loh, E. J. Bieske. *Int. J. Mass Spectrom.* 220 (2002) 273.
[26] Z. M. Loh, R. L. Wilson, D. A. Wild, E. J. Bieske, M. S. Gordon. *J. Phys. Chem. A* 109 (2005) 8481.
[27] D. A. Wild, Z. M. Loh, P. P. Wolynec, P. S. Weiser, E. J. Bieske. *Chem. Phys. Lett.* 332 (2000) 531.
[28] B. L. J. Poad, C. D. Thompson, E. J. Bieske. *Chem. Phys.* 346 (2008) 176.
[29] V. Dryza, E. J. Bieske. *Int. J. Mass Spectrom.* 297 (2010) 46.
[30] O. Rodriguez Jr, J. M. Lisy. *Chem. Phys. Lett.* 502 (2011) 145.
[31] Y. C. Cheng, J. Chen, L. N. Ding, T. H. Wong, P. D. Kleiber, D. K. Liu. *J. Chem. Phys.* 104 (1996) 6452.
[32] J. Chen, Y. C. Cheng, P. D. Kleiber. *J. Chem. Phys.* 106 (1996) 3884.
[33] P. Atkins, J. de Paula, *Physical Chemistry*, W.H. Freeman and Co, New York, 2002.

[34] S. K. Shukla. *Chromatographia* 6 (1973) 371.
[35] M. T. Benson, T. R. Cundari, E. W. Moody. *J. Organomet. Chem.* 504 (1995) 1.
[36] V. D. Makhaev. *Russ. Chem. Rev.* 72 (2003) 257.
[37] G. N. Patwari, J. M. Lisy. *J. Phys. Chem. A* 111 (2007) 7585.
[38] R. H. Staley, J. L. Beauchamp. *J. Am. Chem. Soc.* 97 (1975) 5920.
[39] D. J. Miller, J. M. Lisy. *J. Am. Chem. Soc.* 130 (2008) 15393.
[40] W. Eastes, U. Ross, J. P. Toennies. *J. Chem. Phys.* 70 (1979) 1652.
[41] M. A. Duncan. *Int. Rev. Phys. Chem.* 22 (2003) 407.
[42] T. D. Vaden, B. Forinash, J. M. Lisy. *J. Chem. Phys.* 117 (2002) 4628.
[43] D. J. Miller, J. M. Lisy. *J. Am. Chem. Soc.* 130 (2008) 15381.
[44] C. E. Klots. *J. Chem. Phys.* 83 (1985) 5854.
[45] Origin (OriginLab, Northampton, MA), 2003.
[46] J. Kong, C. A. White, A. I. Krylov, C. D. Sherrill, R. D. Adamson, T. R. Furlani, M. S. Lee, A. M. Lee, S. R. Gwaltney, T. R. Adams et al., SPARTAN'02, Wavefunction, Inc., Irvine CA, 2002.
[47] M. J. Frisch, G. W. Trucks, H. B. Schlegel, G. E. Scuseria, M. A. Robb, J. R. Cheeseman, J. A. Montgomery Jr., T. Vreven, K. N. Kudin, J. C. Burant et al., Gaussian 03, Revision B.04, Gaussian, Inc., Pittsburgh, PA, 2003.
[48] D. R. Lidle, *CRC Handbook of Chemistry and Physics*, Boca Raton, 2009.
[49] G. E. Froudakis, S. C. Farantos, M. Velegrakis. *Chem. Phys.* 258 (2000) 13.
[50] J. J. Szymczak, K. T. Giju, S. Roszak, J. Leszczynski. *J. Phys. Chem. A* 108 (2004) 6570.
[51] P. Polak-Dingels, M. S. Rajan, E. A. Gislason. *J. Chem. Phys.* 77 (1982) 3983.
[52] J. P. Beck, J. M. Lisy. *J. Phys. Chem. A* 114 (2010) 10011.
[53] A. L. Nicely, D. J. Miller, J. M. Lisy. *J. Am. Chem. Soc.* 131 (2009) 6314.
[54] A. L. Nicely, D. J. Miller, J. M. Lisy. *J. Mol. Spectrosc.* 257 (2009) 157.
[55] J. D. Rodriguez, J. M. Lisy. *Int. J. Mass Spectrom.* 283 (2009) 135.

Chapter 4

IRPD Spectroscopy of $Li^+(CH_4)_n$, n=1-9, Clusters[1]

4.1 Introduction

The lithium cation has the smallest ionic radius [1] of the alkali metals and correspondingly the highest charge density. [2] This can result in strong ion•••ligand interactions that can significantly perturb the molecular properties of those ligands. For instance, spectral shifts of ~100 cm^{-1} have been reported for the C-H stretches of $Li^+(C_6H_{12})_1Ar$. [3] These strong electrostatic interactions make Li^+ a prime candidate to test long range interactions, or perturbations beyond the first solvent shell.

Mass selective-gas phase spectroscopy is an excellent way to study ion•••ligand interactions in small clusters, while eliminating counter ion and bulk solvent effects. Duncan and co-workers have extensively reported on $M^+(CO_2)_n$ clusters, where M=Al [4], Fe [5], Mg [6], Ni [7,8], and V [9]. In each case, second solvent shell ligands were characterized by a vibrational feature essentially unshifted from the asymmetric stretch of neutral CO_2 and were labeled as "surface molecules". Furthermore, as more CO_2 ligands were added, new features were observed to slightly higher frequency from the asymmetric stretch of CO_2 and were assigned as "caged molecules", i.e. molecules in the second shell interacting with outer shell molecules. This suggested that there were spectroscopically observable ligand•••ligand interactions between CO_2 molecules in different solvent shells.

[1] This Chapter is reproduced in part and reprinted with permission from Oscar Rodriguez Jr. and James M. Lisy. *Chemical Physics Letters*. 2011, 502, pp. 145-149.

Considerable attention in our group has focused on the gas phase hydration of alkali metal cations. [10,11] However, understanding the effect of the ion on water ligands occupying the second solvent shell is challenging because of the strong hydrogen bond interactions between the first and second solvent shell waters. This intermolecular interaction can be reduced or eliminated by using ligands with weak pairwise interactions. Such considerations led us to non-polar methane, CH_4, as an ideal species for this project. The CH_4 dimer interaction energy is reported to be ~1.86 kJ/mol based on various calculations [12], while the enthalpy of vaporization, $\Delta_{vap}H$, is 8.18 kJ/mol [1] These values provide some estimate for an approximate CH_4 binding energy in large $Li^+(CH_4)_n$ cluster ions. Furthermore, the first solvent shell for Li^+ is anticipated to be small making the study of second shell occupation feasible.

Because of its convenient size for experimental and computational studies, both neutral and charged CH_4-bearing complexes have been studied. [13-28] For the solvated halides, $X^-(CH_4)_n$, X = F [25,27,29], Cl [25,26,28], and Br [29], the anion lifts the spherical symmetry of CH_4 and gives rise to infrared features shifted to lower frequencies for both ν_1 and ν_3 vibrational modes associated with the C−H stretch. The minimum energy configurations reported all contain a localized C_{3v} symmetry for CH_4 with an η_1 binding configuration and an anionic hydrogen bond, i.e. X^-•••H-CH_3.

In two studies most closely related to this work, Beiske and co-workers reported the infrared spectra in the C−H stretching region for $M^+(CH_4)_n$, M=Al and Mn; n=1-6, clusters [30,31]. For these cations, the η_3 binding configuration was preferred where the ion interacts with three C-H groups at the face of the CH_4 tetrahedron, while the remaining C-H points away from the ion. While the binding interaction is different, the

localized CH_4 symmetry reduction is similar to the halide-$(CH_4)_n$ clusters, from T_d to C_{3v} symmetry, which lends infrared activity in the nominally IR inactive (Raman active) totally symmetric stretch, ν_1, now involving the three C-H groups facing the ion and induces a shift to lower frequency of bands corresponding to the ν_1 and ν_3 vibrational modes. There have been no observations reported of second solvent shell CH_4 for either cations or anions.

In this study, we wish to probe the electrostatic effects of Li^+ on CH_4 in the first and second solvent shells, and to gauge whether intershell CH_4•••CH_4 interactions influence the vibrational spectra. These systems can then serve as simple models for relatively weak ion•••hydrocarbon interactions as those associated in methane clathrates [32-37] and Hofmeister ion effects in biochemical systems containing hydrophobes. [38-40]

4.2 Experimental Methods

$Li^+ (CH_4)_{1-9}$ cluster ions were studied via tandem mass spectrometry with a triple quadrupole apparatus and infrared predissociation spectroscopy. Details of the experimental apparatus are described elsewhere. [11] Briefly, 0.7-2.5% CH_4 in argon is introduced into the source chamber through a 30º conical nozzle (180 μm diameter) at backing pressures of 500-600 torr and undergoes a continuous supersonic expansion to form neutral clusters. Li^+ is generated by thermionic emission from a tungsten filament coated by a lithium halide based paste. The ion beam, perpendicular to the neutral beam, intercepts the neutral CH_4/Ar clusters about 100 nozzle diameters downstream, imparting significant energy by collision and subsequent solvation to form hot, unstable cluster

ions. These nascent cluster ions stabilize through evaporative cooling, rapidly lowering the internal energy and thus the effective temperature [41] of the cluster ions.

Following formation, cluster ions pass through a 1 mm diameter skimmer and are guided through a differentially pumped chamber and into the detection chamber. Here, the cluster ion of interest is mass selected by the first quadrupole mass filter, then guided through the second (r.f. only) quadrupole where interaction with a pulsed tunable infrared laser occurs (Laservision OPO/OPA pumped by a 1064 nm output of a Surelite II 10 Hz Continuum Nd:YAG laser). If the laser is resonant with a cluster vibrational mode, absorption of a photon can occur. The photon energy is then dissipated in the cluster leading to vibrational predissociation. Following dissociation, the fragment ions are mass selected in a third quadrupole and subsequently detected using a conversion dynode and a channeltron electron multiplier. A spectrum is recorded by stepping the laser in 3 cm^{-1} increments over the region of interest (in this case from 2800-3100 cm^{-1}) and reporting the photodissociation cross section (the fraction of dissociation corrected for laser fluence) as a function of frequency. Features in each spectra are fitted using Origin 7.5 [42] to obtain vibrational frequencies and integrated photodissociation cross sections of the bands. Absolute frequency calibration is accomplished by simultaneously recording the IR spectrum of CH_4 or HCl in a reference gas cell.

The reported Li^+•••CH_4 binding energy is 0.38 eV (36.66 kJ/mol) [43], near the photon energies (33.48-37.07 kJ/mol) of the C−H stretching region. The Li^+···Ar dimer interaction is ~30 kJ/mol [44] and even lower (<20 kJ/mol) when other ligands are present. [45,46] Therefore the argon-tagging technique was used to efficiently detect photodissociation [45,47] for $Li^+(CH_4)_nAr_m$, n=1-4, cluster ions, where different numbers

of argon atoms were used to optimize the photodissociation spectra. For consistency only the spectra of mono-argonated species, m=1, are reported here. Direct photodissociation of $Li^+(CH_4)_n$ was observed starting at n=3. The low binding energy of CH_4 in larger clusters, n>5, can result in multiple ligand loss upon absorption of an IR photon, thus the specific fragment channel monitored for the photodissociation spectrum of a given cluster ion is identified (*vide infra*).

4.3 Computational Methods

To better characterize the experimental results, density functional theory (DFT) calculations were carried out at the B3LYP/6-31+G* level. Initial minimum energy geometries were obtained using SPARTAN 02 [48] and vibrational frequencies were calculated using GAUSSIAN 03 [49] software. The calculated frequencies were scaled by 0.9576, the factor to fit the calculated CH_4 vibrational frequencies to the reported experimental gas phase values. Zero-point binding energies were calculated at the MP2/6-31+G* level.

4.4 Results and Discussion

For $Li^+(CH_4)_n$ clusters, an η_3 binding configuration is predicted in the DFT calculations and is consistent with the study of $M^+(CH_4)_{1\text{-}6}$, M=Al and Mn, reported by Bieske and co-workers. [30,31] This results in the lowering of the localized CH_4 symmetry from T_d to C_{3v} symmetry. Under these conditions, the IR inactive (Raman active) totally symmetric C−H stretching mode, ν_1, at 2917 cm^{-1} [50] now correlates to an IR active symmetric stretch and is shifted to lower frequency. The triply degenerate IR active C−H stretching mode, ν_3, at 3019 cm^{-1} [50] is split into two modes, a doubly

degenerate (perpendicular transition) C−H stretch, ν_3(e), shifted to lower frequency and a weak symmetric stretch, $\nu_3(a_1)$, of the lone C−H oscillator pointing away from the ion shifted to higher frequency. A full spectral summary of the $Li^+(CH_4)_{1\text{-}9}$ series is reported in Figure 4.1. The neutral CH_4 gas phase values, ν_1 and ν_3, are indicated by the labeled lines. Experimental and calculated vibrational frequencies are included in Table 4.1 while the frequency shifts and zero-point binding energies for CH_4 and argon ligands are reported in Table 4.2.

Spectra of the smallest argonated clusters, $Li^+(CH_4)_nAr_1$, n=1-4, are shown in Figure 4.2. For n=1, the now IR active symmetric stretch, ν_1, is the prominent feature observed at 2859 cm^{-1}, while the broad ν_3(e) mode is weakly observed above background near 2965 cm^{-1}. The significant binding energy (see Table 4.2) of both argon and methane in this cluster allows considerable internal energy to be retained, leading to the breadth of both bands. For n=2-4, the gradual shift to higher frequency of these features indicates that the added CH_4 ligands compete for interaction with the ion, weakening the individual Li^+•••CH_4 interactions. Interestingly, calculations predict a dramatic decline in binding energy for the argon atom from n=3 to n=4, 14.63 kJ/mol to 4.26 kJ/mol respectively (see Table 4.2), and place the argon in a second solvent shell for n=4, where one would expect it to be more weakly bound. This would suggest a Li^+ coordination number of four in methanated clusters and will be discussed further in the next section.

The summary for $Li^+(CH_4)_n$, n=5-9 is shown in Figure 4.3. The neutral CH_4 gas phase values, ν_1 and ν_3, are indicated by the labeled lines. For better comparison, all the spectra are scaled so that each band at 2880 cm^{-1} is equal in intensity.

The bands for n=5-9 centered at ~2880 cm^{-1} represent the perturbed ν_1 modes for first shell CH_4 ligands and are unshifted from the ν_1 band frequency from n=4. However, a new band located at ~2909 cm^{-1} grows in intensity relative to the 2880 cm^{-1} band with increasing CH_4. This suggests that the additional methanes are more weakly perturbed by the ion and their respective ν_1 bands are not as strongly shifted to lower frequency as compared to the ν_1 band for first shell CH_4. This is consistent with occupation of the second solvent shell starting at n=5 (and noted in the case of $Li^+(CH_4)_4Ar_1$). This is the first report of second shell occupation in the solvation of an ion by methane; bands were not observed for $M^+(CH_4)_{1\text{-}6}$, M=Al [30] and Mn [31], or $X^-(CH_4)_n$, X = F [27] and Cl [26].

Supporting *ab initio* calculations confirm that solvation of Li^+ by methane has a first solvent shell size of four, with subsequent methanes entering the second shell. Stable 5-coordinated $Li^+(CH_4)_5$ structures (i.e. all ligands in the first shell) were not found. Predicted vibrational frequencies (see Table 4.1) for the ν_1 band further support this assignment in two ways. First, the calculated frequency of the ν_1 band for the first shell CH_4 is essentially unchanged for n=4-9, a result reproduced by experiment, which also indicates minimal interaction between the first and second shell ligands. Second, the modest shift of 8-10 cm^{-1} of the second shell ν_1 feature, from the neutral gas phase value, demonstrates that the electrostatic effect of the ion on the second shell ligands is reduced. This is unlike the cases of $M^+(CO_2)_n$ clusters (M=Al [4], Fe [5], Mg [6], Ni [7,8], and V [9]). For these systems the asymmetric stretch band of second shell CO_2 ligands appeared to be nearly unshifted from the neutral gas-phase values. In contrast, bands from "caged molecules" suggested interactions between ligands in the second and third shells.

At higher frequency for n=5-9, the ν_3(e) mode due to CH_4 in first shell is clearly observed around ~2983 cm^{-1}, again unshifted compared to the same feature in $Li^+(CH_4)_4Ar_1$. There is a clear broadening to higher frequency for n=5 which becomes more clearly resolved for n=6-9. The features centered about ~3005 cm^{-1} and ~3021 cm^{-1} represent the ν_3(e) and $\nu_3(a_1)$ modes for second shell CH_4 ligands. These inferences are well supported by the *ab initio* calculations in Table 4.1, where the agreement between the calculated and experimental frequencies of these modes is excellent.

In addition to the difference in frequency shifts between first and second shell CH_4, there is a substantial change in the relative photodissociation cross-sections of the ν_1 versus ν_3(e) and $\nu_3(a_1)$ modes that clearly demonstrates the differences in the ion•••ligand interactions for methanes in the two solvent shells. For the strongly perturbed ligands in the first shell, the enhancement of the ν_1 mode (a parallel transition) makes this feature more intense than the IR-allowed ν_3(e) mode (perpendicular transition). To help illustrate this, we report the ratio of the integrated IRPD cross sections for the ν_3(e) band versus ν_1 band in Table 4.3. The data for bands associated with first shell CH_4 are plotted in Figure 4.4a. The ν_3(e) versus ν_1 band intensity ratio increases linearly as the ν_3(e) band gains intensity with additional CH_4. As the solvent shell fills, the electrostatic influence of the ion on each methane decreases and this is reflected by the decrease in the intensity of the ν_1 band, relative to the ν_3 band. Once the first shell is filled, the ν_3(e) versus ν_1 band intensity ratio is essentially constant. The ratios are based on spectra using the optimal photodissociation loss channel for the given cluster ion. Fragmentation to other CH_4 loss channels is possible since large $Li^+(CH_4)_n$ clusters can lose multiple ligands upon IR absorption. However over this narrow frequency range, we expect the integrated

photodissociation cross-sections to be proportional to the IR absorption intensity, so the presence of other loss channels should not affect the ratios. For the second shell methanes, the intensity of the ν_1 and ν_3 bands are significantly different from the first shell as seen in Figure 4.4b. The weakening of the electrostatic interaction deprives the ν_1 band of intensity. As this occurs, the intensities of the $\nu_3(e)$ and $\nu_3(a_1)$ do not decrease. As can be seen in the integrated IRPD cross section ratio of the ν_3 band versus ν_1 band for second shell ligands (in Table 4.3), this ratio sharply increases to between 2.34 - 3.22, another clear indication of the different environments experienced by methanes in the first and second shells. The n=5 data were not used in this analysis, due to weak intensity of the second shell ν_1 band and difficulties in deconvoluting the ν_3 portion of the spectrum into first and second shell contributions.

The weak ion•••second shell CH_4 interactions are further characterized by the substantial drop in binding energy of CH_4 (see Table 4.2). Binding energies of 5.42 kJ/mol, 5.65 kJ/mol, 5.51 kJ/mol, 6.56 kJ/mol, and 5.21 kJ/mol are calculated for n=5-9 respectively. These predicted values are slightly less than to the enthalpy of vaporization for CH_4, 8.18 kJ/mol. [1] The low binding energy of CH_4 allows for easy photofragmentation with the loss of multiple methanes, thus, no argon tagging was necessary for larger clusters. Structurally, a tetrahedral configuration in the first solvent shell is preferred. Each subsequent second shell CH_4 ligand then binds to a face of the tetrahedral; minimizing the ion•••second shell CH_4 distance until each face is occupied. This could have a stabilizing effect on the n=8 cluster, which has a slightly higher binding energy relative to the n=7 and 9 species.

4.5. Conclusions

The infrared spectra of $Li^+(CH_4)_n$, n=1-9, clusters were reported. Due to the strong interaction with Li^+, the nominally IR-inactive, Raman-active ν_1 symmetric mode of CH_4 becomes IR active and shifts to lower frequency. The triply degenerate ν_3 mode is split into two modes, $\nu_3(e)$, which is also shifted to lower frequency and a weak $\nu_3(a_1)$, which is only observed for weakly interacting second shell ligands. The first solvent shell of Li^+ is observed to fill with four CH_4, and occupation of a spectrally distinct CH_4 second shell is reported for the first time.

The second CH_4 shell was associated with the ν_1 and ν_3 modes at frequencies between those for first shell methanes and gas phase, neutral CH_4. All IRPD features originating from first and second shell ligands for n=5-9 show no significant shifts in frequency. This consistency strongly suggests little or no perturbing interactions between the first and second shell CH_4 ligands. Also, the small shifts in second shell features from the neutral gas phase values indicate a weakened perturbation by the ion beyond the first solvent shell. The intensity of the ν_1 mode is also a fairly sensitive measure of the electrostatic influence of the ion on the methane. In the second solvent shell, the intensity of the ν_1 band relative to the slightly perturbed $\nu_3(e)$ and $\nu_3(a_1)$ modes was found to dramatically decrease, confirming the electrostatic interaction of the Li^+ on the second shell CH_4 is substantially reduced.

This report lays the ground work for characterizing weak ion•••hydrocarbon interactions. We are currently studying the alkali metal ion series to compare solvent shell sizes and the electrostatic effects of these ions on methane. By including water molecules into the clusters we can probe ion•••water•••hydrophobe interactions to model

the initiation of methane clathrate formation in natural seawater or physiological hydrophilic-hydrophobic interactions occurring in biochemistry.

4.6 Figures and Tables

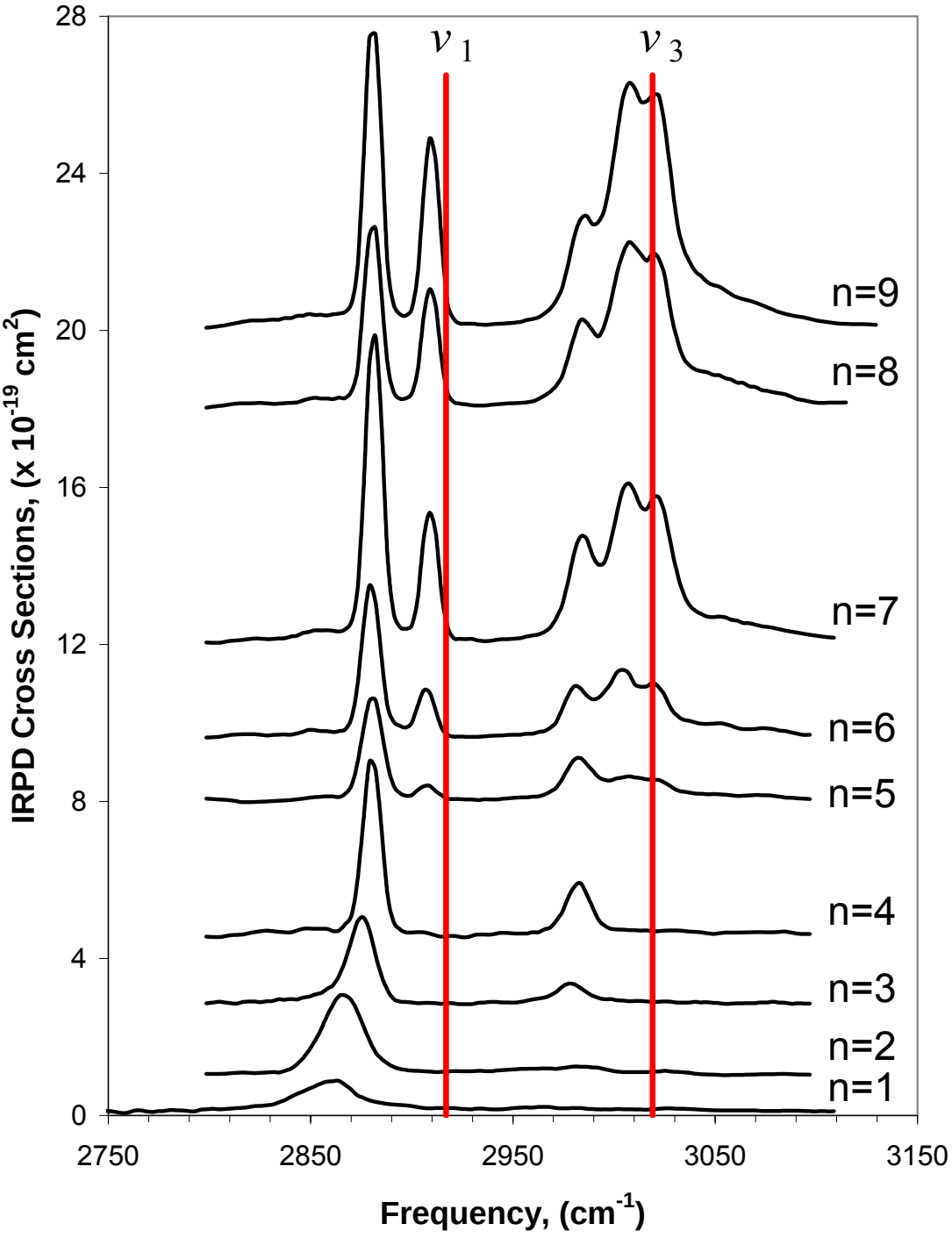

Figure 4.1. Full infrared predissociation (IRPD) summary of $Li^+(CH_4)_{1\text{-}9}$. In this series n=1-4 are singly-argonated, $Li^+(CH_4)_{1\text{-}4}Ar_1$, although efficient fragmentation was observed as early as n=3 for non-argonated species. New features beginning at n=5 indicate the onset of a second solvent shell.

Table 4.1
Experimental and B3LYP/6-31+G* calculated frequencies, (cm^{-1}).

	Exp	Calc	Exp	Calc	Exp	Calc	Exp	Calc	Exp	Calc
	1° ν_1	1° ν_1	2° ν_1	2° ν_1	1° ν_3(e)	1° ν_3(e)	2° ν_3(e)	2° ν_3(e)	2° $\nu_3(a_1)$	2° $\nu_3(a_1)$
$Li^+(CH_4)_1Ar_1$	2859	2858	-	-	2965	2962	-	-	-	-
$Li^+(CH_4)_2Ar_1$	2866	2867	-	-	2973	2973	-	-	-	-
$Li^+(CH_4)_3Ar_1$	2875	2880	-	-	2979	2987	-	-	-	-
$Li^+(CH_4)_4Ar_1$	2880	2885	-	-	2982	2994	-	-	-	-
$Li^+(CH_4)_5$	2880	2885	2907	2908	2981	2997	3003	3008	-	-
$Li^+(CH_4)_6$	2879	2886	2907	2910	2981	2996	3003	3007	3021	3026
$Li^+(CH_4)_7$	2881	2886	2909	2910	2984	2996	3006	3007	3022	3027
$Li^+(CH_4)_8$	2880	2886	2909	2910	2983	2998	3006	3007	3022	3027
$Li^+(CH_4)_9$	2880	2886	2909	2910	2984	2998	3005	3008	3020	3027

1° and 2° represent first shell and second shell ligands respectively. The $\nu_3(a_1)$ modes for first shell ligands are barely observed above background and are not included in the table.

Table 4.2
Magnitude of frequency shift for each observed vibrational mode (cm^{-1}) relative to the gas-phase value; CH_4 and Ar binding energies; D_o, (kJ/mol), and loss channel monitored.

	1° Δv_1	2° Δv_1	1° Δv_3(e)	2° Δv_3(e)	2° Δv_3(a_1)	D_o (CH_4)	D_o (Ar)	Channel
$Li^+(CH_4)_1Ar_1$	-58	-	-54	-	-	44.21	25.24	Ar
$Li^+(CH_4)_2Ar_1$	-51	-	-46	-	-	35.03	17.29	Ar
$Li^+(CH_4)_3Ar_1$	-42	-	-40	-	-	27.63	14.63	Ar
$Li^+(CH_4)_4Ar_1$	-37	-	-37	-	-	23.35*	4.26	Ar + CH_4
$Li^+(CH_4)_5$	-37	-10	-38	-16	-	5.42	-	2 CH_4
$Li^+(CH_4)_6$	-38	-10	-38	-16	+2	5.65	-	2 CH_4
$Li^+(CH_4)_7$	-36	-8	-35	-13	+3	5.51	-	3 CH_4
$Li^+(CH_4)_8$	-37	-8	-36	-13	+3	6.56	-	4 CH_4
$Li^+(CH_4)_9$	-37	-8	-35	-14	+1	5.21	-	4 CH_4

Magnitude of frequency shift determined from comparing the experimental observed fitted peaks to the neutral gas phase CH_4 v_1 and v_3 modes. 1° and 2° represent first shell and second shell ligands respectively. The binding energy for $Li^+(CH_4)_4Ar_1$, labeled (*), represents the approximated binding energy of a CH_4 in the $Li^+(CH_4)_4$ cluster assuming that the second shell argon atom does not affect first shell interactions.

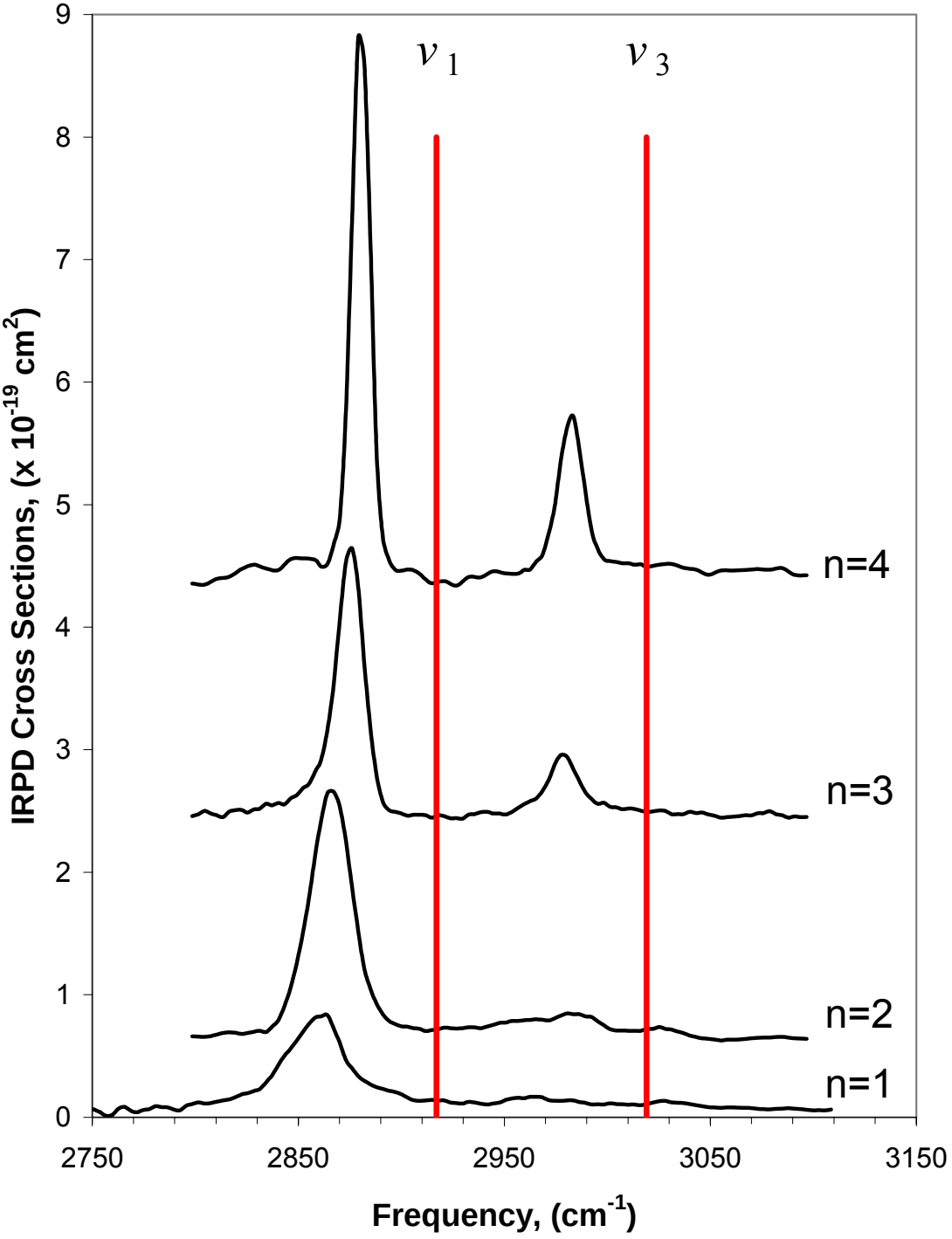

Figure 4.2. IRPD summary for $Li^+(CH_4)_nAr_1$, n=1-4.

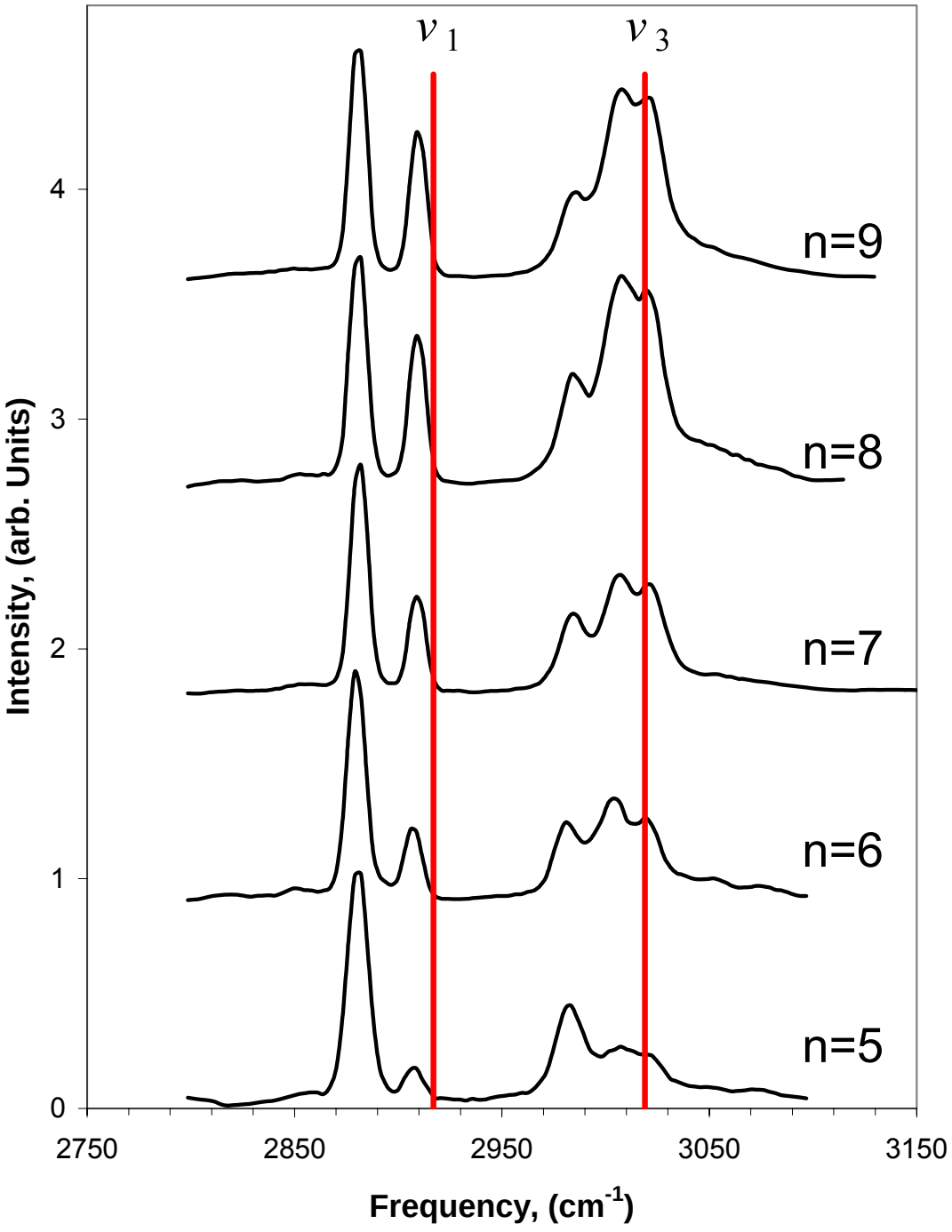

Figure 4.3. IRPD summary for $Li^+(CH_4)_n$, n=5-9. The spectra for n=6-9 are scaled so that each band at 2880 cm^{-1} are equal in intensity for comparison. The second solvent shell is first observed at n=5 as indicated by the bands near the neutral CH_4 ν_1 and ν_3 values (red lines). Each band is unshifted in the series indicating minimal CH_4•••CH_4 interactions.

Table 4.3
Intensity ratio of ν_3(e) bands versus ν_1 bands.

n	First Shell Ligands $I(\nu_3(e))/I(\nu_1)$ (±1σ)	Second Shell Ligands $I(\nu_3(e))/I(\nu_1)$ (±1σ)
1	0.16 (0.04)	–
2	0.25 (0.04)	–
3	0.35 (0.03)	–
4	0.40 (0.03)	–
6	0.38 (0.05)	3.07 (0.47)
7	0.41 (0.04)	2.34 (0.26)
8	0.46 (0.05)	3.21 (0.28)
9	0.37 (0.06)	2.64 (0.28)

Each band for n=5-9 was fit with a Lorentzian line shape and the integrated IRPD cross section was obtained and used for the intensity calculations. Using these values, the intensity ratio of ν_3(e) versus ν_1 was calculated for first shell and second shell ligands.

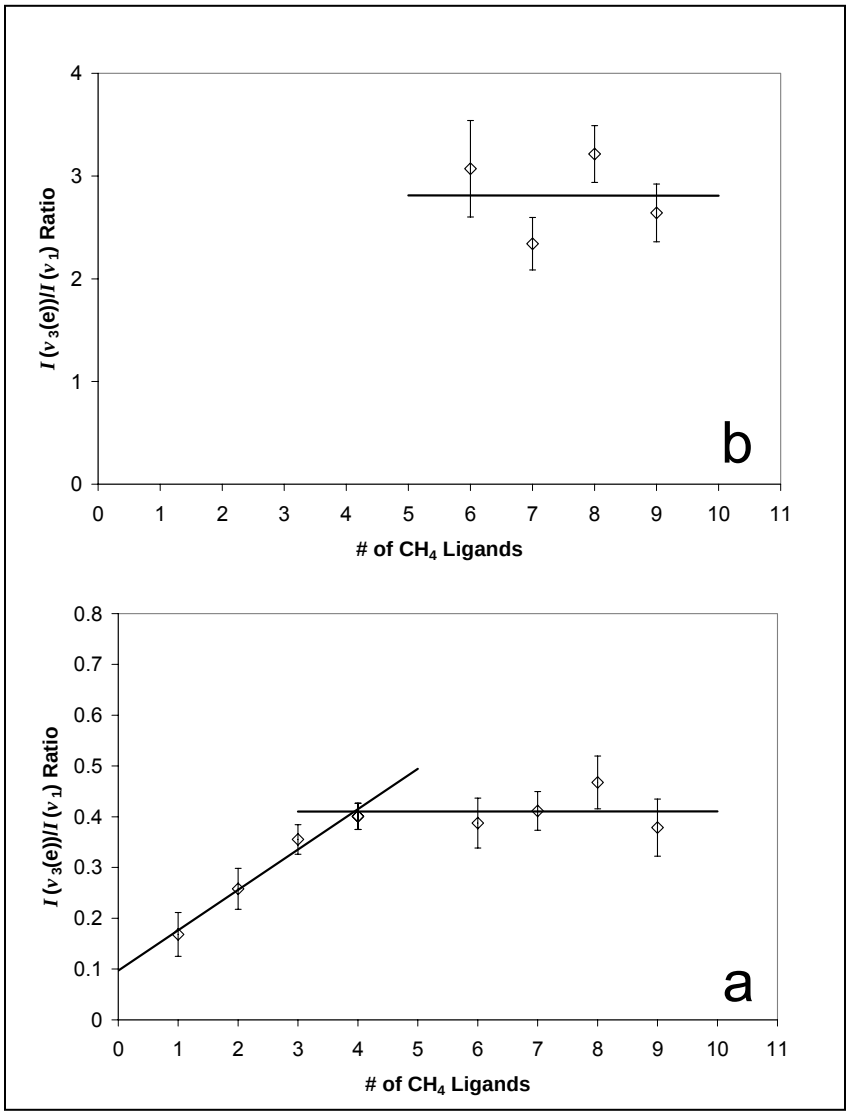

Figure 4.4. Intensity ratio of ν_3(e) versus ν_1 for bands associated with first shell CH_4 (a) and second shell CH_4 (b).

4.7 References

[1] P. Atkins, J. de Paula, Physical Chemistry, W.H. Freeman and Co, New York, 2002.
[2] S. K. Shukla. *Chromatographia* 6 (1973) 371.
[3] G. N. Patwari, J. M. Lisy. *J. Phys. Chem. A* 111 (2007) 7585.
[4] R. S. Walters, N. R. Brinkmann, H. F. Schaefer, M. A. Duncan. *J. Phys. Chem. A* 107 (2003) 7396.
[5] G. Gregoire, M. A. Duncan. *J. Chem. Phys.* 117 (2002) 2120.
[6] G. Gregoire, N. R. Brinkmann, D. van Heijnsbergen, H. F. Schaefer, M. A. Duncan. *J. Phys. Chem. A 107* (2003) 218.
[7] N. R. Walker, G. A. Grieves, R. S. Walters, M. A. Duncan. *Chem. Phys. Lett.* 380 (2003) 230.
[8] N. R. Walker, R. S. Walters, G. A. Grieves, M. A. Duncan. *J. Chem. Phys.* 121 (2004) 10498.
[9] N. R. Walker, R. S. Walters, M. A. Duncan. *J. Chem. Phys*. 120 (2004) 10037.
[10] D. J. Miller, J. M. Lisy. *J. Am. Chem. Soc.* 130 (2008) 15393.
[11] D. J. Miller, J. M. Lisy. *J. Am. Chem. Soc.* 130 (2008) 15381.
[12] L. Ferrighi, G. K. H. Madsen, B. Hammer. *Chem. Phys. Lett.* 492 (2010) 183.
[13] M. Geleijns, N. Halberstadt, J. Millan, P. E. S. Wormer, A. Van der Avoird. *Faraday Discuss.* 118 (2001) 143.
[14] M. Geleijns, A. Van Der Avoird, P. E. S. Wormer, N. Halberstadt. *J. Chem. Phys.* 117 (2002) 7562.
[15] T. G. A. Heijmen, P. E. S. Wormer, A. Van Der Avoird, R. E. Miller, R. Moszynski. *J. Chem. Phys.* 110 (1999) 5639.
[16] R. E. Miller, T. G. A. Heijmen, P. E. S. Wormer, A. Van Der Avoird, R. Moszynski. *J. Chem. Phys.* 110 (1999) 5651.
[17] M. Wangler, D. A. Roth, I. Pak, G. Winnewisser, P. E. S. Wormer, A. Van der Avoird. *J. Mol. Spectrosc.* 222 (2003) 109.
[18] J. Chen, Y. C. Cheng, P. D. Kleiber. *J. Chem. Phys.* 106 (1996) 3884.
[19] Y. C. Cheng, J. Chen, L. N. Ding, T. H. Wong, P. D. Kleiber, D. K. Liu. *J. Chem. Phys.* 104 (1996) 6452.
[20] K. K. Irikura, J. L. Beauchamp. *J. Am. Chem. Soc.* 113 (1991) 2769.
[21] K. K. Irikura, J. L. Beauchamp. *J. Phys. Chem.* 95 (1991) 8344.
[22] F. X. Li, P. B. Armentrout. *J. Chem. Phys*. 125 (2006) 133114.
[23] F.-X. Li, X.-G. Zhang, P. B. Armentrout. *Int. J. Mass Spectrom.* 255-256 (2006) 279.
[24] F. Liu, X. G. Zhang, R. Liyanage, P. B. Armentrout. *J. Chem. Phys.* 121 (2004) 10976.
[25] Z. M. Loh, R. L. Wilson, D. A. Wild, E. J. Bieske, M. S. Gordon. *Aust. J. Chem*. 57 (2004) 1157.
[26] Z. M. Loh, R. L. Wilson, D. A. Wild, E. J. Bieske, M. S. Gordon. *J. Phys. Chem. A* 109 (2005) 8481.
[27] Z. M. Loh, R. L. Wilson, D. A. Wild, E. J. Bieske, J. M. Lisy, B. Njegic, M. S. Gordon. *J. Phys. Chem. A* 110 (2006) 13736.
[28] D. A. Wild, Z. M. Loh, P. P. Wolynec, P. S. Weiser, E. J. Bieske. *Chem. Phys. Lett.* 332 (2000) 531.

[29] D. A. Wild, Z. M. Loh, E. J. Bieske. *Int. J. Mass Spectrom.* 220 (2002) 273.
[30] B. L. J. Poad, C. D. Thompson, E. J. Bieske. *Chem. Phys.* 346 (2008) 176.
[31] V. Dryza, E. J. Bieske. *Int. J. Mass Spectrom.* 297 (2010) 46.
[32] Q. Chen, C. Liu, Y. Ye. J. *Nat. Gas Chem.* 18 (2009) 217.
[33] G. R. Dickens, M. S. Quinby-Hunt. *Geophys. Res. Lett.* 21 (1994) 2115.
[34] G. R. Dickens, M. S. Quinby-Hunt. *J. Geophys. Res*., B 102 (1997) 773.
[35] H. Sato, T. Tsuji, T. Nakamura, K. Uesugi, T. Kinoshita, M. Takahashi, H. Mimachi, T. Iwasaki, K. Ohgaki. *Int. J. Chem. Eng.* 2009 (2009) 1.
[36] P. Tishchenko, C. Hensen, K. Wallmann, C. S. Wong. *Chem. Geol.* 219 (2005) 37.
[37] S. H. Yeon, J. Seol, Y. Seo, Y. Park, D. Koh, K. Park, D. Huh, J. Lee, H. Lee. *J. Phys. Chem. B* 113 (2009) 1245.
[38] B. Hribar, N. T. Southall, V. Vlachy, K. A. Dill. *J. Am. Chem. Soc.* 124 (2002) 12302.
[39] L. M. Pegram, M. T. Record Jr. *J. Phys. Chem. B* 112 (2008) 9428.
[40] D. J. Tobias, J. C. Hemminger. *Science* 319 (2008) 1197.
[41] C. E. Klots. *J. Chem. Phys.* 83 (1985) 5854.
[42] Origin (OriginLab, Northampton, MA),
[43] W. Eastes, U. Ross, J. P. Toennies. *J. Chem. Phys.* 70 (1979) 1652.
[44] P. Polak-Dingels, M. S. Rajan, E. A. Gislason. *J. Chem. Phys.* 77 (1982) 3983.
[45] T. D. Vaden, B. Forinash, J. M. Lisy. *J. Chem. Phys.* 117 (2002) 4628.
[46] T. D. Vaden, J. M. Lisy, P. D. Carnegie, E. Dinesh Pillai, M. A. Duncan. *Phys. Chem. Chem. Phys.* 8 (2006) 3078.
[47] M. A. Duncan. *Int. Rev. Phys. Chem.* 22 (2003) 407.
[48] J. Kong, C. A. White, A. I. Krylov, C. D. Sherrill, R. D. Adamson, T. R. Furlani, M. S. Lee, A. M. Lee, S. R. Gwaltney, T. R. Adams et al., SPARTAN'02, Wavefunction, Inc., Irvine CA, 2002.
[49] M. J. Frisch, G. W. Trucks, H. B. Schlegel, G. E. Scuseria, M. A. Robb, J. R. Cheeseman, J. A. Montgomery Jr., T. Vreven, K. N. Kudin, J. C. Burant et al., Gaussian 03, Revision B.04, Gaussian, Inc., Pittsburgh, PA, 2003.
[50] R. Toth, L. R. Brown, R. H. Hunt, L. S. Rothman. *Appl. Opt.* 20 (1981) 932.

Chapter 5

Methanation of Alkali Metal Ions: Infrared Spectroscopy of $M^+(CH_4)_{1-12}$, M=Na, K, Rb, and Cs, Clusters[1]

5.1 Introduction

In chapter 4 of this Thesis, the infrared predissociation (IRPD) spectra of $Li^+(CH_4)_n$ clusters in the C-H stretching region were reported in order to investigate alkali metal ion•••hydrocarbon interactions.[1] We found that upon interaction with Li^+, the tetrahedral symmetry of CH_4 is lowered to C_{3v}, giving rise to an intense, red-shifted IR band correlating to the totally symmetric ν_1 vibrational mode of CH_4, which is infrared inactive in neutral CH_4.

An advantage of using CH_4 as a solvent is it allows us to directly study long range electrostatic effects, or influence of Li^+ beyond the first solvent shell, because of weak CH_4•••CH_4 pairwise interactions. This is difficult in cluster ions with polar solvent molecules wherein first- and second-shell molecules tend to interact with each other.[2-5] Indeed, new bands in the IRPD spectra of n=5 correspond to less perturbed CH_4 vibrational modes, relative to first shell CH_4 vibrational modes, indicating a coordination number of four.

$Al^+(CH_4)_{1-6}$ [6] and $Mn^+(CH_4)_{1-6}$ [7] clusters have been studied by Bieske and co-workers computationally and using IRPD spectroscopy. For both ions they were able to

[1] This Chapter is reproduced in part from a manuscript in preparation by Oscar Rodriguez Jr. and James M. Lisy.

observe an infrared active, red-shifted, totally symmetric ν_1 band of η_3 configured CH_4 ligands. However, no second solvent shell CH_4 features were observed in their IRPD spectra. Their calculations predict a first solvent shell size of six methanes for both Al^+ and Mn^+.

Bieske and co-workers also reported the solvation of F^- [8] and Cl^- [9] by methane. They found that methane molecules bind to anions via a single hydrogen bond, or η_1 configuration. However, similar to the cation complexes mentioned above, the localized symmetry of CH_4 ligands is C_{3v}. Unfortunately, large enough clusters could not be generated to determine a coordination number for F^- or Cl^- ions.

$M^+(CH_4)_n$ clusters provide the foundation for understanding ion•••hydrocarbon interactions. As we have already reported IRPD spectra $Li^+(CH_4)_n$ clusters, we aim to extend the study of alkali metal ion solvation by CH_4 to Na^+, K^+, Rb^+, and Cs^+ in order to characterize electrostatic effects of alkali metal ions on CH_4 molecules.

5.2 Experimental Methods

$M^+(CH_4)_{1\text{-}12}$ clusters, M= Li, Na, K, Rb, and Cs, are reported using a triple quadrupole mass spectrometer and infrared predissociation spectroscopy. Our experimental details are described elsewhere.[4,5,10] Briefly, 1.0-2.5% CH_4 seeded in argon is introduced into the source chamber through a 30º conical nozzle (180 μm diameter). Neutral cluster form via continuous supersonic expansion. Approximately100 nozzle diameters downstream from the nozzle exit, alkali metal ions of interest, generated by thermionic emission from a homemade ion gun, collide with neutral clusters. The resulting $M^+(CH_4)_n$ cluster ions have significant internal energy from both the collisional

and solvation processes, which exceeds the binding energy of methane to the cluster ion. The nascent cluster ions stabilize by evaporative cooling,[11] dissipating internal energy until a quasistable cluster ion (with a unimolecular lifetime greater than the flight time through the apparatus) is formed. The quasi-stable cluster ions are skimmed into a differential pumping chamber and guided into the first of three quadrupoles where the cluster ion of interest is mass selected. The second quadrupole acts as an ion guide (radio frequency mode only) where the output of a counter propagating tunable pulsed infrared beam (Laservision OPO/OPA pumped by a 1064 nm output of a Surelite II 10 Hz Continuum Nd:YAG laser) is gently focused to overlap with the cluster ion beam. Cluster ions with vibrational modes on resonance with the IR laser can absorb a photon leading to fragmentation of one or more ligands. The fragment cluster ion is then mass selected in the third quadrupole and subsequently detected using a conversion dynode/channeltron electron multiplier.

Infrared spectra are reported by plotting the photodissociation cross section (corrected for laser fluence) as a function of laser frequency. The infrared laser is stepped in 3 cm^{-1} increments over the C-H stretching region (2800 -3100 cm^{-1}). Bands are fit with Lorentzian lineshapes using Origin 7.5.[12]

5.3 Computational Methods

MP2 level, *ab inito* geometry optimization and frequency calculations of $M^+(CH_4)_n$ clusters were carried out to supplement experimental results. Initial structures generated using Spartan 02 [13] were allowed to optimize using Gaussian 03 [14] software to obtain minimum energy geometries. Li^+ and Na^+ cations and carbon and

hydrogen atoms are treated using augmented correlation-consistent all-electron, aug-cc-pVDZ, basis set while K^+, Rb^+, and Cs^+ cations are treated using the Los Alamos double-ζ basis sets with effective core potentials, LANL2DZ.[15-17] Calculated spectra were generated using the SWizard [18] program with calculated CH_4 frequencies scaled by 0.9471 to fit experimental neutral CH_4 gas phase values.

5.4 Results and Discussion

Upon complexation with a cation, methane's tetrahedral symmetry is lowered to C_{3v} symmetry and configured in an η_3 manner.[1,6,7,19] The normally infrared inactive totally symmetric stretch, ν_1, becomes infrared active and shifts to lower frequency from the neutral CH_4 ν_1 value [20], 2917 cm^{-1}. The neutral CH_4 triply degenerate ν_3 mode, 3019 cm^{-1},[20] is split into two weak modes. The first is a doubly degenerate mode corresponding to a perpendicular transition vibrational mode, $\nu_3(e)$, shifted to lower frequency. The second is a weak single mode, $\nu_3(a_1)$, corresponding to the C-H stretch pointing away from the ion, shifted to higher frequency.

IRPD spectra for $Na^+(CH_4)_n$ clusters are shown in Figure 5.1. The dominant band at 2880 cm^{-1} in the n=1 spectrum correlates to the ν_1 totally symmetric stretching mode. This band is ~21 cm^{-1} higher in frequency compared to the same band in the n=1 spectrum of $Li^+(CH_4)_1Ar_1$. This indicates a weaker Na^+•••CH_4 electrostatic interaction compared to Li^+•••CH_4.

As more CH_4 ligands are added, the ν_1 band gradually shifts to 2897 cm^{-1} for n=6 and remains at the same frequency for n=7, 8, and 12. Furthermore, a new band appears at 2912 cm^{-1} starting at n=7, which grows in intensity and exhibits no frequency shifts as

more CH_4 is added. The appearance of this feature coincides with the onset of the second solvent shell at n=7 and confirms a coordination number of six for Na^+ when solvated by methane. The difference in relative IR intensities between the first- and second-shell ν_1 features is noteworthy. Since we were able to determine a coordination number of six, we can safely say that six CH_4 molecules reside

in each solvent shell for n=12; yet their respective ν_1 bands differ in relative intensity. This is because the ion's electrostatic effect is weaker for second shell molecules compared to those in the first shell. As a result, the second shell CH_4 molecule tends toward its neutral, tetrahedral configuration resulting in the ν_1 totally symmetric vibrational mode tending toward IR inactivity, thus losing intensity.

Also, we conclude that there are negligible CH_4•••CH_4 interactions between first- and second-shell CH_4 molecules since no frequency shifts in all ν_1 bands are observed when second shell CH_4 molecules are present. An identical effect was reported in chapter 4 of this Thesis for $Li^+(CH_4)_{5\text{-}9}$ clusters which contained a second solvent shell.[1]

At higher frequency, the ν_3(e) shifts to higher frequency as more CH_4 ligands are added. This corresponds to a weakening Na^+•••CH_4 electrostatic interaction with increasing cluster size. First- and second-shell ν_3(e) bands could not be resolved and only a broad feature centered ~3000 cm^{-1} is observed for n=6-12. Also, a weak shoulder feature corresponding to the $\nu_3(a_1)$ symmetric stretching vibrational mode is first observed in the n=3 spectrum near the 3019 cm^{-1} and becomes prominent with increasing cluster size.

IRPD spectra for selected $K^+(CH_4)_n$ clusters is shown in Figure 5.2. For n=8, 10, and 12, the ν_1, ν_3(e), and $\nu_3(a_1)$ bands are observed near 2900 cm^{-1}, 3000 cm^{-1}, and 3020

cm^{-1} respectively. A weak shoulder feature of the ν_1 band is first observed in the spectrum for n=10 and is more pronounced for n=12. At higher frequency, ν_3(e) bands are relatively broad and features distinguishing first- and second shell-ligands can not be resolved. Therefore, a clear second solvent shell designation can not be made for K^+. See appendix A.1 for other $K^+(CH_4)_n$ spectra.

IRPD summaries for selected $Rb^+(CH_4)_n$ and $Cs^+(CH_4)_n$ clusters are shown together in Figure 5.3 because their trends are similar. For both Rb^+ and Cs^+ cluster ions, the ν_1, ν_3(e), and $\nu_3(a_1)$ bands are all observed at n=2 and are only modestly shifted as more CH_4 molecules are added. For $Rb^+(CH_4)_n$ clusters, a weak shoulder feature appears in the spectrum for n=12, and appears similar to the spectra for large $K^+(CH_4)_n$ clusters described earlier. However, no clear solvent shell size could be determined for either $Rb^+(CH_4)_n$ or $Cs^+(CH_4)_n$.

Next, we will compare non-argonated $M^+(CH_4)_1$ clusters. P and R branches associated with the parallel transition mode appear between 2850 cm^{-1} – 2900 cm^{-1} in the IRPD spectra shown in Figure 5.4. This is useful because by approximating a M^+•••CH_4 as a pseudo-diatomic complex, an average cluster temperature can be estimated by using the equation $\Delta\nu_{PR}^{max}=(8BkT/hc)^{1/2}$ [21] where $\Delta\nu_{PR}^{max}$ is the frequency splitting in cm^{-1} between the P and R branch maxima, B is the rotational constant of the pseudo-diatomic complex, T is the temperature, and k, h, and c are constants. M^+•••CH_4 equilibrium distances from calculations can be used to solve for the pseudo-diatomic rotational constant, B (cm^{-1}). The results are shown in Table 5.1.

The average cluster temperatures follow the same trend as the ion•••ligand interaction energies, $Na^+ > K^+ > Rb^+ > Cs^+$ and can be explained by the evaporative

cooling process reported in chapter 2 of this thesis and elsewhere.[22] Evaporation of ligands during cluster stabilization carry away energy which lowers the internal energy (effective temperature) of the cluster. The process occurs until the internal energy of the cluster is less that the energy required to induce another ligand evaporative event. Thus, more evaporative events occur in Cs^+ compared to Na^+ cluster stabilization resulting in a colder temperature for Cs^+ clusters.

Warm cluster temperatures result in broad, structureless intensity of the ν_3(e) mode for all spectra except for $Cs^+(CH_4)_1$ where some ΔK subbands can be resolved. The peak intensities for ΔK subbands follow a strong-weak-weak-strong pattern consistent with nuclear spin statistics of a symmetric top molecule [23] which has been reported before for $X^-(CH_4)_1$ complexes [9,24-26] and supports the predicted C_{3v} structure of the complex. Higher frequency ΔK subbands are not resolved due to an overlap in intensity from the $\nu_3(a_1)$ vibrational stretching feature at 3028 cm^{-1}.

Finally, we examine how the ion•••CH_4 interaction strength affects the intensity ratios of the ν_3(e) and $\nu_3(a_1)$ bands versus the ν_1 band. We chose to use tetra-methanated clusters as an example because all four methane molecules bind directly to the ion.

IRPD spectra of selected $M^+(CH_4)_4$ clusters are shown in Figure 5.5 (we include $Li^+(CH_4)Ar_1$ data from the previous chapter of this Thesis for comparison). The ν_1 bands gradually shift to higher frequency from Li^+ to K^+. Compared to the $Li^+(CH_4)_4Ar_1$ spectrum, the ν_3(e) and $\nu_3(a_1)$ bands gradually gain IR intensity (relative to the ν_1 band intensity) in the Na^+ and K^+ spectra. These results indicate that as the ion size increases, ion•••CH_4 electrostatic interaction decreases and CH_4 vibrational modes will trend toward neutral vibrational frequencies.

5.5 Conclusions

IRPD spectra are reported for $M^+(CH_4)_n$, M= Na, K, Rb, Cs, cluster ions. For $Na^+(CH_4)_n$ clusters a coordination number of n=6 is determined based on the appearance of a new, less perturbed ν_1 band for n=7. For n ≥ 7, there are no measurable frequency shifts in the ν_1 bands corresponding to first- and second-shell CH_4 molecules indicating weak, if any, interactions between molecules in the two shells. Coordination numbers could not be determined for $K^+(CH_4)_n$, $Rb^+(CH_4)_n$, and $Cs^+(CH_4)_n$, due to the lack of resolvable ν_1 bands.

The strength of ion•••CH_4 interaction was also determined to trend as $Na^+ > K^+ > Rb^+ > Cs^+$ based on the magnitude of frequency shifts. Furthermore we were able to show that as the ion•••CH_4 interaction weakens, the ν_3(e) and $\nu_3(a_1)$ features gain intensity (relative to the ν_1 band) as the CH_4 molecules tend toward the neutral CH_4 vibrational modes.

Also, we determine an average temperature of $M^+(CH_4)$ dimers based on the PR branch splitting, with $Na^+(CH_4)_1$ clusters the warmest, 540 K, and $Cs^+(CH_4)_1$ the coolest, 297 K.

5.6 Figures and Tables

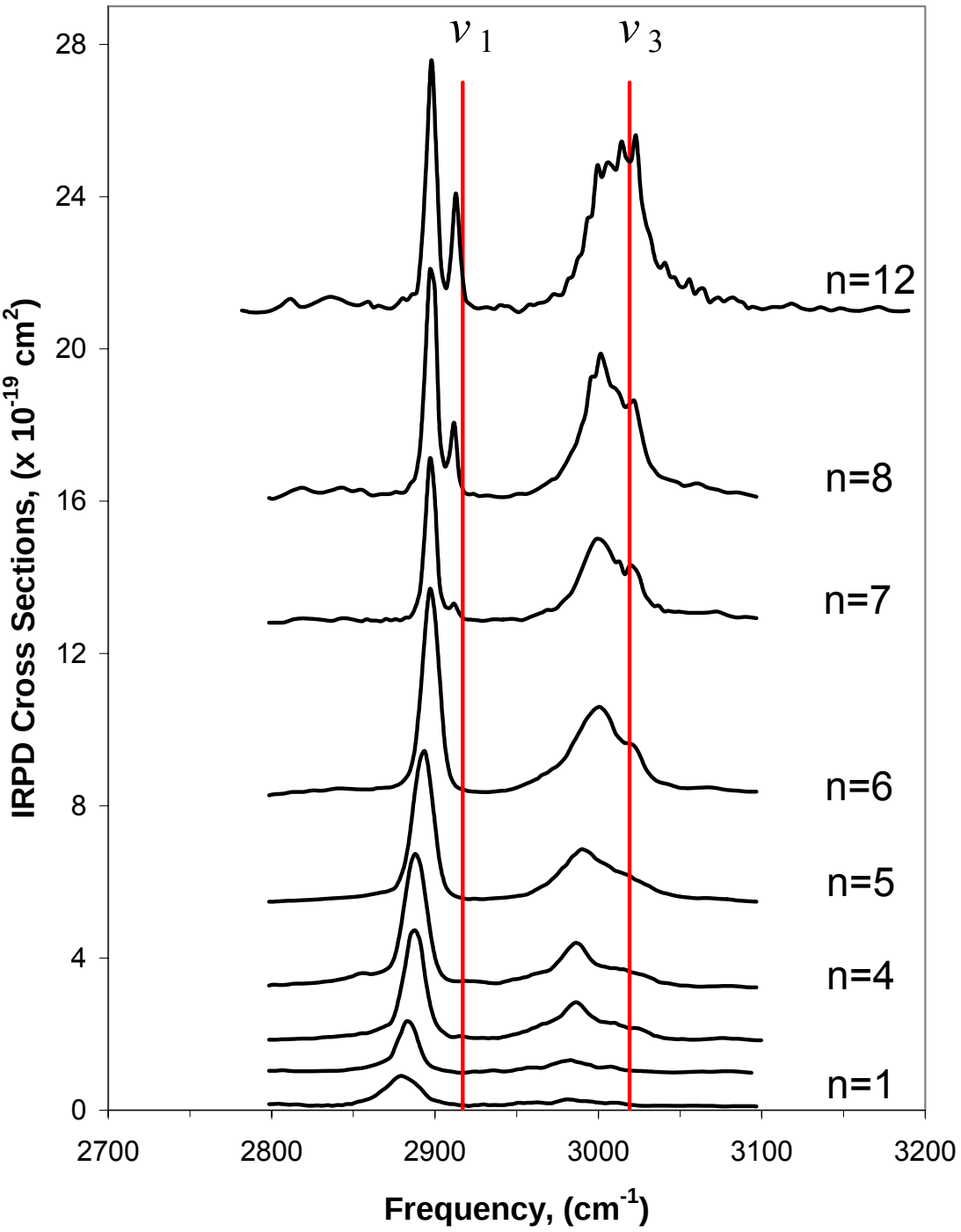

Figure 5.1: IRPD spectra for $Na^+(CH_4)_n$ clusters; n=1 clusters are argon tagged. Neutral CH_4 ν_1 and ν_3 values are labeled with red vertical lines.

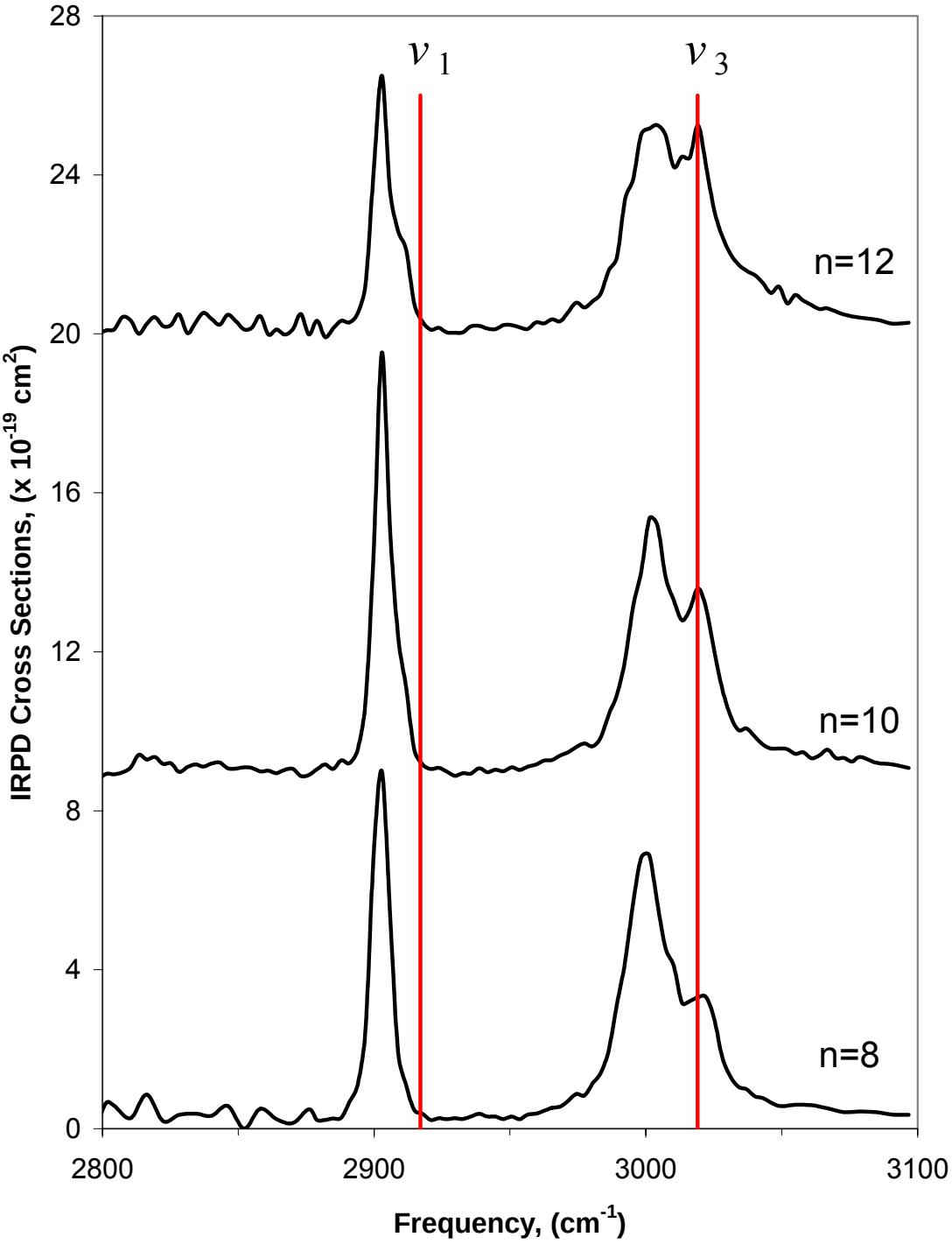

Figure 5.2. IRPD spectra for $K^+(CH_4)_n$, n=8, 10, and 12, clusters. Neutral CH_4 ν_1 and ν_3 values are shown in red vertical lines.

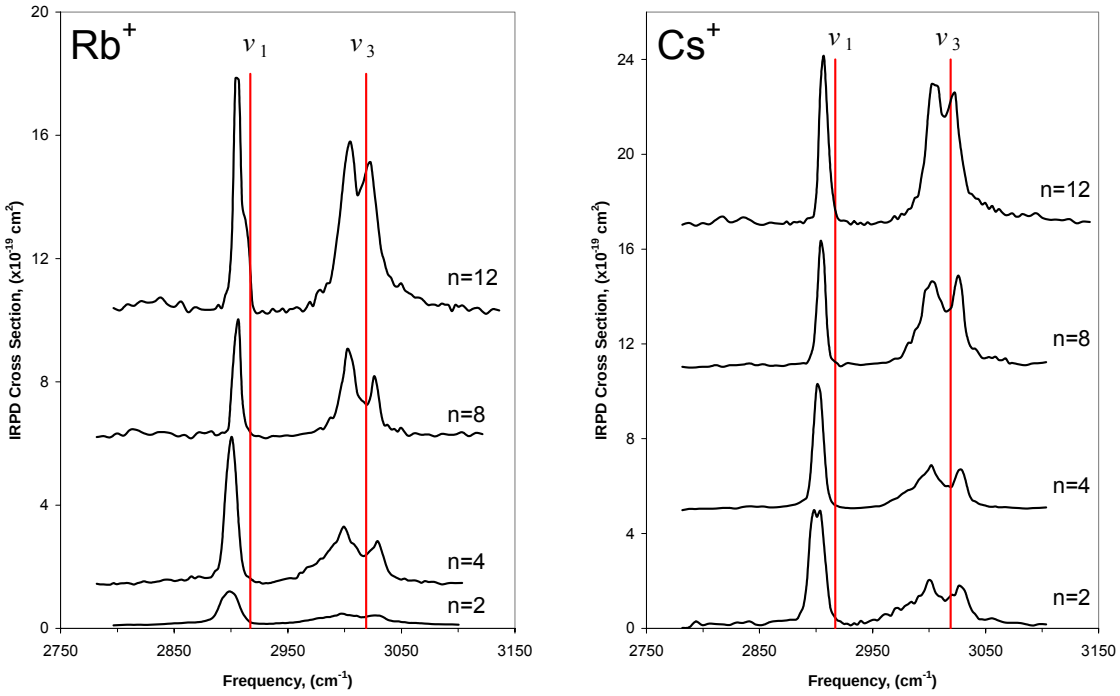

Figure 5.3. IRPD spectra of $Rb^+(CH_4)_n$ (left) and $Cs^+(CH_4)_n$ (right) clusters. Neutral CH_4 ν_1 and ν_3 values are shown in red vertical lines.

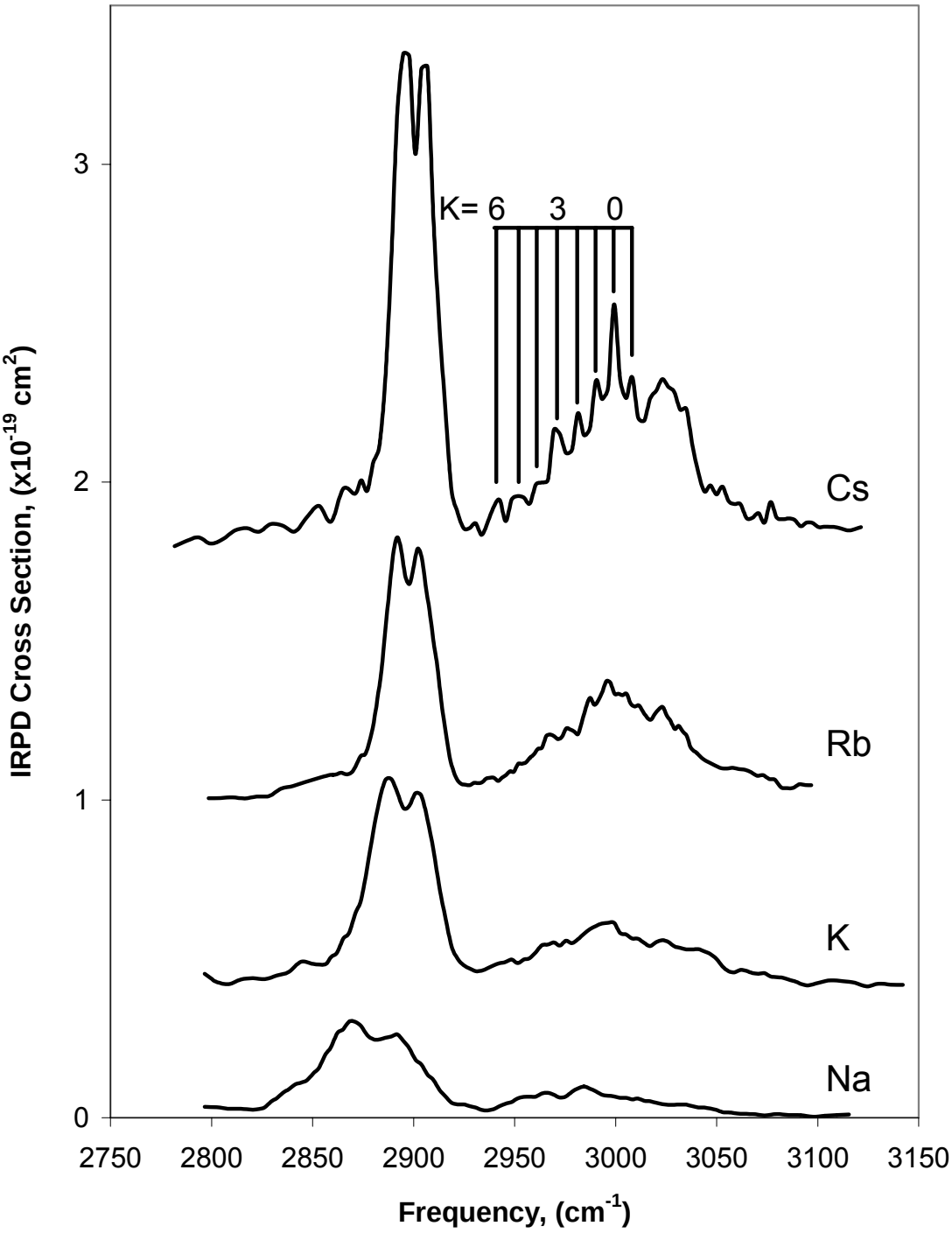

Figure 5.4: IRPD spectra for $M^+(CH_4)_1$, M= Na, K, Rb, and Cs, dimers. Rotational structure is only observed for $Cs^+(CH_4)_1$ clusters. ν_1 PR branch splitting can be used to estimate dimer temperature.

Table 5.1: $M^+(CH_4)_1$ Dimer Data and Experimental Temperatures.

	$\Delta\nu_{PR}^{Max}$, (cm^{-1})	Calc. M^+CH_4 Dist. (Å)	B, (cm^{-1})	T, (K)
$Na^+(CH_4)_1$	27	2.71	0.243	540
$K^+(CH_4)_1$	18	3.17	0.147	395
$Rb^+(CH_4)_1$	14	3.42	0.107	329
$Cs^+(CH_4)_1$	12	3.68	0.087	297

$\Delta\nu_{PR}^{max}$ obtained from experiment. Rotational constant, B (cm^{-1}), was obtained using M^+CH_4 distances from MP2 calculations.

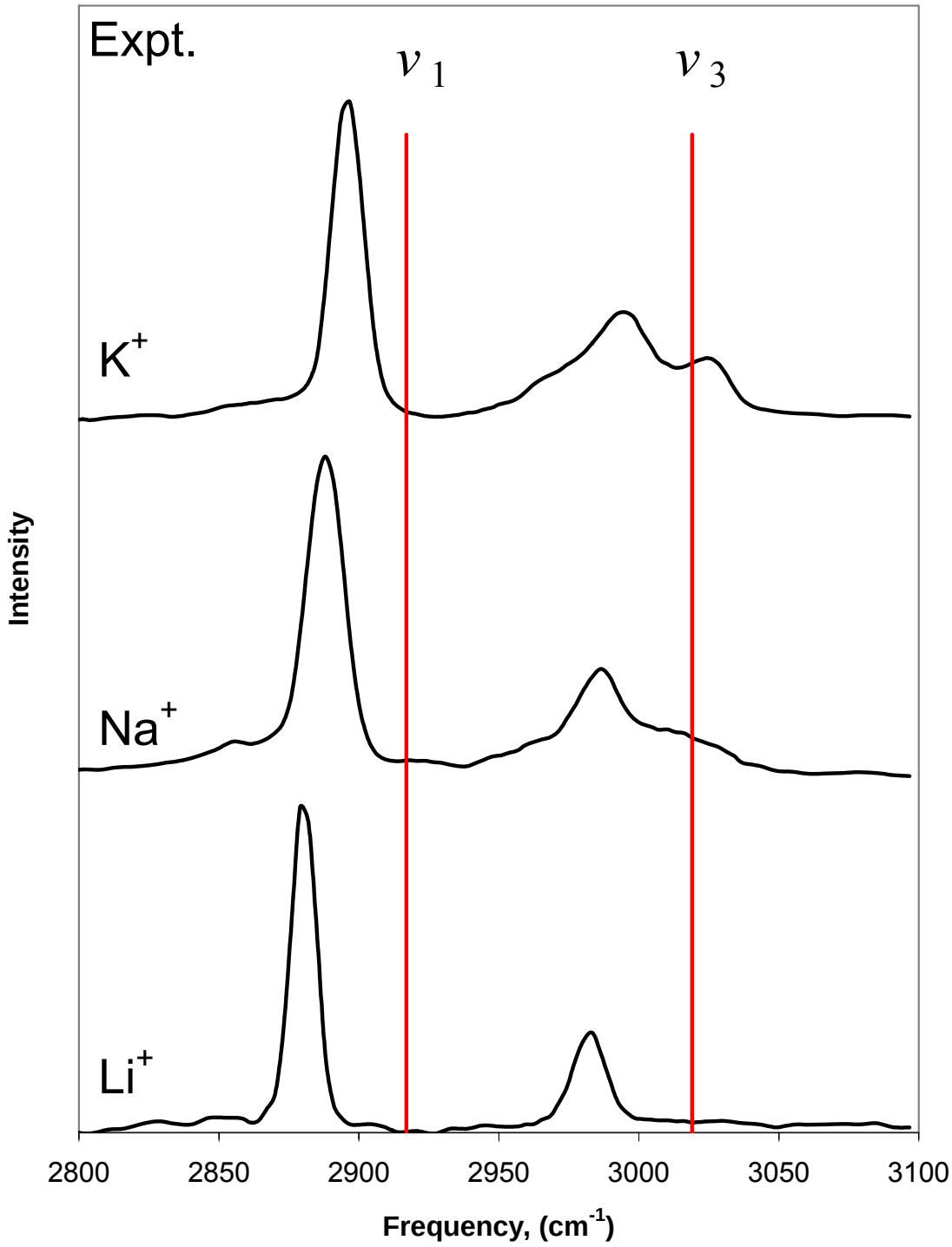

Figure 5.5. IRPD spectra of $M^+(CH_4)_4$, M=Li, Na, and K cluster ions (Li^+ cluster contains one argon tagging atom). Spectra are scaled so that all ν_1 bands are equal in peak IRPD intensity. Neutral CH_4 ν_1 and ν_3 values are labeled in each panel.

5.7 References

[1] O. Rodriguez Jr, J. M. Lisy. *Chem. Phys. Lett.* 502 (2011) 145.
[2] J. P. Beck, J. M. Lisy. *J. Phys. Chem. A* 114 (2010) 10011.
[3] O. M. Cabarcos, C. J. Weinheimer, J. M. Lisy. *J. Chem. Phys.* 110 (1999) 8429.
[4] D. J. Miller, J. M. Lisy. *J. Am. Chem. Soc.* 130 (2008) 15393.
[5] D. J. Miller, J. M. Lisy. *J. Am. Chem. Soc.* 130 (2008) 15381.
[6] B. L. J. Poad, C. D. Thompson, E. J. Bieske. *Chem. Phys.* 346 (2008) 176.
[7] V. Dryza, E. J. Bieske. *Int. J. Mass Spectrom.* 297 (2010) 46.
[8] Z. M. Loh, R. L. Wilson, D. A. Wild, E. J. Bieske, J. M. Lisy, B. Njegic, M. S. Gordon. *J. Phys. Chem. A* 110 (2006) 13736.
[9] Z. M. Loh, R. L. Wilson, D. A. Wild, E. J. Bieske, M. S. Gordon. *J. Phys. Chem. A* 109 (2005) 8481.
[10] J. M. Lisy. *Int. Rev. Phys. Chem.* 16 (1997) 267.
[11] C. E. Klots. *J. Chem. Phys.* 83 (1985) 5854.
[12] Origin (OriginLab, Northampton, MA), 2003.
[13] J. Kong, C. A. White, A. I. Krylov, C. D. Sherrill, R. D. Adamson, T. R. Furlani, M. S. Lee, A. M. Lee, S. R. Gwaltney, T. R. Adams et al., SPARTAN'02, Wavefunction, Inc., Irvine CA, 2002.
[14] M. J. Frisch, G. W. Trucks, H. B. Schlegel, G. E. Scuseria, M. A. Robb, J. R. Cheeseman, J. A. Montgomery Jr., T. Vreven, K. N. Kudin, J. C. Burant et al., Gaussian 03, Revision B.04, Gaussian, Inc., Pittsburgh, PA, 2003.
[15] P. J. Hay, W. R. Wadt. *J. Chem. Phys.* 82 (1985) 299.
[16] P. J. Hay, W. R. Wadt. *J. Chem. Phys.* 82 (1985) 270.
[17] W. R. Wadt, P. J. Hay. *J. Chem. Phys.* 82 (1985) 284.
[18] S. I. Gorelsky, *SWizard program*, 4.1, University of Ottawa, Canada, 2005.
[19] V. D. Makhaev. *Russian Chemical Reviews* 72 (2003) 257.
[20] D. R. Lidle, CRC Handbook of Chemistry and Physics, Boca Raton, 2009.
[21] G. Herzberg, Molecular Spectra and Molecular Structure I. Spectra of Diatomic Molecules, Van Nostrand Reinhold, New York, 1950.
[22] O. M. Cabarcos, C. J. Weinheimer, J. M. Lisy. *J. Phys. Chem. A* 103 (1999) 8777.
[23] G. Herzberg, Molecular Spectra and Molecular Structure II. Infrared and Raman Spectra of Polyatomic Molecules, Van Nostrand, New York, 1945.
[24] Z. M. Loh, R. L. Wilson, D. A. Wild, E. J. Bieske, M. S. Gordon. *Aust. J. Chem.* 57 (2004) 1157.
[25] D. A. Wild, Z. M. Loh, E. J. Bieske. *Int. J. Mass Spectrom.* 220 (2002) 273.
[26] D. A. Wild, Z. M. Loh, P. P. Wolynec, P. S. Weiser, E. J. Bieske. *Chem. Phys. Lett.* 332 (2000) 531.

Chapter 6

Revisiting $Li^+(H_2O)_{3-4}Ar_1$ Clusters: Evidence of High Energy Conformers from Infrared Spectra[1]

6.1 Introduction

When the internal energy in argon-bearing cluster ions (hereafter referred to as argon-tagged) is adequately low, there can be insufficient kinetic energy to overcome energetic barriers to rearrange into a lower, or global-minimum energy conformer. As a result, the cluster ion beam can contain multiple conformers, including kinetically-trapped, high energy clusters in addition to minimum energy clusters.

Previous studies of cluster ion conformers have been performed using a two laser IR-IR double resonance technique.[1,2] However, we have discovered that by monitoring different photofragmentation channels, selective IRPD spectra of kinetically-trapped, high energy conformers, can be obtained using a single laser.[3,4] It was proposed that the amount of energy stored in high energy conformers can be released upon infrared excitation, resulting in unique fragmentation pathways.[3,4]

While these high energy conformers may not be the dominant species in the ion cluster beam, their infrared spectra can be obtained, revealing unique hydrogen bonding motifs, and used to gain a more rounded description of ion solvation, the interplay between competing non-covalent interactions, and cluster photodissociation dynamics. In

[1] This Chapter is reproduced in part from a manuscript in preparation by Oscar Rodriguez Jr. and James M. Lisy.

a previous IRPD study, our group reported spectroscopic features from high energy conformer of $Li^+(H_2O)_4Ar_1$ [5] which were only observed using the argon-tagging method and monitoring the loss of argon. With our recent experience obtaining different IRPD spectra by monitoring additional fragmentation channels, we chose to reexamine some of the simplest hydrated ion species, $Li^+(H_2O)_{3\text{-}4}Ar_1$, to see if other high energy conformers could be observed in IRPD experiments.

6.2 Experimental Methods

Infrared predissociation spectroscopy of $Li^+(H_2O)_{3\text{-}4}Ar_1$ cluster ions are carried out using a triple-quadrupole mass spectrometer and IR laser. Details of our experimental apparatus are described elsewhere.[5,6] Briefly, water vapor seeded in argon gas is introduced into the source chamber through a 30° conical nozzle (180 μm diameter). Neutral water clusters in an argon bath are generated via supersonic expansion forming a neutral cluster beam. A tungsten filament coated with an alkali halide paste is heated to thermionically emit ions which are collimated to intercept the neutral cluster beam at 90°. The subsequent ion-neutral cluster collision and ion solvation forms energetically "hot", unstable cluster ions which dissipate energy by evaporation of the most labile ligands [7], argon in this case, until the evaporative lifetime is comparable to the flight time through the apparatus. The quasi-stable cluster ion beam goes through a stage of differential pumping, then enters a third chamber where the first of three quadrupoles is used to mass-select the cluster ion of interest. These ions proceed to the second r.f. (radio frequency)-only quadrupole (which acts as an ion guide) where the output of a counter propagating pulsed tunable Laservision OPO/OPA, pumped by the 1064 nm output of a Surelite II 10 Hz Continuum Nd:YAG laser, is gently focused along the axis of the 60 cm

long quadrupole. Absorption of a mid-IR photon by a resonant vibrational mode within the cluster ion in this quadrupole induces photofragmentation. The fragment cluster ions are mass-selected by the third quadrupole and detected using a conversion dynode/channeltron electron multiplier. Spectra are obtained by stepping the laser frequency in 3 cm^{-1} increments and reporting the photodissociation cross section (cm^2) (corrected for laser fluence) as a function of laser frequency (cm^{-1}). Absolute frequency calibration is obtained by simultaneously recording a photoacoustic spectrum of ambient atmospheric H_2O vapor. Experimental frequencies were obtained by fitting experimental bands with Lorentizan lineshapes using Origin 7.5.[8]

6.3 Computational Methods

Calculations were carried out at the MP2/aug-cc-pVDZ level. Initial structures were generated using Spartan 02 [9] and minimum energy structures and harmonic vibrational frequencies were obtained using Gaussian 03 software.[10] Calculated spectra (12 cm^{-1} FWHM) were generated using SWizard.[11] Calculated frequencies are scaled by 0.9577 to match the reported neutral water frequencies.

6.4 Results and Discussion

Spectra of $Li^+(H_2O)_4Ar_1$ monitoring the [Ar + H_2O] and [Ar] fragmentation channels are reported in Figure 6.1 (spectra will be referred to as [Ar + H_2O] and [Ar] herein). The differences between the two IRPD spectra are striking and suggest the presence of multiple conformers that appear in specific photofragmentation channels. Most notably, there are features in the region between 3200 cm^{-1} and 3450 cm^{-1}

associated with hydrogen bonding in the [Ar + H_2O] spectrum that are absent in the [Ar] spectrum. This suggests that there must be conformers containing different H_2O•••H_2O interactions.

In addition, the [Ar + H_2O] spectrum contains a band at 3678 cm^{-1} which is absent in the [Ar] spectrum and in a region associated with a free O-H stretch of a 3-coordinated, double proton acceptor and single proton donor [12] (AAD), H_2O molecule. This is intriguing given the presence of only four H_2O molecules in these clusters. Typically, the 3-coordinated H_2O free O-H stretching feature is observed in spectra of large, bulk-like water clusters [13-16], surfaces or interfaces [17], and ice [18,19], but has been observed before in IRPD spectra of $H^+(H_2O)_7$ [20], $NH_4^+(H_2O)_6$ [12], and $CH_3NH_3^+(H_2O)_4$ [21] clusters.

The O-H vibrational bands of the [Ar] spectrum have been previously reported and assigned [5] (although we rescanned the spectrum below 3450 cm^{-1} to insure that there were no additional vibrational features). The [Ar] spectrum is shown in Figure 6.2 with simulated spectra for two lowest energy conformers, 4a and 4b, calculated at the MP2/aug-cc-pVDZ level. Briefly, the most intense band in the spectrum, at 3533 cm^{-1}, corresponds to a bent hydrogen bond O-H stretching modes associated with the two O-H groups involved as proton-donors (see structure 4b in Figure 6.2). Bands observed at 3625 and 3655 cm^{-1}, are assigned to the symmetric O-H stretches for second- and first-shell water molecules, respectively, that are not involved as proton donors. The remaining bands due to the free O-H groups (of the first shell hydrogen-bonded waters) and asymmetric O-H stretches of the nonproton-donating waters overlap and are centered at 3726 cm^{-1}. Conformer 4b, although 9 kJ/mol higher in energy than the global minimum

energy conformer, 4a, appears to be the dominant species in the cluster ion beam based on the relative peak intensities in the IRPD spectrum.

However, the simulated spectra of conformers 4a and 4b in Figure 6.2 do not contain any hydrogen bonding features below 3450 cm^{-1}, therefore can not explain the O-H stretching features observed in the [Ar + H_2O] spectrum (see Figure 6.1). In order to assign the observed experimental features in the [Ar + H_2O] spectrum, it was necessary to extend our search for stable conformers containing more extensive hydrogen bonding. Calculations at the MP2/aug-cc-pVDZ level revealed five additional stable conformers, 4c-4g, of $Li^+(H_2O)_4Ar_1$ shown in Figure 6.3.

Conformers 4c-4g all contain H_2O•••H_2O hydrogen bonding and are ~42 – 53 kJ/mol higher in energy than the global minimum energy conformer, 4a (see Figure 6.2). The corresponding calculated spectra (harmonic frequencies) for conformers 4c-4g are shown in Figure 6.4.

The calculated spectra of conformers 4d and 4f each contain features between 3560 – 3630 cm^{-1} and conformer 4g contains a hydrogen bond feature near 3054 cm^{-1} which are notably absent from the [Ar + H_2O] spectrum. Therefore we consider these conformers to be absent from the cluster ion beam. The calculated spectrum of conformer 4c contains four features which are in reasonable agreement with the [Ar + H_2O] spectrum, while the calculated spectrum for conformer 4e appears to give the best overall agreement with the [Ar + H_2O] spectrum and is the only simulated spectrum containing a feature correlating to a signature 3-coordinated H_2O free O-H stretching mode.

A simple analysis of ligand binding energies in the minimum energy conformer and relative energies of the high energy conformers explain why spectral features from

the [Ar] spectrum are absent in the [Ar + H_2O] spectrum and *vice versa*. First, at the MP2/aug-cc-pVDZ level, the argon binding energy in conformer 4a (see Figure 6.2) is only ~ 5 kJ/mol and binding energy of a water molecule from the subsequent $Li^+(H_2O)_4$ fragment cluster ion is ~67 kJ/mol; thus ~72 kJ/mol of energy is required to induce [Ar + H_2O] fragmentation. Absorption of an IR photon in the O-H stretching region imparts ~38-45 kJ/mol of energy into the cluster ion. Clearly from the binding energies, the absorbed photon energy is sufficient to cause argon fragmentation only.

Now consider high energy conformer 4b (see Figure 6.2) which is ~9 kJ/mol higher in energy than 4a. Thus, the total energy required to access the [Ar + H_2O] fragmentation channel for 4b is reduced from ~72 to ~63 kJ/mol; still well above the IR photon energy (~38-45 kJ/mol). Therefore, spectral features of conformer 4b are only observed in the [Ar] spectrum.

However, high energy conformers 4c and 4e from Figure 6.3 are ~42-44 kJ/mol higher in energy (relative to the global minimum energy conformer), reducing the energy required to access the [Ar + H_2O] fragmentation channel from ~72 to ~28-30 kJ/mol. Since energy from an absorbed photon in the O-H stretching region exceeds this threshold, spectral features from conformers 4c and 4e are observed in spectra obtained by monitoring the [Ar + H_2O] fragmentation channel. These features are absent in the [Ar] spectrum, as the remaining energy in the cluster ion following argon fragmentation would be greater than the water binding energy, ~67 kJ/mol, causing water fragmentation. Thus the [Ar + H_2O] channel is unique to the high (+42-44 kJ/mol) conformers.

As the conformers, 4c-g, all have the argon directly bound to the lithium ion, we were interested in seeing if the position of the argon was responsible for the stability of these calculated structures. We performed additional calculations without argon and identified stable structures similar to those shown in Figure 6.3 (see appendix A.2 for calculated structures for non-argonated $Li^+(H_2O)_4$ clusters). These stable argonated and non-argonated structures have not been previously reported in literature to the best of our knowledge and represent new minima on the potential energy surface of $Li^+(H_2O)_4Ar_{0-1}$ at the MP2/aug-cc-pVDZ level of theory.

The results from $Li^+(H_2O)_4Ar_1$ experiments compelled us to search for high energy conformers and unique fragmentation channels for $Li^+(H_2O)_3Ar_1$ clusters. A spectrum of $Li^+(H_2O)_3Ar_1$ has been previously reported [5] in the frequency region 3600 – 3850 cm^{-1}. We have obtained a new spectrum monitoring the [Ar] fragmentation channel and extended the frequency range to 3200 – 3850 cm^{-1} as shown in Figure 6.5. The bands at 3648 cm^{-1} and 3723 cm^{-1} correspond to symmetric and asymmetric O-H stretching modes, and are indicative of water molecules where the O-H groups are not involved in hydrogen bonds. However, by scanning to lower frequency, we observed an additional minor feature corresponding to a hydrogen-bonded O-H stretching feature, at 3508 cm^{-1}

Two stable conformers were identified at the MP2/aug-cc-pVDZ level. Their simulated spectra (see Figure 6.5) correspond to structures containing an argon atom. Calculations indicated that these structures did not require the presence of an argon atom. The calculated bands corresponding to the minimum energy conformer, labeled 3a, are assigned as H_2O symmetric and asymmetric vibrational stretches at 3634 and 3740 cm^{-1}

respectively. The high energy conformer (+28 kJ/mol), labeled 3b, contains the characteristic bent hydrogen bond out-of-phase/in-phase modes near ~3500 cm^{-1}, symmetric stretch of the second shell H_2O at 3617 cm^{-1}, and free O-H and H_2O asymmetric stretches centered at 3723 cm^{-1}. We note that the feature at 3508 cm^{-1} is analogous to the 3533 cm^{-1} band in conformer 4b of $Li^+(H_2O)_4Ar_1$. The lower degree of hydration in $Li^+(H_2O)_3Ar_1$ leads to a stronger electrostatic enhancement of the hydrogen bonds and thus a slightly lower value for the hydrogen-bonded O-H stretching mode.

The bent hydrogen bonded O-H stretching feature intensity is weak relative to the other bands in the experimental spectrum. Since the formation of O-H•••O hydrogen bonds are accompanied by a significant increase in infrared intensity [22,23], we conclude that conformer 3b is only a minor constituent in the cluster ion beam.

Finally we will briefly discuss fragmentation energetics for $Li^+(H_2O)_3Ar_1$. According to MP2/aug-cc-pVDZ level calculations, the binding energies of argon and water in the global minimum energy conformer are ~7 and 88 kJ/mol respectively (i.e. 95 kJ/mol is required to access the [Ar + H_2O] fragmentation channel). Thus an absorbed photon in the O-H stretching region of interest (3500 – 3800 cm^{-1} for $Li^+(H_2O)_3Ar_1$) imparting ~42-45 kJ/mol of energy into the cluster ion is sufficient to cause only [Ar] fragmentation.

Let's turn our focus to high energy conformer 3b which is +28 kJ/mol higher in energy than the global minimum energy conformer. Therefore the required energy to access the [Ar + H_2O] fragmentation channel is decreased from 95 kJ/mol to 67 kJ/mol. The imparted energy from an absorbed IR photon (~42-45 kJ/mol) does not meet the

energetic requirement to access the [Ar + H_2O] fragmentation channel. Thus, only the [Ar] fragmentation channel (~10 kJ/mol required) is accessible.

6.5 Conclusions

Infrared spectra of $Li^+(H_2O)_{3\text{-}4}Ar_1$ cluster ions are reported. For $Li^+(H_2O)_4Ar_1$ a spectrum corresponding to one or more high energy conformers is obtained by monitoring the [Ar + H_2O] fragmentation channel. This spectrum exhibits a features corresponding to a free O-H vibrational mode for a 3-coordinated H_2O and those corresponding to hydrogen bonding modes from previously unknown H_2O•••H_2O interactions. The features prominent in the [Ar + H_2O] spectrum are noticeably absent from the [Ar] spectrum and *vice versa*. Using ligand binding energies and relative conformer energies, we have shown the energetic requirements behind unique fragmentation channels for $Li^+(H_2O)_4Ar_1$.

For $Li^+(H_2O)_3Ar_1$ a hydrogen bonded O-H stretching mode corresponding to a conformer calculated to be +28 kJ/mol higher in energy than the global minimum energy conformer was observed monitoring the [Ar] fragmentation channel. No other photofragmentation channels were detected for $Li^+(H_2O)_3Ar_1$.

We have reported a simple way to obtain IRPD spectra of high energy conformers utilizing unique fragmentation channels. The $Li^+(H_2O)_{3\text{-}4}Ar_1$ clusters reported here are prime candidates for further theoretical exploration. These structures and energies will be useful in mapping out the potential energy surface and to determine the barrier heights between different conformers in this deceptively complex cluster ion system. While this

has been done previously in flexible biomolecules [24], it is a new frontier for clusters and ion clusters.

6.6 Figures

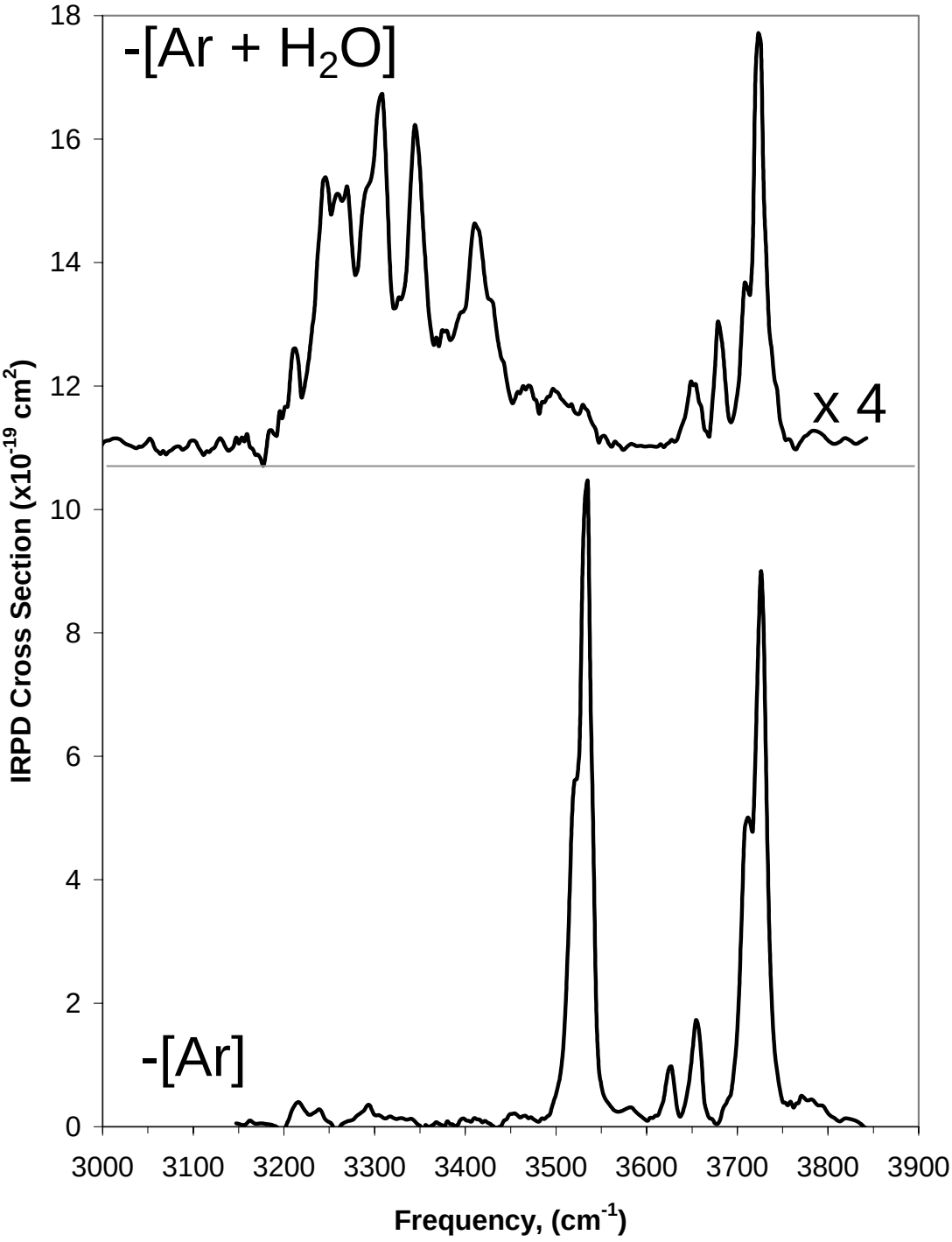

Figure 6.1: IRPD spectra of $Li^+(H_2O)_4Ar_1$ by monitoring the argon loss channel [Ar] and argon and water loss channel [Ar + H_2O].

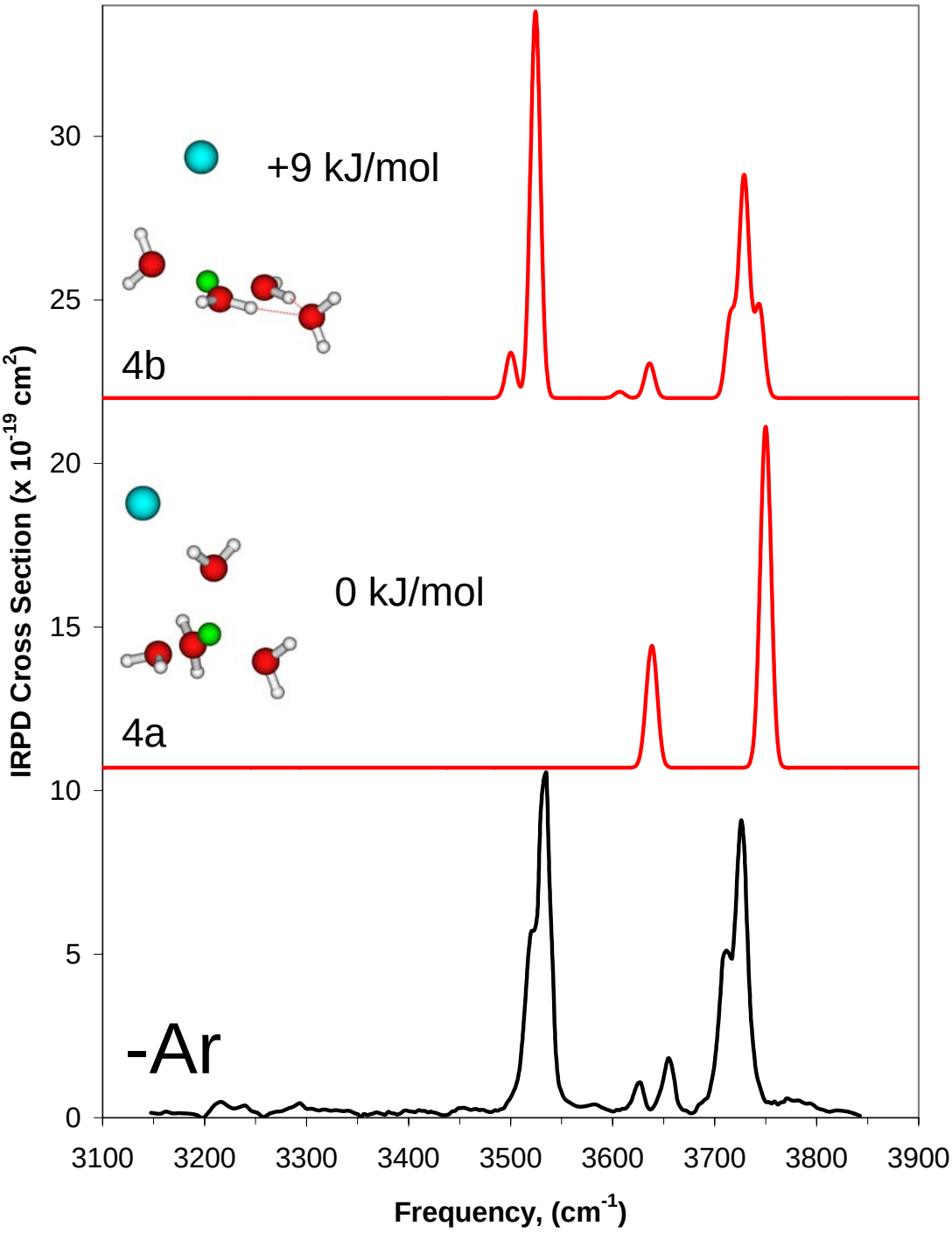

Figure 6.2: IRPD spectrum of $Li^+(H_2O)_4Ar_1$ monitoring the [Ar] fragmentation channel (black). The simulated spectra (red) and structures 4a and 4b are calculated at the MP2/aug-cc-pVDZ level of theory. The relative energies are corrected for zero-point energy.

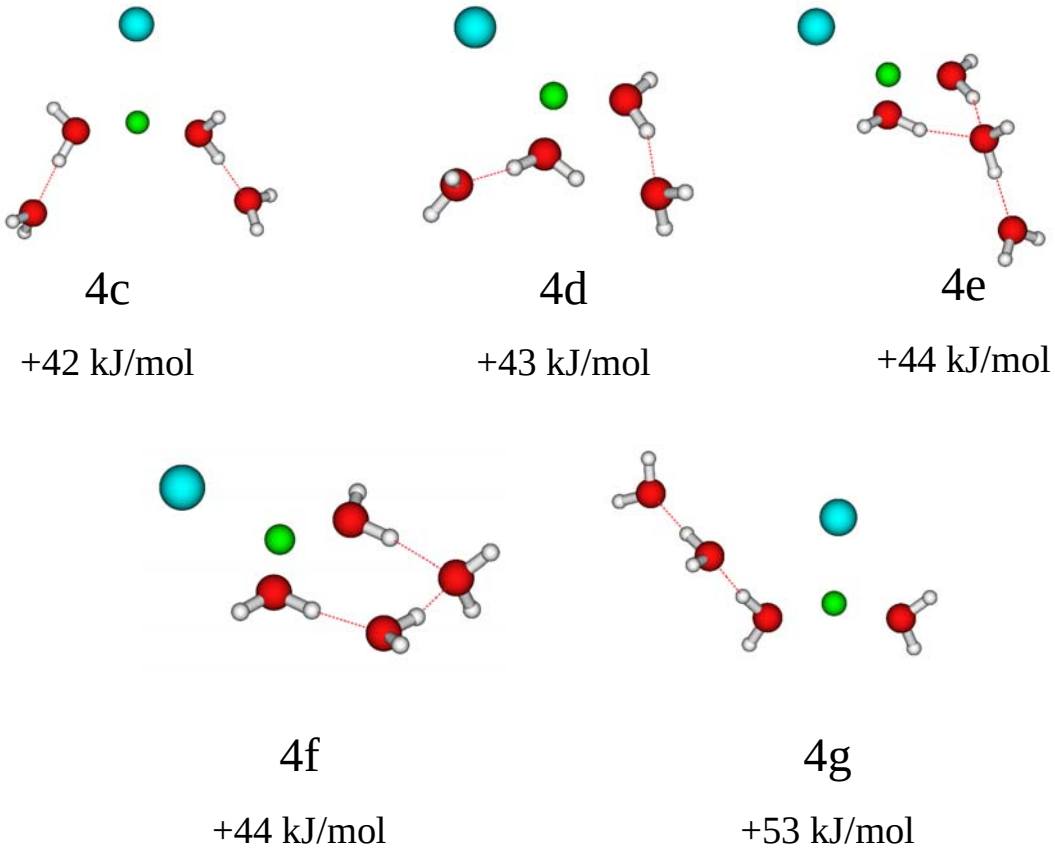

Figure 6.3: Five stable conformers (4c-4g) containing hydrogen bonding for $Li^+(H_2O)_4Ar_1$ calculated at the MP2/aug-cc-pVDZ level. Relative energies (compared to the global minimum energy structure 4a from Figure 2) are corrected for zero-point energy. Li^+ is shown in green and argon in light blue.

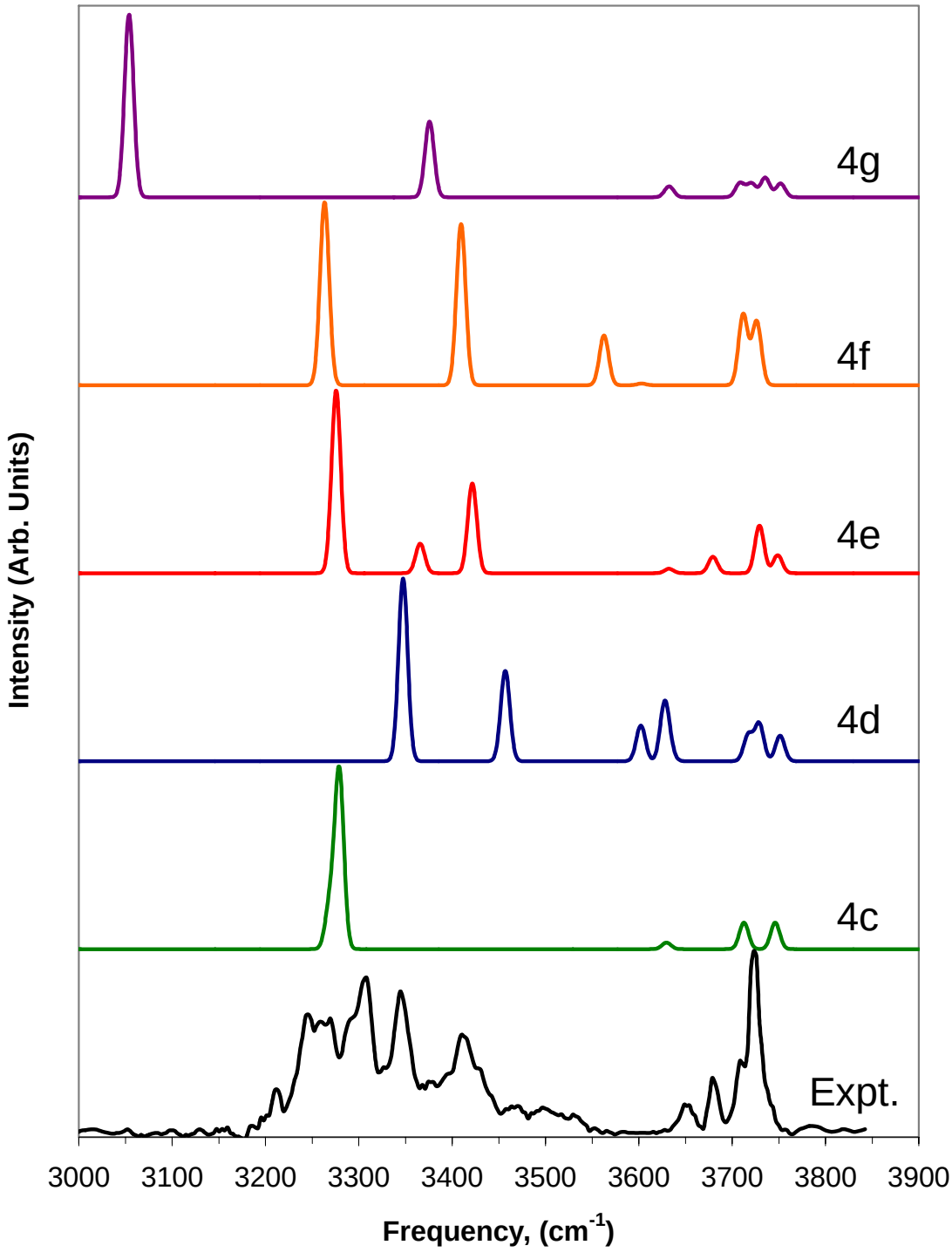

Figure 6.4: IRPD spectrum for $Li^+(H_2O)_4Ar_1$ monitoring the [Ar + H_2O] fragmentation channel along with the calculated spectra (MP2/aug-cc-pVDZ level) for conformers 4c-4g from Figure 6.2.

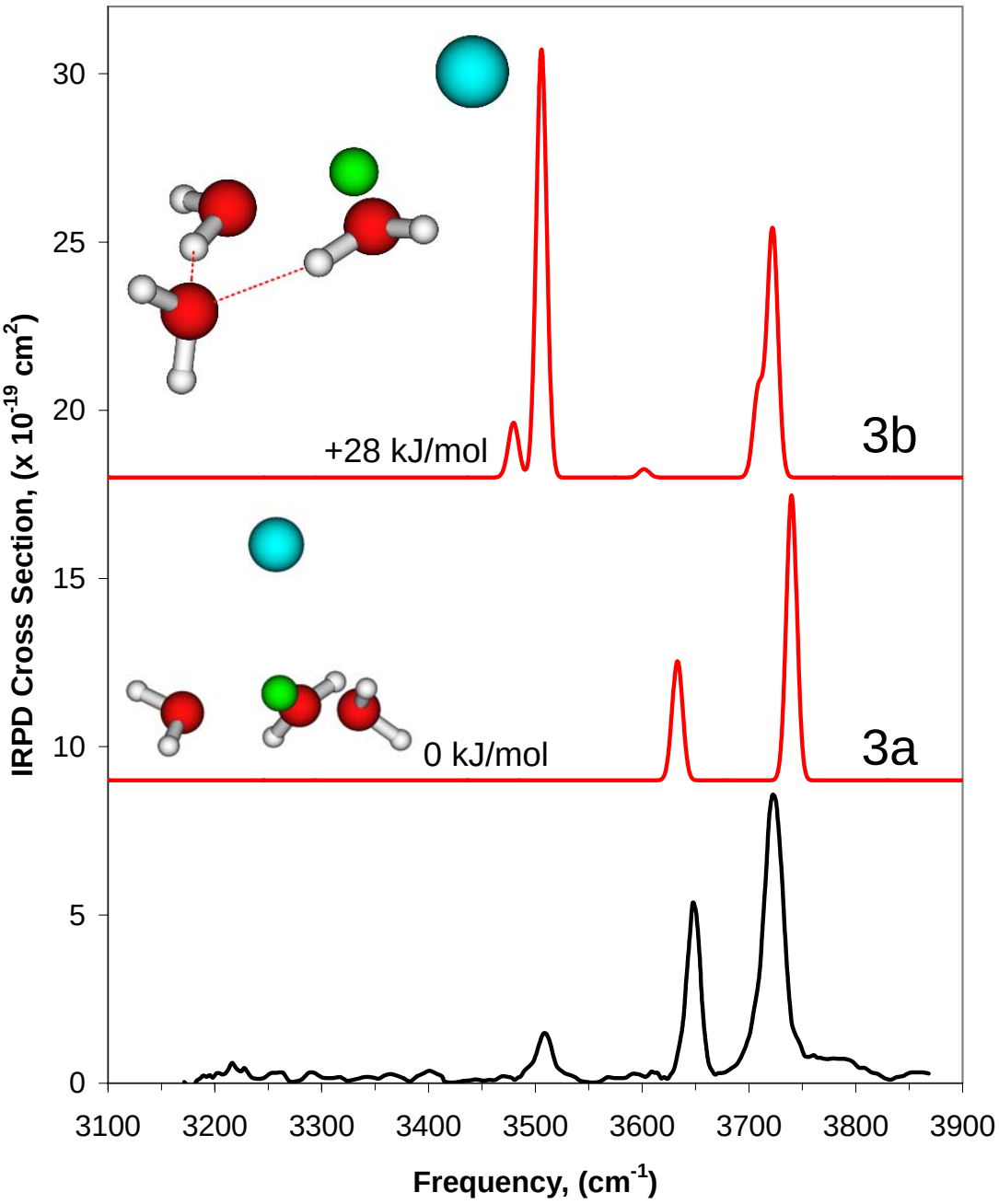

Figure 6.5: IRPD spectrum of $Li^+(H_2O)_3Ar_1$ cluster ions monitoring the [Ar] fragmentation channel. MP2/aug-cc-pVDZ level structures and calculated spectra for two stable conformers are shown in 3a and 3b with their respective relative energies (corrected for zero-point energy).

6.7 References

[1] B. M. Elliott, R. A. Relph, J. R. Roscioli, J. C. Bopp, G. H. Gardenier, T. L. Guasco, M. A. Johnson. *J. Chem. Phys.* 129 (2008) 943031.
[2] T. L. Guasco, B. M. Elliott, M. A. Johnson, J. Ding, K. D. Jordan. *J. Phys. Chem. Lett.* 1 (2010) 2396.
[3] J. D. Rodriguez, J. M. Lisy. *Int. J. Mass Spectrom.* 283 (2009) 135.
[4] O. Rodriguez Jr, J. M. Lisy. *J. Phys. Chem. A* In Press (2011)
[5] D. J. Miller, J. M. Lisy. *J. Am. Chem. Soc.* 130 (2008) 15381.
[6] D. J. Miller, J. M. Lisy. *J. Am. Chem. Soc.* 130 (2008) 15393.
[7] C. E. Klots. *J. Chem. Phys.* 83 (1985) 5854.
[8] Origin (OriginLab, Northampton, MA), 2003.
[9] J. Kong, C. A. White, A. I. Krylov, C. D. Sherrill, R. D. Adamson, T. R. Furlani, M. S. Lee, A. M. Lee, S. R. Gwaltney, T. R. Adams et al., SPARTAN'02, Wavefunction, Inc., Irvine CA, 2002.
[10] M. J. Frisch, G. W. Trucks, H. B. Schlegel, G. E. Scuseria, M. A. Robb, J. R. Cheeseman, J. A. Montgomery Jr., T. Vreven, K. N. Kudin, J. C. Burant et al., Gaussian 03, Revision B.04, Gaussian, Inc., Pittsburgh, PA, 2003.
[11] S. I. Gorelsky, *SWizard program*, 4.1, University of Ottawa, Canada, 2005.
[12] Y. S. Wang, J. C. Jiang, C. L. Cheng, S. H. Lin, Y. T. Lee, H. C. Chang. *J. Chem. Phys.* 107 (1997) 9695.
[13] G. E. Douberly, A. M. Ricks, M. A. Duncan. *J. Phys. Chem. A* 113 (2009) 8449.
[14] M. Miyazaki, A. Fujii, T. Ebata, N. Mikami. *J. Phys. Chem. A* 108 (2004) 10656.
[15] M. Miyazaki, A. Fujii, T. Ebata, N. Mikami. *Science* 304 (2004) 1134.
[16] J. W. Shin, N. I. Hammer, E. G. Diken, M. A. Johnson, R. S. Walters, T. D. Jaeger, M. A. Duncan, R. A. Christie, K. D. Jordan. *Science* 304 (2004) 1137.
[17] H. C. Allen, E. A. Raymond, G. L. Richmond. *Curr. Opin. Colloid Interface Sci.* 5 (2000) 74.
[18] J. C. Jiang, J. C. Chang, B. C. Wang, S. H. Lin, Y. T. Lee, H. C. Chang. *Chem. Phys. Lett.* 289 (1998) 373.
[19] C. Steinbach, P. Andersson, J. K. Kazimirski, U. Buck, V. Buch, T. A. Beu. *J. Phys. Chem. A* 108 (2004) 6165.
[20] J. C. Jiang, Y.-S. Wang, H.-C. Chang, S. H. Lin, Y. T. Lee, G. Niedner-Schatteburg, H.-C. Chang. *J. Am. Chem. Soc.* 122 (2000) 1398.
[21] K. Y. Kim, W. H. Han, U. I. Cho, Y. T. Lee, D. W. Boo. *Bull. Korean Chem. Soc.* 27 (2006) 2028.
[22] G. A. Jeffrey, An Introduction to Hydrogen Bonding, Oxford University Press, New York, 1997.
[23] S. S. Xantheas, Recent Theorectical and Experimental Advances in Hydrogen Bonded Clusters, Kluwer Academic Publishers, Dordrecht, 2000.
[24] J. R. Carney, T. S. Zwier. *J. Phys. Chem. A* 104 (2000) 8677.

Chapter 7

Ion-Water-Alkane Cluster Ions I: Infrared Spectroscopy of $Li^+(H_2O)_{1-4}(CH_4)_n$ Clusters[1]

7.1 Introduction

Methane hydrates, or clathrates, occur when water molecules entrain one or more CH_4 molecules in ice-like structures and have been suggested as a lucrative fuel source if harvested efficiently.[1,2] However, clathrates are a nuisance in oceanic gas lines and pose atmospheric issues if methane gas escapes from the structure.[3] Therefore, studying complexes, or clusters, containing H_2O and CH_4 molecules is of great economic and environmental interest. Furthermore, ions are essentially unavoidable in the environment, so it is important to understand roles of ions in these structures.

Since CH_4 is the smallest alkane, clusters containing H_2O and CH_4 serve as a simple water-hydrocarbon model which has been studied before. Until recently, nearly all calculated neutral water•••methane structures exhibited a O•••H-C orientation where the water oxygen acted as a proton acceptor.[4-6] However, new *ab initio* and atoms in molecules (AIM) calculations indicate that CH_4 in fact acts as the proton acceptor wherein a water hydrogen interacts with a tetrahedral face of CH_4 in the global minimum energy structure.[7,8] This type of weak hydrogen bond and orientation was reported in a microwave spectrum of the water•••methane complex.[9]

Olesen *et al.* have used *ab initio* methods to study the proton accepting and hydrogen bonding capabilities of alkanes, including methane.[10] In a theoretical and

[1] This Chapter is reproduced in part from a manuscript in preparation by Oscar Rodriguez Jr. and James M. Lisy.

IRPD (infrared predissociation) study of argon tagged $CH_4 \bullet H_3O^+$ complexes, [11] Olesen *et al.* illustrate that CH_4 acts as a proton acceptor. This leads to the elongation of the hydrogen bonded O-H and all C-H bonds resulting in a red shift of their respective vibrational features. In addition, the authors report a shallow potential energy surface for CH_4 internal rotation which indicates a weak water•••methane interaction.

Since the goal is to study the solvation of Li^+ by water and methane simultaneously, it is useful to discuss prior work by our group of $Li^+(L)_n$, $L=H_2O$ [12] and CH_4 [13,14], clusters. For $Li^+(H_2O)_n$ clusters, water•••water O-H hydrogen bonded features appeared in the IRPD spectrum when a fifth water was added.[12] However, we reported in the previous chapter of this Thesis and in Ref [15] that argon tagging can be used to generate, and kinetically trap, multiple $Li^+(H_2O)_4Ar_1$ conformers which contain extensive hydrogen bonding.

In chapter 4 of this Thesis, we showed that weak CH_4•••CH_4 interactions in $Li^+(CH_4)_n$ clusters allowed us to directly probe the electrostatic effect by the ion beyond the first solvent shell. This is difficult to evaluate in hydrated clusters where first- and second-shell molecules readily form hydrogen bonds.

In this chapter, Li^+ solvation studies are extended to clusters containing water and a hydrocarbon component, methane. Infrared predissociation spectroscopy (IRPD), together with density functional theory calculations, are used to study the electrostatic effects of the ion, competing non-covalent interactions, determine cluster structures, and examine the water•••methane interaction.

7.2 Experimental Methods

IRPD spectra of $Li^+(H_2O)_{1-4}(CH_4)_n$ clusters are reported using a triple quadrupole apparatus and IR laser. The particulars of the experimental [12,15] methods have been detailed in Chapter 2 of this Thesis. Briefly, CH_4 and H_2O gas seeded in argon gas is introduced into the source chamber through a 30°, 180 μm conical nozzle. Neutral methane-water-argon clusters are generated via supersonic expansion. Ions are ejected by thermionic emission from a homemade ion gun containing a coiled tungsten filament coated with a LiCl paste. Ions collide with neutral clusters forming hot, unstable cluster ions which reach a quasi-stable state by evaporative cooling [16] The cluster ions then travel through a radio-frequency only octopole ion guide and then enter the detection chamber containing three quadrupoles.

The cluster ion of interest is mass selected in the first quadrupole and allowed to pass to a second, radio-frequency only, quadrupole. Here the cluster ions can interact with the output of a counter propagating pulsed tunable infrared laser (Laservision OPO/OPA pumped by a 1064 nm output of a Surelite II 10 Hz Continuum Nd:YAG laser). If the frequency of the laser is on resonance with a vibrational mode of the cluster ion, photon absorption can occur. Imparted energy from the photon can induce fragmentation of one or more ligands. The fragment cluster ion is mass selcted in the third quadrupole and subsequently detected.

Spectra are obtained by stepping the IR laser in 3 cm^{-1} increments over the spectral region of interest and reporting photodissociation cross sections (corrected for laser fluence) as a function of laser frequency. Spectral features are fitted using Origin 7.5 [17] to obtain peak frequencies. Absolute frequency calibration is achieved by

simultaneously recording a reference spectrum of ambient H_2O vapor or CH_4 in a reference gas cell.

7.3 Computational Methods

DFT calculations at the B3LYP/6-31+G* level were carried out to better characterize the experimental data. Initial structures were generated using SPARTAN 02 [18] then allowed to optimize using Gaussian 03 [19] to obtain structures, relative energies (corrected for zero-point energy), and vibrational frequencies. Simulated spectra were generated using SWizard [20] and O-H frequencies were scaled by 0.9758 to match neutral H_2O values.

7.4 Results and Discussion

IRPD (top) and simulated (bottom) spectra in the O-H stretching region, along with optimized structures (right) of selected $Li^+(H_2O)_1(CH_4)_n$ clusters are shown in Figure 7.1 (see appendix A.3 for n=1-5 summary). The simulated spectra agree with the experimental spectra. The low and high frequency features in n=3 spectra correspond to H_2O symmetric and asymmetric stretches respectively. The spectra for n=4 is vastly different. The symmetric stretching feature from n=3 appears shifted below 3600 cm^{-1} in the n=4 spectra. This type of shift is typically associated with hydrogen bonding. Thus, we assign the bands at 3588 cm^{-1} and 3693 cm^{-1} in the n=4 IRPD spectrum to O-H•••CH_4 hydrogen bonded and free O-H stretching modes respectively. Furthermore, the absence of an H_2O symmetric stretching feature in n=4 spectra strongly suggests that a single

structural conformer is responsible for the observed bands (see optimized n=4 structure in Figure 7.1).

The appearance of an O-H•••CH_4 hydrogen bond also shows that a CH_4 molecule can act as a proton acceptor and form a weak hydrogen bond with a first shell H_2O molecule. The shift induced by the O-H•••CH_4 hydrogen bond (~52 cm^{-1} relative to the H_2O symmetric stretch in n=3) is much smaller compared to the 100 – 300 cm^{-1} shifts caused by stronger proton accepting molecules such as H_2O.[12,15]

The spectra for n=5 in the Figure 7.1 contain two features which have been shifted to lower frequency compared to the n=4 spectra. Having established that CH_4 can act as proton acceptor, a fifth CH_4 molecule likely binds to the available O-H site. Hence the symmetric and asymmetric stretch motions of a double proton-donating H_2O molecule are observed spectroscopically and supported by calculations.

$Li^+(H_2O)_1(CH_4)_n$ clusters also present a situation where CH_4 molecules are located in two solvent shells. By obtaining spectra in the C-H stretching region, we can compare the ion effects on first- and second-shell CH_4 in the presence and absence of H_2O to $Li^+(CH_4)_n$ spectra that were reported in chapter 4 of this Thesis.

Briefly, first shell CH_4 molecules bind via η_3 configuration with the face of the tetrahedral toward the ion, changing the symmetry from T_d to C_{3v}.[14,21,22] The IR inactive totally symmetric vibrational mode at 2917 cm^{-1} [23], ν_1, is rendered IR active and shifted to lower frequency, while the triply degenerate (perpendicular transition) vibrational mode at 3019 cm^{-1} [23], ν_3, is split into a doubly degenerate mode, $\nu_3(e)$, also shifted to lower frequency, and a weak, symmetric mode, $\nu_3(a_1)$, shifted to higher frequency.

IRPD spectra in the C-H stretching region for $Li^+(H_2O)_1(CH_4)_n$, n=3-5, clusters are shown in Figure 7.2. From the discussion above, we determined that all molecules were in the first solvent shell for n=3 (see Figure 7.1); thus the two bands in the n=3 spectrum, at 2885 cm^{-1} and 2986 cm^{-1}, correspond to first shell CH_4 ν_1 and ν_3(e) modes respectively. The $\nu_3(a_1)$ is too weak to be observed. These frequencies are ~4-5 cm^{-1} higher in frequency compared to the same bands reported for $Li^+(CH_4)_4$ clusters (see chapter 4 of this Thesis) where all ligands were determined to be in the first shell. This indicates that substitution of a single H_2O molecule weakens the overall Li^+•••CH_4 interaction.

As more CH_4 molecules are added, two resolved peaks at are observed 2887 cm^{-1} and 2899 cm^{-1} in the n=5 spectrum and correspond to ν_1 bands from first- and second-shell CH_4 molecules respectively. The ν_3(e) modes from both first- and second-shell CH_4 molecules are not resolved while the $\nu_3(a_1)$ band at 3021 cm^{-1} arises from second shell CH_4 molecules. A calculated spectrum (and structure) for n=5 are shown in Figure 7.3 to support the assignment of the bands.

Resolved ν_1 bands in the n=5 spectrum originating from first- and second-shell CH_4 molecules allow us to further investigate the effect of water on CH_4 in the cluster. In chapter 4 of this Thesis, we reported that ν_1 bands originating from second shell CH_4 molecules in $Li^+(CH_4)_n$ clusters were observed at 2909 cm^{-1}. Interestingly, the second shell CH_4 ν_1 band in the $Li^+(H_2O)_1(CH_4)_5$ spectrum is 10 cm^{-1} lower in frequency, 2899 cm^{-1}, indicating the second shell CH_4 in the $Li^+(H_2O)_1(CH_4)_5$ cluster is more perturbed. We attribute this extra perturbation to the induced dipole moment on the second shell CH_4 molecule(s) by H_2O, which is enhanced by the presence of the ion.

We obtained spectra for $Li^+(H_2O)_2(CH_4)_n$ clusters and observed features very similar to those described thus far. Therefore the series will not be discussed here and the reader is encouraged to see appendices A.4 – A.5 for full IRPD summaries in the O-H and C-H stretching regions.

An IRPD spectrum for $Li^+(H_2O)_3(CH_4)_1$ in the O-H stretching region is shown in Figure 7.4. The spectrum appears similar to the spectrum for $Li^+(H_2O)_3Ar_1$, reported in Chapter 6 of this Thesis and shown in Figure 7.4 for comparison. Using the information obtained earlier in this chapter, and in Chapter 6, we can assign the bands at 3510 cm^{-1} and 3610 cm^{-1} in the $Li^+(H_2O)_3(CH_4)_1$ spectrum to $H_2O•••H_2O$ bent- and O-H•••CH_4 hydrogen bonded O-H stretching modes while bands at 3650 cm^{-1} and 3718 cm^{-1} correspond to H_2O symmetric and free/asymmetric O-H stretching modes respectively.

Interestingly, the $H_2O•••H_2O$ bent hydrogen bonded O-H stretching feature is more intense in the $Li^+(H_2O)_3(CH_4)_1$ spectrum than in the $Li^+(H_2O)_3Ar_1$ spectrum (see Figure 7.4). This indicates that a conformer containing a bent hydrogen bonded motif is more prominent in the $Li^+(H_2O)_3(CH_4)_1$ cluster ion beam than the $Li^+(H_2O)_3Ar_1$ cluster ion beam.

B3YLP/6-31+G* calculations are used to confirm the assignments. Results indicate three stable conformers of $Li^+(H_2O)_3(CH_4)_1$. Their simulated spectra and respective structures are shown in Figure 7.5. Conformers 3a (0 kJ/mol) and 3b (+1 kJ/mol) are nearly isoenergetic, with the spectrum for conformer 3a containing bands corresponding to an O-H•••CH_4 hydrogen bonded and free O-H stretching modes. The conformer 3c spectrum contains features near ~3500 cm^{-1} arising from $H_2O•••H_2O$ bent hydrogen bonded out-of-phase/in-phase O-H stretching modes. The free/asymmetric O-H

stretches calculated to be near 3700 cm^{-1}. The second shell H_2O contributes a weak symmetric stretch mode near 3620 cm^{-1}.

The appearance of infrared bands in the $Li^+(H_2O)_3(CH_4)_1$ spectrum arising from H_2O•••H_2O interactions is surprising since ion•••dipole interactions are expected to be maximized during the cluster generation process. In addition, the conformer containing the H_2O•••H_2O bent hydrogen bond, 3c, is +19 kJ/mol higher in energy than the minimum energy conformer. Yet, based on the relative intensities, we conclude that this conformer is rather prominent in the cluster ion beam. This indicates that CH_4, like argon reported in chapter 6 of this Thesis, seems to effectively trap high energy conformers. We also obtained spectra in the C-H stretching region, however different conformers could not be distinguish because the C-H stretches are not as sensitive to their environment as O-H stretches. Please see appendices A.6 – A.7 for a full spectral summary of $Li^+(H_2O)_3(CH_4)_n$, n=1-3, clusters in the O-H and C-H stretching regions.

Next, we examine an IRPD spectrum for $Li^+(H_2O)_4(CH_4)_2$ in the O-H stretching region, seen in Figure 7.6 (see appendix A.8 for full $Li^+(H_2O)_4(CH_4)_n$ summary in the O-H stretching region). Although the spectrum is complex, we can use the results from the $Li^+(H_2O)_3(CH_4)_1$ discussion earlier to assign peaks at 3537 cm^{-1}, 3619 cm^{-1}, 3654 cm^{-1}, and 3722 cm^{-1} to a H_2O•••H_2O bent hydrogen bonded, O-H•••CH_4 hydrogen bonded, H_2O symmetric, and free/asymmetric O-H stretching modes respectively. In addition, there are bands between 3100 – 3450 cm^{-1} suggesting additional conformers containing extensive H_2O•••H_2O hydrogen bonds. Furthermore, a peak at 3682 cm^{-1} appears in a region commonly associated with a 3-coordinated, or acceptor-acceptor-donor (AAD), H_2O molecule.

B3LYP/6-31+G* calculations were used to search for several possible conformers and obtain their respective simulated spectra. Calculations reveal seven stable conformers, labeled 4a-4g in Figure 7.7. Relative energies are corrected for zero-point energy. The simulated spectra for conformers 4a-4c simply confirm assignments for bands above 3500 cm^{-1} (see appendix A.9). Simulated spectra for conformers 4d-4g are compared to the IRPD spectrum of $Li^+(H_2O)_4(CH_4)_2$ in Figure 7.8.

The spectrum for conformer 4g contains a feature near 3110 cm^{-1} corresponding to a hydrogen bonded O-H stretching vibrational mode which is completely absent from the IRPD spectrum, thus we rule out its presence in the cluster ion beam. Conformers 4d-4f all contain O-H stretching features which are in reasonable agreement with the IRPD spectrum, with the simulated spectrum for conformer 4d giving the best overall agreement. Also, 4d contains three hydrogen bonded O-H stretching modes between 3300 – 3450 cm^{-1} and is the only calculated spectrum exhibiting the signature free O-H stretching feature of a three-coordinated H_2O molecule which is labeled with an arrow in Figure 7.8. Compared to the results from the previous chapter, we find that the hydrated clusters containing either argon atoms or CH_4 molecules can effectively trap high energy conformers

7.5 Conclusions

IRPD spectra are reported for $Li^+(H_2O)_{1-4}(CH_4)_n$ clusters in the O-H and C-H stretching regions along with supporting B3LYP/6-31+G* calculations. It is established that CH_4 can act as a proton acceptor and form an O-H•••CH_4 hydrogen bond with H_2O based on a ~40 – 70 cm^{-1} shift of the O-H stretching frequency. In turn, the O-H•••CH_4

hydrogen bond, in a cooperative effect with the ion, causes a shift to lower frequency of the C-H stretches of CH_4. However, shifts are greatest for C-H stretches arising from CH_4 molecules in direct contact with the ion.

H_2O•••H_2O hydrogen bonded O-H stretching features are observed in the $Li^+(H_2O)_3(CH_4)_1$ spectrum. The conformer containing a H_2O•••H_2O interaction is calculated to be +19 kJ/mol higher in energy than the minimum energy conformer.

O-H hydrogen bonding features between 3200 – 3450 cm^{-1} and a three-coordinated water free O-H stretching feature appear in the $Li^+(H_2O)_4(CH_4)_2$ spectrum indicating the presence of conformers containing extensive hydrogen bonding. Calculations show that conformers ranging from +29 - +33 kJ/mol higher in energy than the minimum energy conformer may be responsible for these features.

Together, these results imply that high energy conformer trapping is feasible in methanated Li^+ clusters and comparable to argonated clusters reported in Chapter 6 of this thesis. These calculated structures and IRPD spectra lay the foundation to possibly map the potential energy surface and open a door to explore effects of other ligands on hydrated alkali metal ion clusters.

7.6 Figures

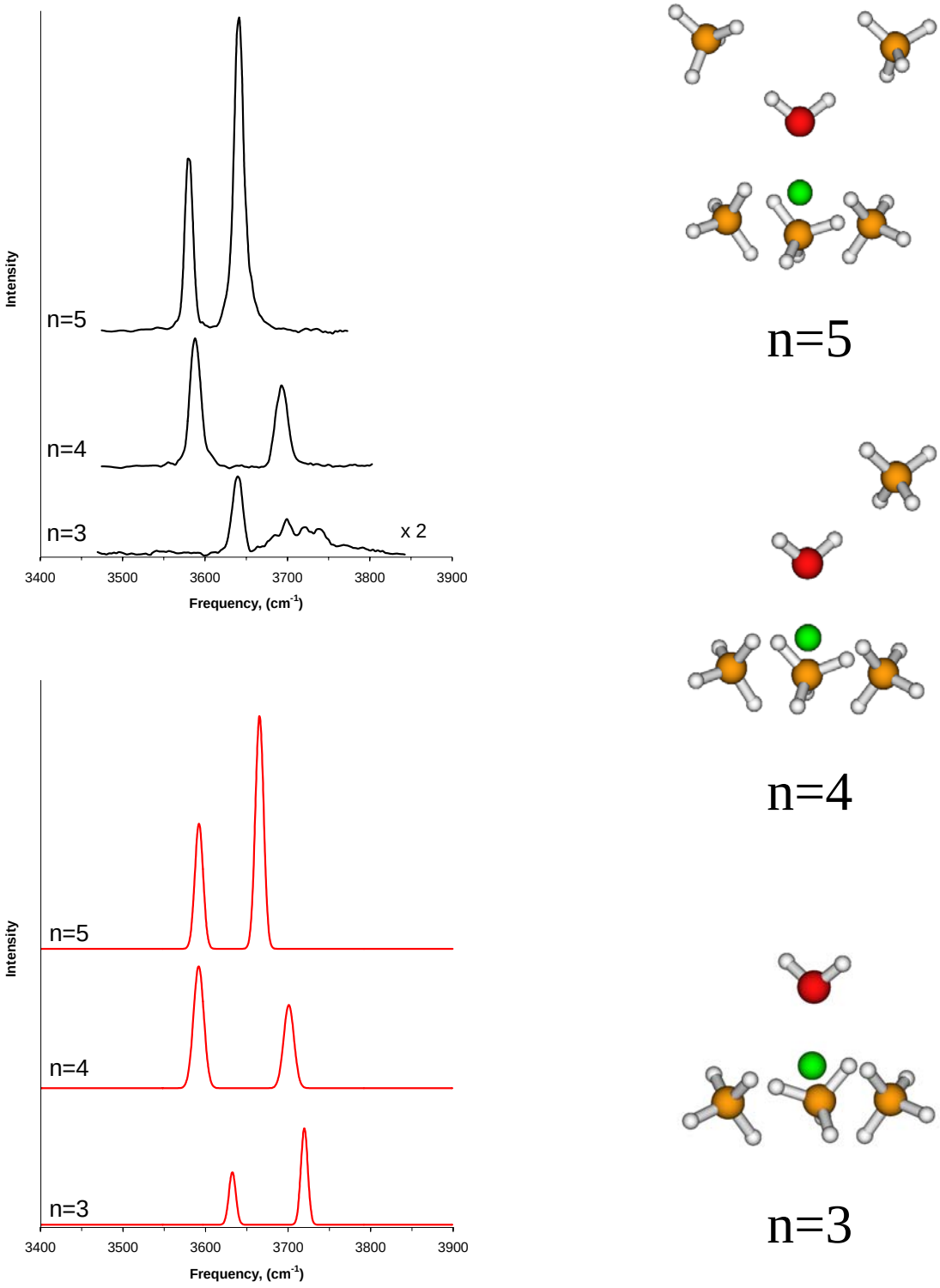

Figure 7.1: IRPD (top) and simulated (bottom) spectra for $Li^{+}(H_2O)_1(CH_4)_n$ clusters along with optimized calculated structures (right) (B3LYP/6-31+G* level calculations).

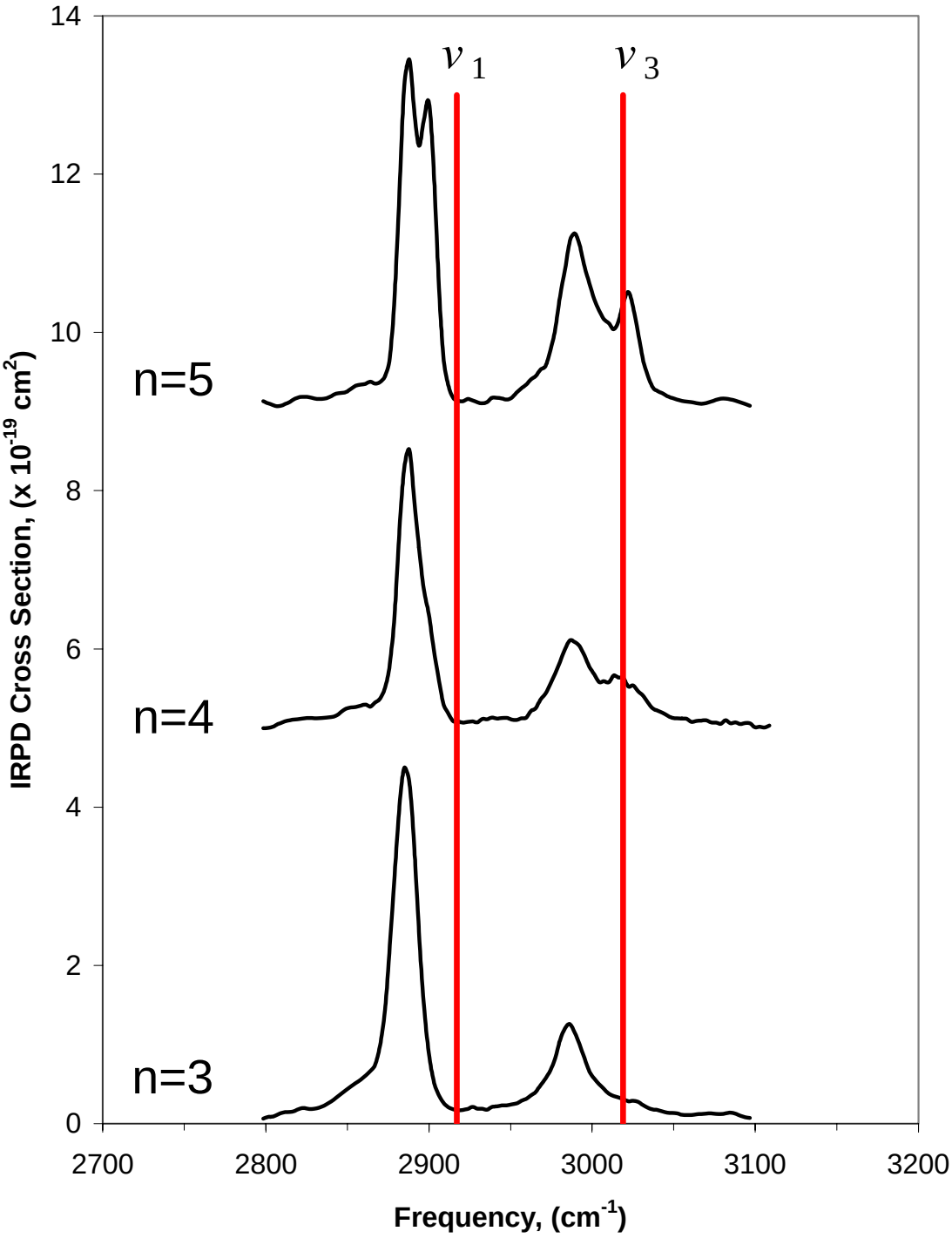

Figure 7.2: IRPD spectra for $Li^+(H_2O)_1(CH_4)_n$, n=3-5, in the C-H stretching region. Neutral CH_4 ν_1 and ν_3 values are labeled.

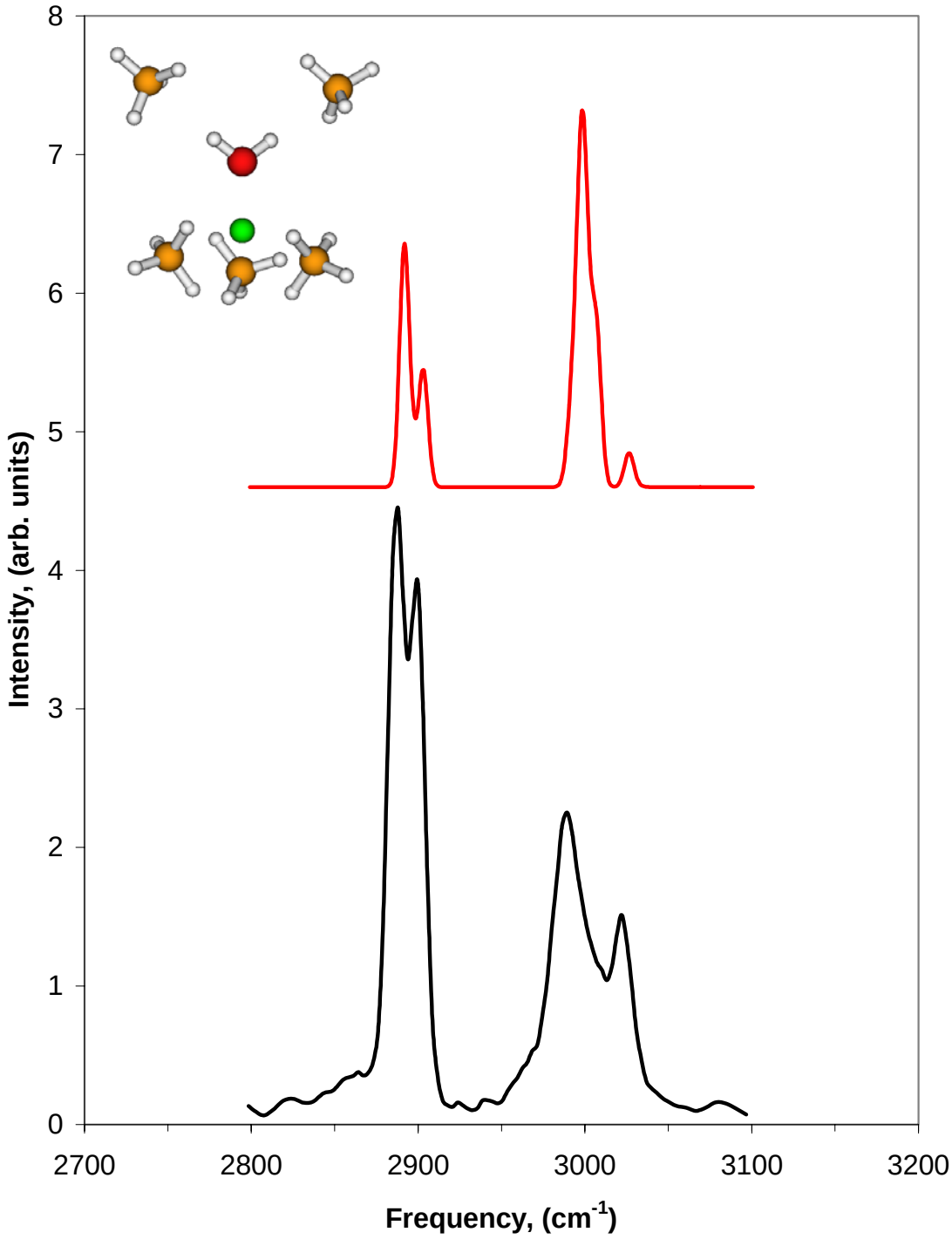

Figure 7.3: IRPD and simulated B3LYP/6-31+G* spectra for $Li^{+}(H_2O)_1(CH_4)_5$ in the C-H stretching region.

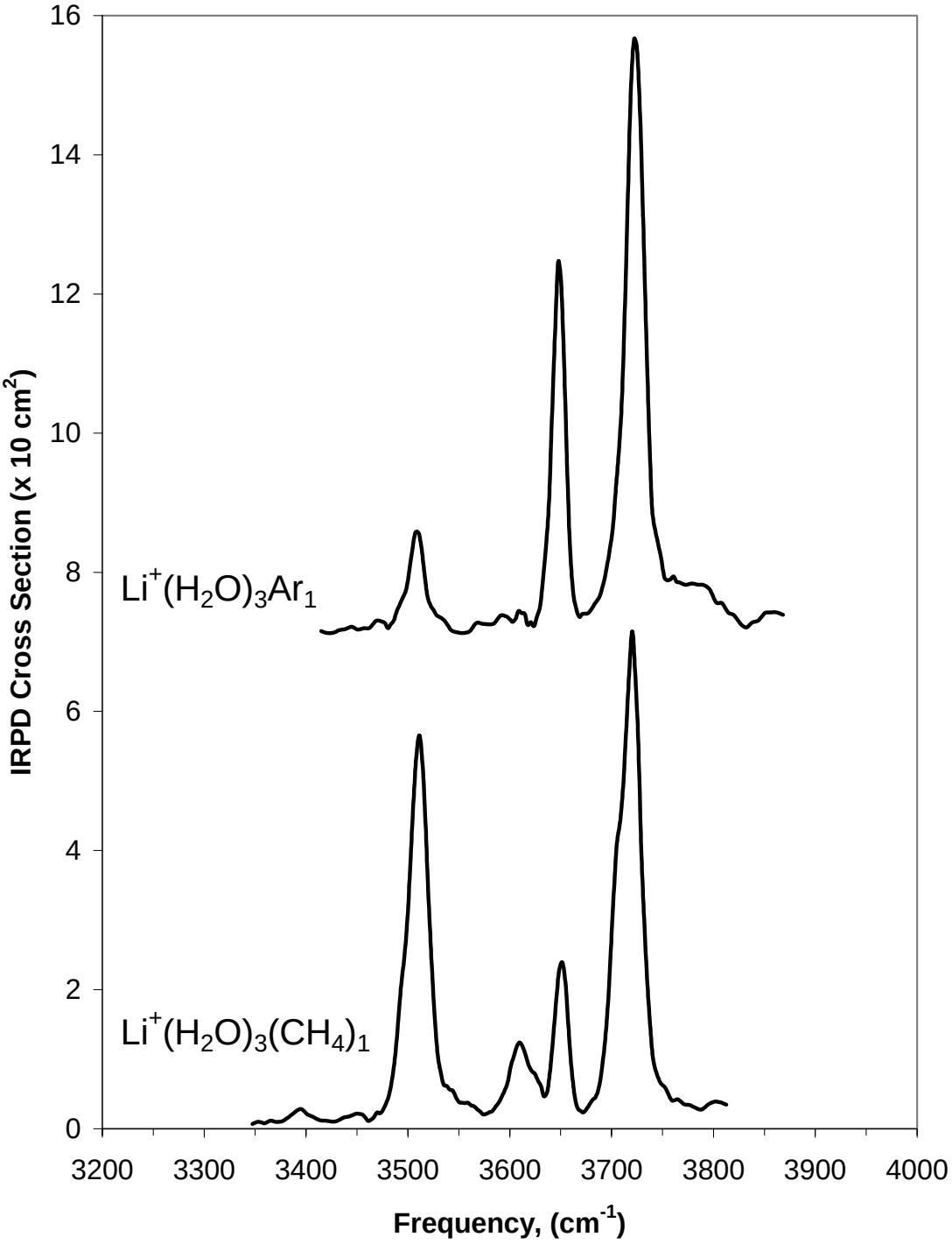

Figure 7.4: IRPD spectra for $Li^+(H_2O)_3(CH_4)_1$ and $Li^+(H_2O)_3Ar_1$.

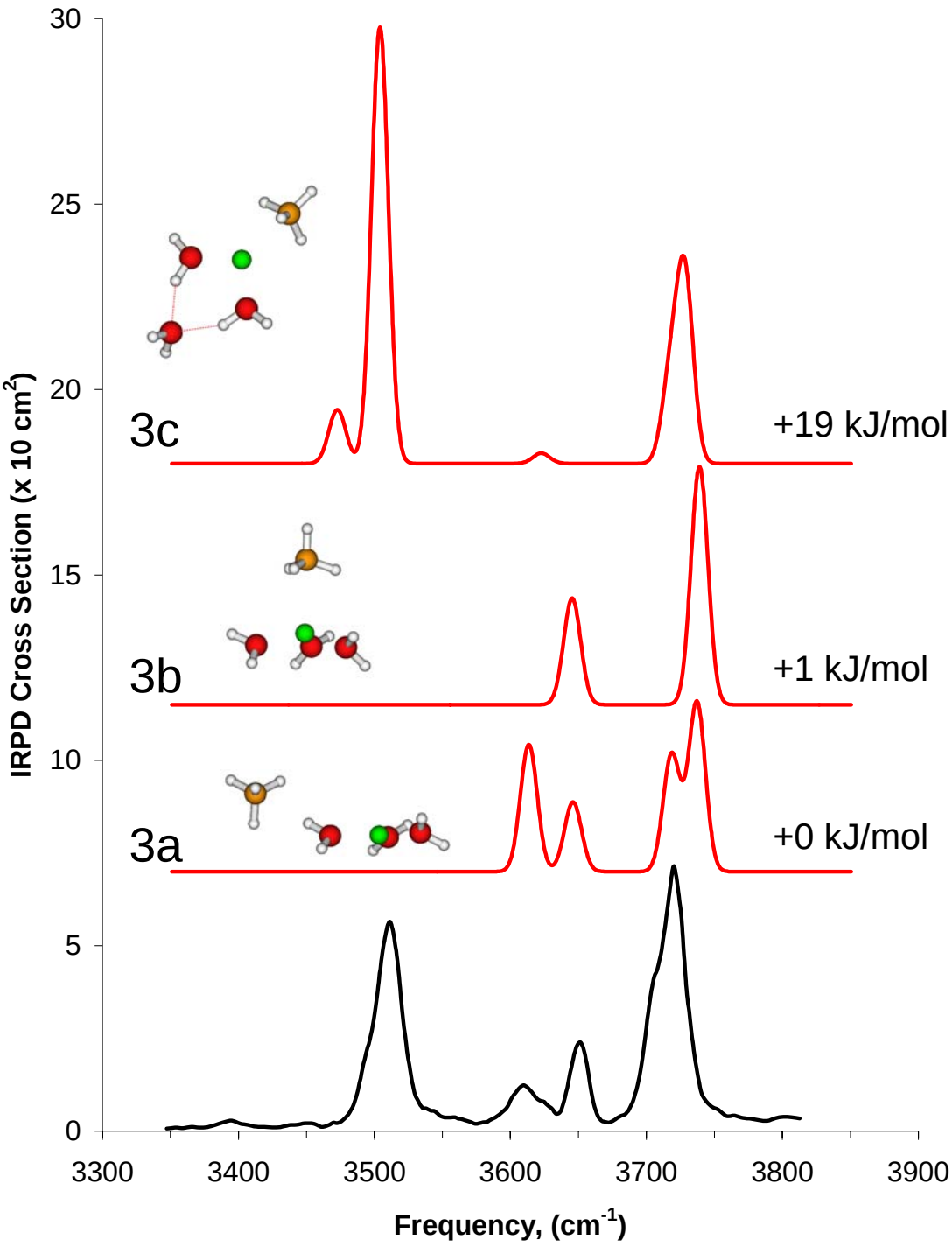

Figure 7.5: IRPD spectrum (black) for $Li^+(H_2O)_3(CH_4)_1$ and simulated (red) B3LYP/6-31+G* spectra for three stable conformers.

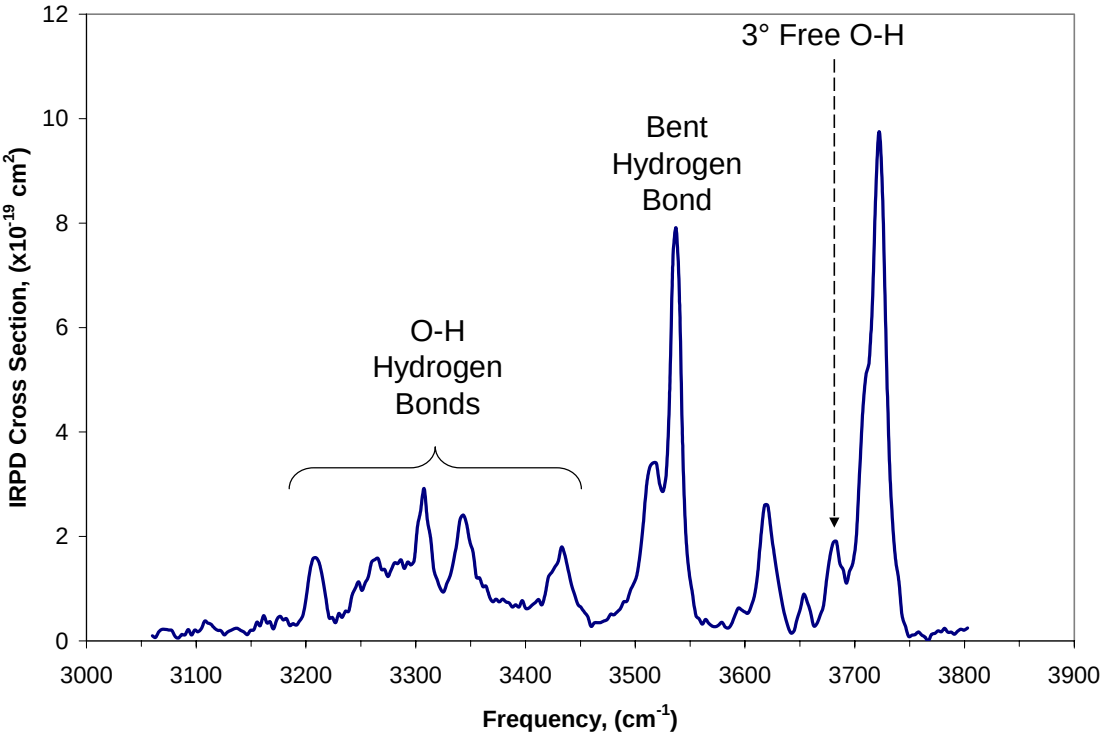

Figure 7.6: IRPD spectrum for $Li^+(H_2O)_4(CH_4)_2$. O-H hydrogen bonded and three-coordinated (3°), AAD, free O-H features are labeled.

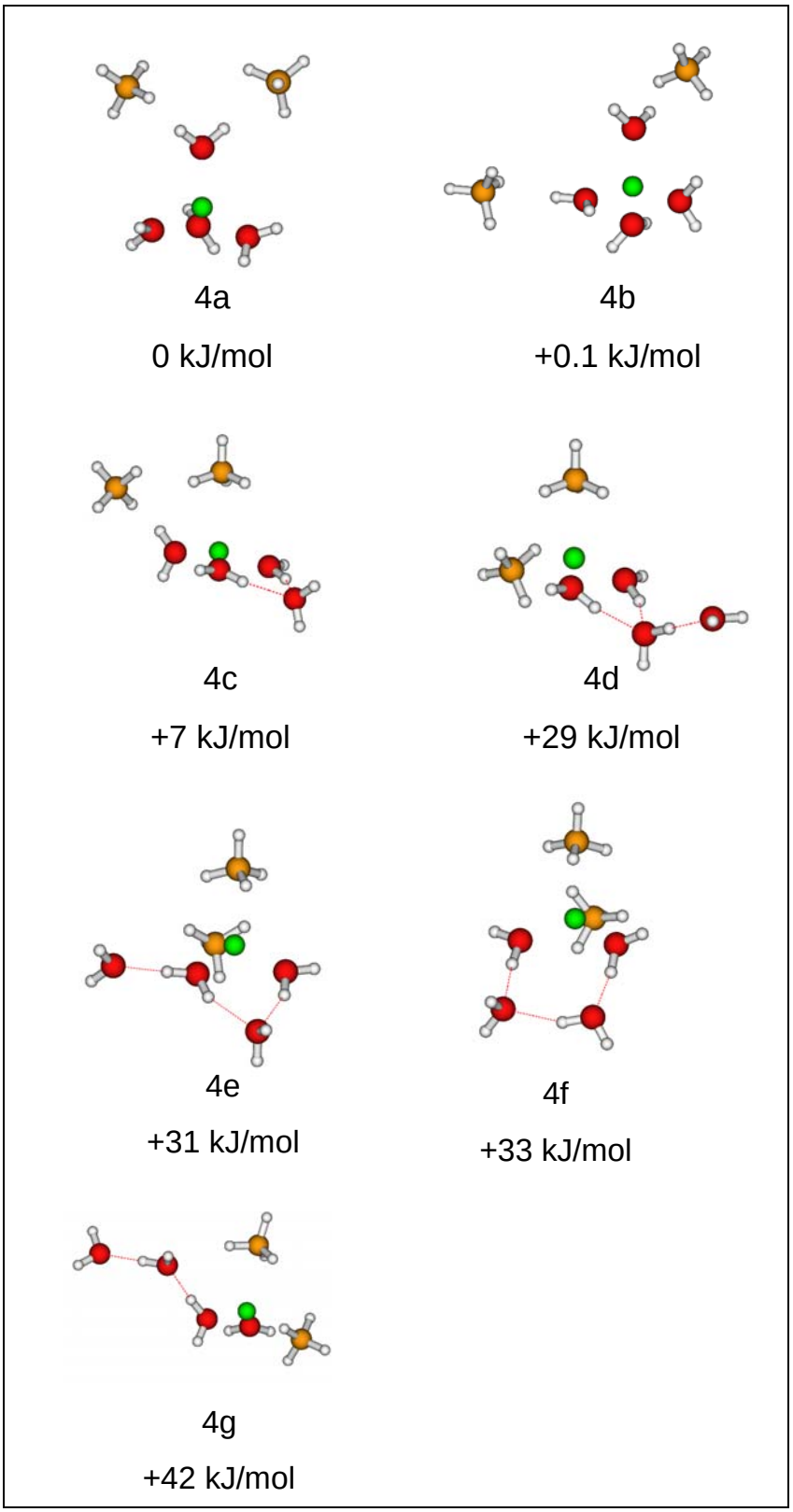

Figure 7.7: Seven stable conformers of $Li^+(H_2O)_4(CH_4)_2$ calculated at the B3LYP/6-31+G* level. Relative energies are corrected for zero-point energy.

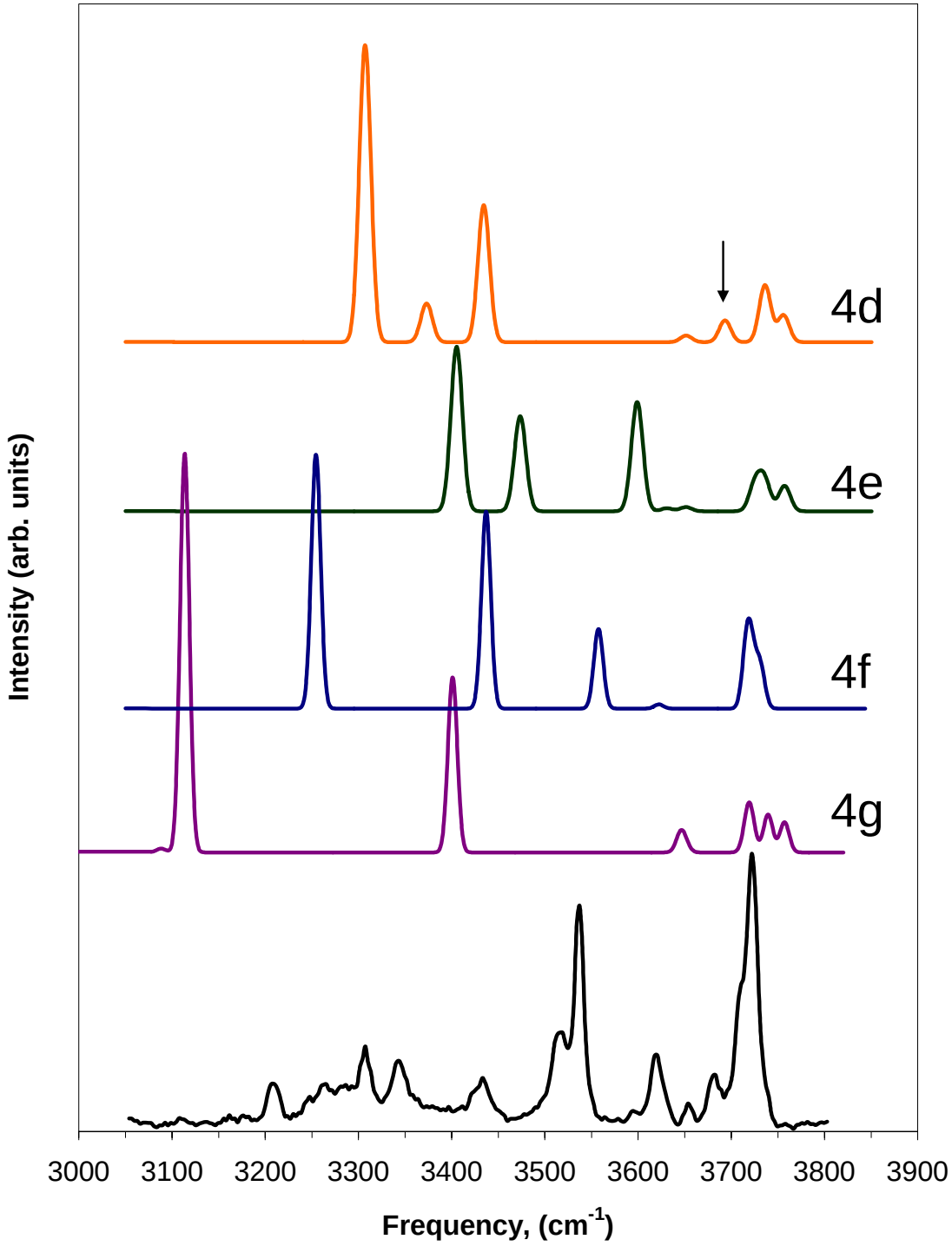

Figure 7.8: IRPD and simulated spectra $Li^+(H_2O)_4(CH_4)_2$. The three-coordinated (3°), AAD, free O-H feature is labeled with an arrow for spectrum 4d

7.7 References

[1] E. D. Sloan, Jr, Clathrate Hydrates of Natural Gases, Marcel Dekker, New York, 1998.
[2] E. D. Sloan. *Energy & Fuels* 12 (1998) 191.
[3] R. A. Kerr. *Science* 303 (2004) 946.
[4] J. J. Novoa, M. Planas, M. C. Rovira. *Chem. Phys. Lett.* 251 (1996) 33.
[5] J. J. Novoa, B. Tarron, M. H. Whangbo, J. M. Williams. *J. Chem. Phys.* 95 (1991) 5179.
[6] M. M. Szczesniak, G. Chalasinski, S. M. Cybulski, P. Cieplak. *J. Chem. Phys.* 98 (1993) 3078.
[7] J. B. L. Martins, J. R. S. Politi, E. Garcia, A. F. A. Vilela, R. Gargano. *J. Phys. Chem. A* 113 (2009) 14818.
[8] B. Raghavendra, E. Arunan. *Chem. Phys. Lett.* 467 (2008) 37.
[9] R. D. Suenram, G. T. Fraser, F. J. Lovas, Y. Kawashima. *J. Chem. Phys.* 101 (1994) 7230.
[10] S. G. Olesen, S. Hammerum. *J. Phys. Chem. A* 113 (2009) 7940.
[11] S. G. Olesen, T. L. Gausco, G. H. Weddle, S. Hammerum, M. A. Johnson. *Mol. Phys.* 108 (2010) 1191.
[12] D. J. Miller, J. M. Lisy. *J. Am. Chem. Soc.* 130 (2008) 15393.
[13] O. Rodriguez, J. M. Lisy. *J. Phys. Chem. A* 115 (2011) 1228.
[14] O. Rodriguez Jr, J. M. Lisy. *Chem. Phys. Lett.* 502 (2011) 145.
[15] D. J. Miller, J. M. Lisy. *J. Am. Chem. Soc.* 130 (2008) 15381.
[16] C. E. Klots. *J. Chem. Phys.* 83 (1985) 5854.
[17] Origin (OriginLab, Northampton, MA), 2003.
[18] J. Kong, C. A. White, A. I. Krylov, C. D. Sherrill, R. D. Adamson, T. R. Furlani, M. S. Lee, A. M. Lee, S. R. Gwaltney, T. R. Adams et al., SPARTAN'02, Wavefunction, Inc., Irvine CA, 2002.
[19] M. J. Frisch, G. W. Trucks, H. B. Schlegel, G. E. Scuseria, M. A. Robb, J. R. Cheeseman, J. A. Montgomery Jr., T. Vreven, K. N. Kudin, J. C. Burant et al., Gaussian 03, Revision B.04, Gaussian, Inc., Pittsburgh, PA, 2003.
[20] S. I. Gorelsky, *SWizard program*, 4.1, University of Ottawa, Canada, 2005.
[21] V. Dryza, E. J. Bieske. *Int. J. Mass Spectrom.* 297 (2010) 46.
[22] B. L. J. Poad, C. D. Thompson, E. J. Bieske. *Chem. Phys.* 346 (2008) 176.
[23] D. R. Lidle, CRC Handbook of Chemistry and Physics, Boca Raton, 2009.

Chapter 8

Ion-Water-Alkane Cluster Ions II: Infrared Spectroscopy of $Li^+(H_2O)_{2-4}(C_6H_{12})_n$ Clusters

8.1 Introduction

In the preceding chapter, we were able to generate and probe high energy $Li^+(H_2O)_{3-4}(CH_4)_n$ conformers containing extensive hydrogen bonding. This was a surprising result since we expected ion•••dipole interactions to dominate in the cluster. But results from CH_4 bearing clusters has changed this paradigm and suggested that including alkanes, like argon reported in chapter 6, in hydrated clusters can cause a significant deviation from what is known about $Li^+(H_2O)_n$ structures. Given the results, it is interesting to delve further into the study of hydrated Li^+ clusters in the presence of hydrocarbons other than CH_4 in order to compare and better understand the role of hydrocarbons in ion hydration.

Cyclohexane, C_6H_{12}, is an intriguing ligand to use in this study. This cyclic alkane is considered an ionophore, or a molecule which selectively binds ions; specifically Li^+.[1-5] Ionophores serve an important role in specific ion transport through membranes and drug delivery in biological systems.[6,7] An ionophore's ion capture or transport capabilities can be greatly enhanced when a cyclohexane ring is part of the complex.[8,9] For example, Suzuki *et al*. reported that the maximum Li^+/Na^+ selectivity ratio (1000:1) was achieved for a 14-crown-4 derivative containing a pair of cyclohexane rings that sandwiched Li^+.[8] Thus, in order for ions in this environment to bind to ionophores, some degree of ion dehydration must take place.

Interestingly, the gas phase Li^+•••cyclohexane interaction energy is ~100 kJ/mol [10] which is comparable to the Li^+•••H_2O interaction energy, ~137 kJ/mol.[11] This suggests there must be a delicate balance between competing non-covalent interactions involving some degree of Li^+ dehydration and leading to a preferred Li^+•••ionophore complex. While condensed- and gas-phase properties can differ, gas phase infrared presdissociation spectroscopy allows us to study non-covalent interactions in cluster ions while controlling the number, and nature, of solvating ligands.[12,13] Thus, an investigation of ion•••water, ion•••cyclohexane, water•••water, and water•••cyclohexane interactions is carried out in order to gauge the effects of cyclohexane in a hydrated Li^+ clusters.

8.2 Experimental Methods

Infrared predissociation (IRPD) spectroscopy is used to analyze $Li^+(H_2O)_{2\text{-}4}(C_6H_{12})_n$ cluster ions using a triple quadrupole apparatus and IR laser. The details of our apparatus have been described in Chapter 2 of this Thesis and elsewhere.[13-15] Briefly, water and cyclohexane vapor are carried by argon gas and introduced into the source chamber through a 30°, 180 μm conical nozzle. A neutral cyclohexane-water-argon cluster beam is formed by supersonic expansion. About 100 nozzle diameters downstream from the nozzle exit, lithium ions ejected from a homemade ion gun consisting of a tungsten filament coated with a LiCl paste perpendicularly intersect the neutral clusters forming unstable cluster ions. The collision and solvation energy is dissipated by evaporative cooling [16] until the cluster ion is quasi-stable. The cluster ion beam is skimmed into a differentially pumped chamber,

guided through an R.F. only octopole ion guide, and into the detection chamber. Here the cluster ion of interest is mass selected in the first quadrupole and allowed to pass to the second, R.F. only, quadrupole where they can interact with photons from a pulsed, tunable infrared laser (Laservision OPO/OPA pumped by a 1064 nm output of a Surelite II 10 Hz Continuum Nd:YAG laser). If on resonance with a vibrational mode of the cluster ion, absorption of a photon can occur. The imparted energy causes the most labile ligand to fragment. The third quadrupole is tuned to the mass of the fragment ion allowing it to pass and be detected.

Spectra are reported as photodissociation cross sections (corrected for laser fluence) as a function of laser frequency, which is stepped in 3 cm^{-1} increments. Absolute frequency calibration is achieved by simultaneously acquiring a photoacoustic spectrum of ambient water vapor.

8.3 Computational Methods

DFT calculations at the B3LYP/6-31+G* level were carried out to support experimental data. Initial geometries generated using Spartan 02 [17] were allowed to optimize using Gaussian 03 [18] to obtain structures, relative energies (corrected for zero-point energy) and vibrational frequencies. Simulated spectra were generated using SWizard.[19] Calculated O-H stretching frequencies were scaled by 0.9758 to match neutral H_2O values.

8.4 Results and Discussion

IRPD spectra in the O-H stretching region for $Li^+(H_2O)_2(C_6H_{12})_n$ are shown in Figure 8.1. Two bands at 3645 cm^{-1} and 3720 cm^{-1} in the n=1 spectrum correspond to the H_2O symmetric and asymmetric stretches respectively. There are no features appearing below 3645 cm^{-1} indicating the absence of O-H hydrogen bonded stretching modes. Thus we conclude all molecules are located in the first solvent shell. Upon addition of a second C_6H_{12} molecule, a new feature appears near 3576 cm^{-1}. This feature is consistent with a weak O-H•••CH_4 hydrogen bonded features reported ~3588 – 3615 cm^{-1} in the previous chapter of this Thesis for $Li^+(H_2O)_{1-4}(CH_4)_n$ clusters. The O-H•••C_6H_{12} hydrogen bond is slightly stronger than that for O-H•••CH_4 based on the greater shift to lower frequency. However, the O-H•••C_6H_{12} hydrogen bonded feature is only a minor band, while the H_2O symmetric and asymmetric stretches dominate the n=2 spectrum. It is likely that the principal conformer responsible for the spectral features contains all four molecules in the first shell for n=2.

The IRPD spectrum for $Li^+(H_2O)_3(C_6H_{12})_1$ in the O-H stretching region is shown at the bottom of Figure 8.2 and has a striking resemblance to the $Li^+(H_2O)_3Ar_1$ and $Li^+(H_2O)_3(CH_4)_1$ spectra reported in the two previous chapters and shown in Figure 8.2 to compare. The features can be easily assigned since the band assignments for the argonated and methanated spectra were reported earlier in this Thesis. The bands in the $Li^+(H_2O)_3(C_6H_{12})_1$ spectrum at 3523 cm^{-1} and 3609 cm^{-1} correspond to water bent- and O-H•••C_6H_{12} hydrogen bonds respectively (see appendix A.10 for simulated spectra of three stable structures shown to support the band assignments). Of the three spectra, the bent hydrogen bonded feature in the $Li^+(H_2O)_3Ar_1$ spectrum is shifted lowest in

frequency. The reason for this lays in the strength of the Li^+•••(C_6H_{12}/CH_4/Ar) interaction. In the conformers containing the bent hydrogen bonded structure, C_6H_{12}, CH_4, or Ar resides in the first shell (see chapters 6 and 7). Of the three ligands, Ar interacts weakest with Li^+, thus the ion can interact strongest with the water motif hence strengthening the hydrogen bonded structure and causing the largest hydrogen bonded O-H red shift.

Three optimized structures for $Li^+(H_2O)_3(C_6H_{12})_1$ are shown in Figure 8.3 along with zero-point energy corrected relative energies. Interestingly, the conformer containing the hydrogen bonded motif, 3c, is 20 kJ/mol higher in energy than the minimum energy conformer and essentially identical to the relative energy reported in chapter 7 for the $Li^+(H_2O)_3(CH_4)_1$ conformer containing the same hydrogen bonded motif. This, together with similar IRPD spectra, indicates that C_6H_{12} and CH_4 have similar high energy conformer trapping effects.

The IRPD spectrum for $Li^+(H_2O)_4(C_6H_{12})_2$ in the O-H stretching region is shown at the bottom of Figure 8.4 and is more complex compared to the spectra shown thus far in this chapter. However, the spectrum closely resembles the $Li^+(H_2O)_4(CH_4)_2$ spectrum reported in the previous chapter of this Thesis. Therefore it is reasonable to estimate that water structural motifs giving rise to features in the $Li^+(H_2O)_4(C_6H_{12})_2$ spectrum are similar to those reported for $Li^+(H_2O)_4(CH_4)_2$.

Because of the complexity and size of the $Li^+(H_2O)_4(C_6H_{12})_2$ system, an exhaustive computational search for all possible conformers was not undertaken, however, several stable structures, were calculated which are shown in Figure 8.5 accompanied by their respective relative energies (simulated spectra for these structures

are shown in appendix A.11). While it is difficult to definitively assign each band using the simulated spectra, it can be concluded based on what has been reported in the preceding two chapters of this Thesis that the features below 3600 cm^{-1} originate from extensive hydrogen bonding which appear to be present in high energy (>20 kJ/mol) $Li^+(H_2O)_4(C_6H_{12})_2$ conformers. This is more evidence that C_6H_{12} can effectively trap high energy conformers in hydrated systems.

8.5 Conclusions

IRPD spectra in the O-H stretching region and DFT calculations for $Li^+(H_2O)_{2\text{-}4}(C_6H_{12})_n$ are reported. O-H stretching features shifted to lower frequency relative to the O-H symmetric stretch suggest that C_6H_{12} can act as a proton acceptor, forming an O-H•••C_6H_{12} hydrogen bond. The frequency shift is larger compared to a similar interaction reported for O-H•••CH_4 in the previous chapter of this Thesis indicating that the O-H•••C_6H_{12} interaction is stronger.

For $Li^+(H_2O)_3(C_6H_{12})_1$, a feature corresponding to a H_2O bent hydrogen bonded O-H stretching mode appears in the IRPD spectrum. Calculations reveal a conformer with the bent hydrogen bonded motif is +20 kJ/mol higher in energy than the global minimum energy conformer. Similarly, the IRPD spectrum and calculations for $Li^+(H_2O)_4(C_6H_{12})_2$ suggests that high energy conformers (>20 kJ/mol) containing extensive hydrogen bonding are present in the cluster ion beam. Interestingly, the IRPD spectra shown for $Li^+(H_2O)_3(C_6H_{12})_1$ and $Li^+(H_2O)_4(C_6H_{12})_2$ are similar to the $Li^+(H_2O)_3(CH_4)_1$ and $Li^+(H_2O)_4(CH_4)_2$ reported in the previous chapter of this Thesis.

Thus, it can be concluded that these hydrocarbons act very similarly in effectively trapping high energy conformers containing $H_2O•••H_2O$ hydrogen bonding. The spectra and calculations presented in this, and in the previous two chapters of this Thesis, will be a useful foundation leading to a better understanding of a particular ligand's role in high energy conformer trapping in cluster ions.

8.6 Figures

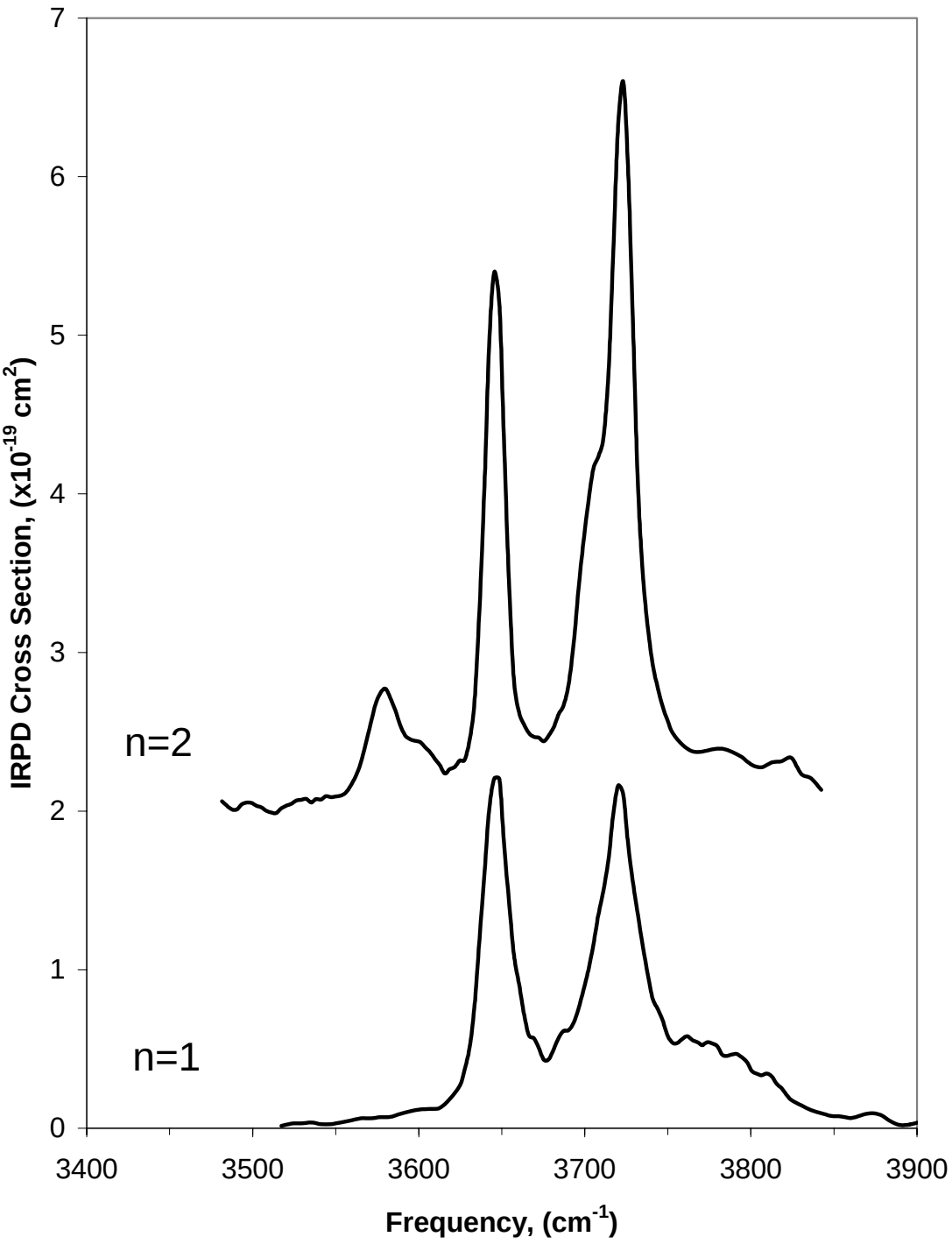

Figure 8.1: IRPD spectra for $Li^+(H_2O)_2(C_6H_{12})_n$ in the O-H stretching region.

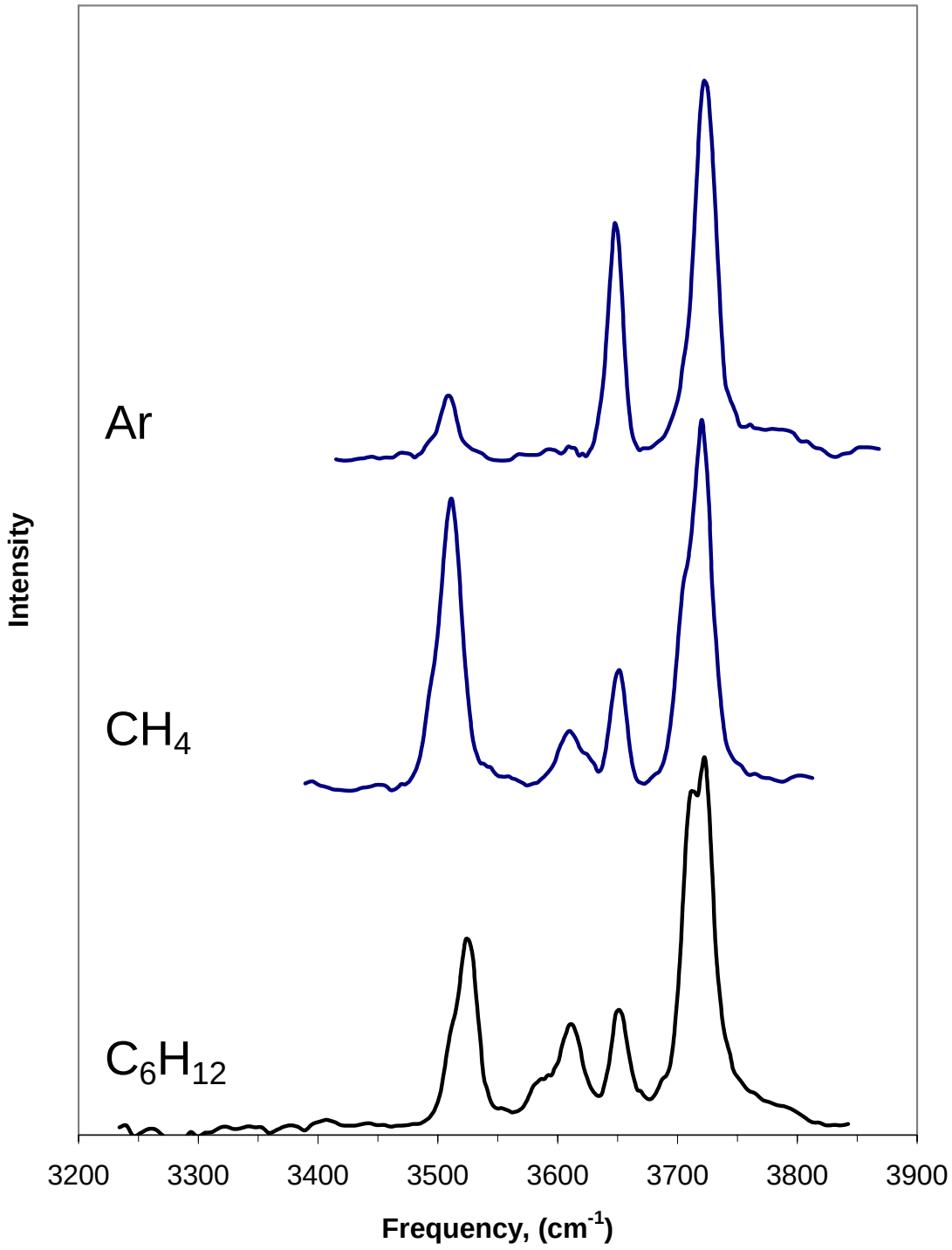

Figure 8.2: IRPD spectra for $Li^+(H_2O)_3(L)_1$, L=Ar, CH_4, and C_6H_{12}, in the O-H stretching region scaled so that the most intense peak in each spectrum has the same maximum intensity.

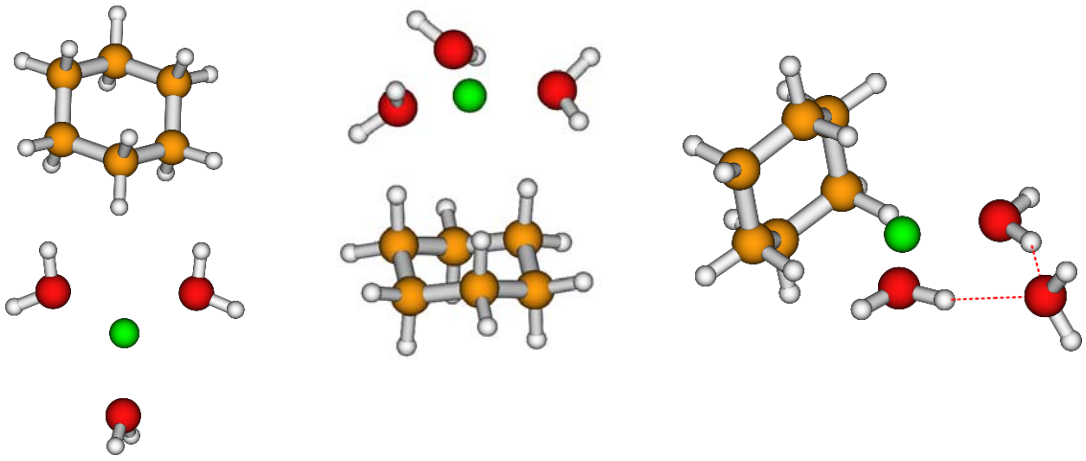

3a	3b	3c
+0 kJ/mol	+5 kJ/mol	+20 kJ/mol

Figure 8.3: Optimized structures for $Li^{+}(H_2O)_3(C_6H_{12})_1$ calculated at the B3LYP/6-31+G* level. Relative energies are corrected for zero-point energy.

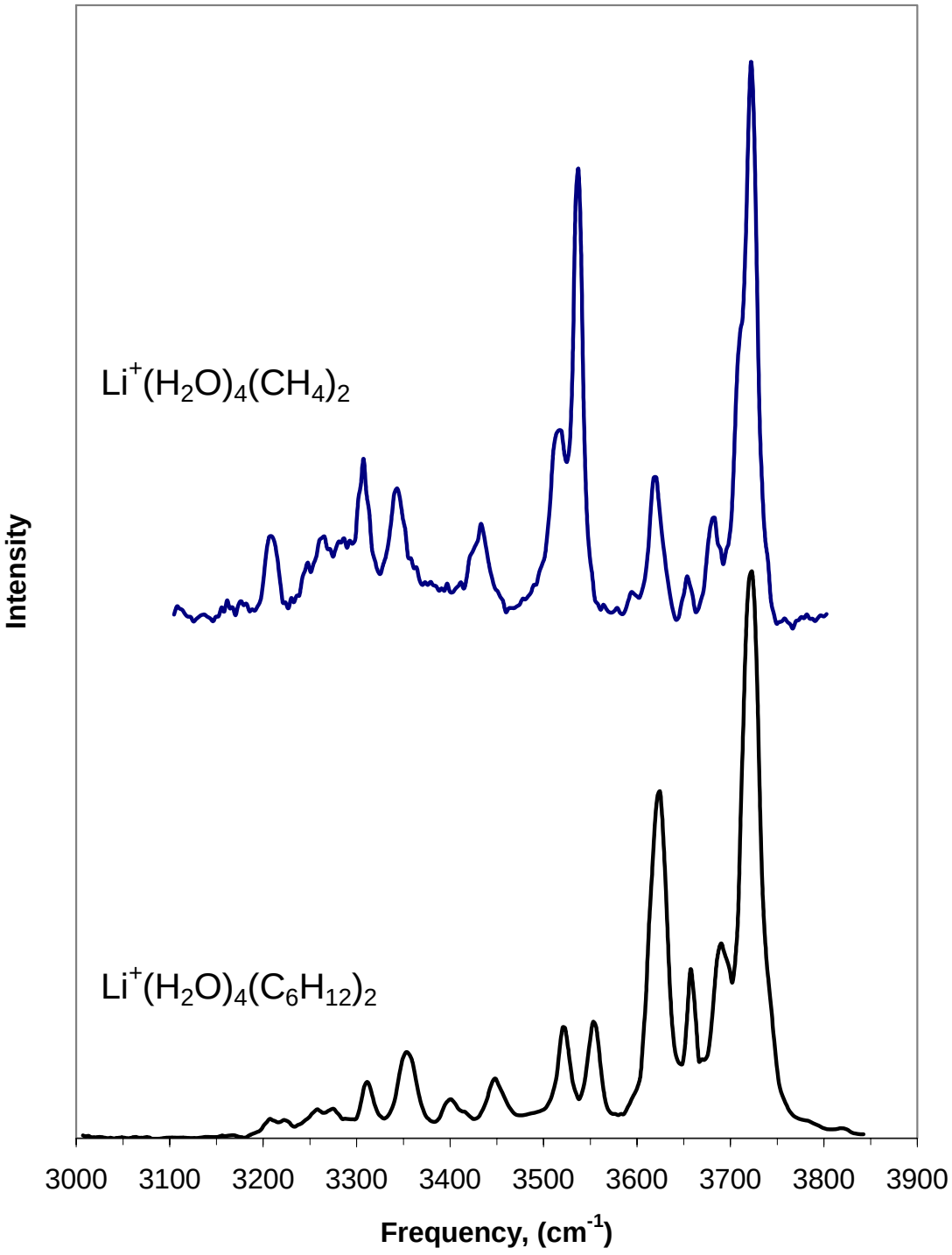

Figure 8.4: IRPD spectra for $Li^+(H_2O)_4(L)_2$, L=CH_4 and C_6H_{12}, in the O-H stretching region. Spectra are scaled so that the most intense peak has the same maximum intensity.

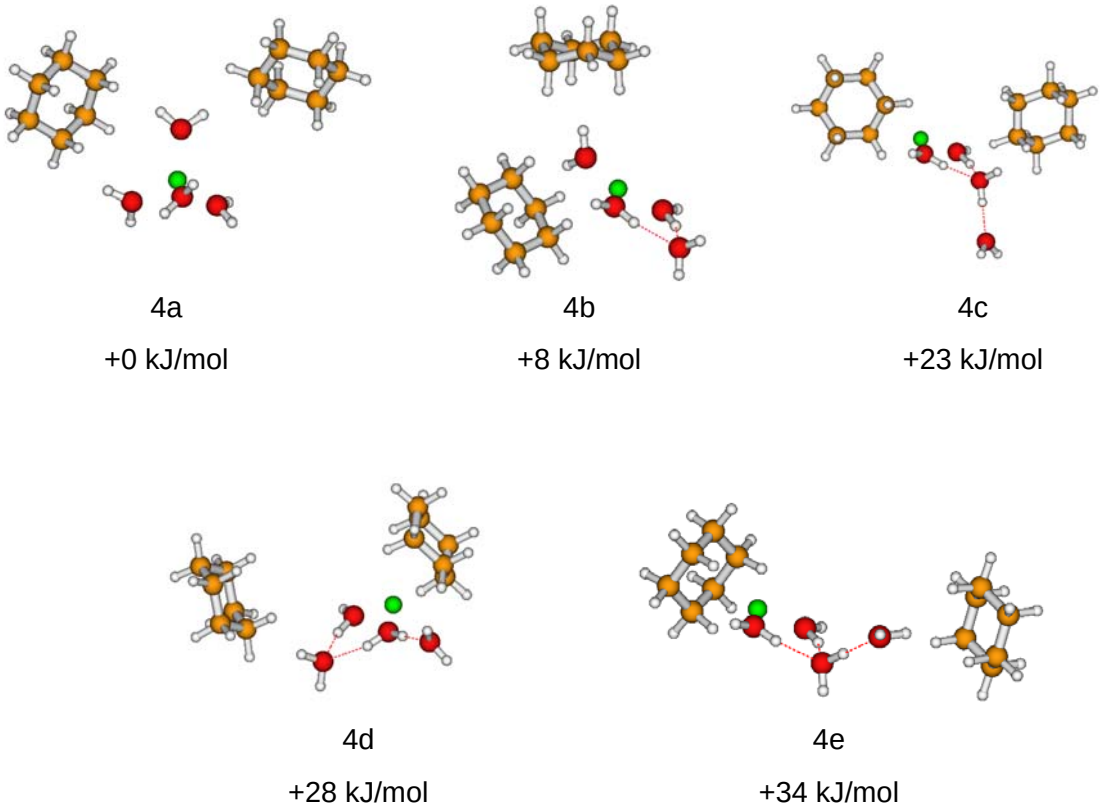

Figure 8.5: Optimized structures for $Li^{+}(H_2O)_4(C_6H_{12})_2$ calculated at the B3LYP/6-31+G* level. Relative energies are corrected for zero-point energy.

8.7 References

[1] R. M. Izatt, J. S. Bradshaw, S. A. Nielsen, J. D. Lamb, J. J. Christensen, D. Sen. *Chem. Rev.* 85 (1985) 271.
[2] R. M. Izatt, J. S. Bradshaw, K. Pawlak, R. L. Bruening, B. J. Tarbet. *Chem. Rev.* 92 (1992) 1261.
[3] R. M. Izatt, K. Pawlak, J. S. Bradshaw, R. L. Bruening. *Chem. Rev.* 91 (1991) 1721.
[4] R. M. Izatt, K. Pawlak, J. S. Bradshaw, R. L. Bruening. *Chem. Rev.* 95 (1995) 2529.
[5] G. N. Patwari, J. M. Lisy. *J. Phys. Chem. A* 111 (2007) 7585.
[6] M. J. Friedrich. *JAMA, J. Am. Med. Assoc.* 281 (1999) 2271.
[7] J. C. Soares, S. Gershon. *Neuropsychopharmacology* 19 (1998)
[8] K. Suzuki, H. Yamada, K. Sato, K. Watanabe, H. Hisamoto, Y. Tobe, K. Kobiro. *Anal. Chem.* 65 (1993) 3404.
[9] S. Tsurubou, S. Umetani, Y. Komatsu. *Anal. Chim. Acta* 394 (1999) 317.
[10] R. H. Staley, J. L. Beauchamp. *J. Am. Chem. Soc.* 97 (1975) 5920.
[11] M. T. Rodgers, P. B. Armentrout. *J. Phys. Chem. A* 101 (1997) 1238.
[12] M. A. Duncan. *Int. Rev. Phys. Chem.* 22 (2003) 407.
[13] J. M. Lisy. *Int. Rev. Phys. Chem.* 16 (1997) 267.
[14] D. J. Miller, J. M. Lisy. *J. Am. Chem. Soc.* 130 (2008) 15393.
[15] D. J. Miller, J. M. Lisy. *J. Am. Chem. Soc.* 130 (2008) 15381.
[16] C. E. Klots. *J. Chem. Phys.* 83 (1985) 5854.
[17] J. Kong, C. A. White, A. I. Krylov, C. D. Sherrill, R. D. Adamson, T. R. Furlani, M. S. Lee, A. M. Lee, S. R. Gwaltney, T. R. Adams et al., SPARTAN'02, Wavefunction, Inc., Irvine CA, 2002.
[18] M. J. Frisch, G. W. Trucks, H. B. Schlegel, G. E. Scuseria, M. A. Robb, J. R. Cheeseman, J. A. Montgomery Jr., T. Vreven, K. N. Kudin, J. C. Burant et al., Gaussian 03, Revision B.04, Gaussian, Inc., Pittsburgh, PA, 2003.
[19] S. I. Gorelsky, *SWizard program*, 4.1, University of Ottawa, Canada, 2005.

Chapter 9

Ion-Water-Alkane Cluster Ions III: Infrared Spectroscopy of $Cl^-(Water)_{1-3}(CH_4)_n$ Clusters

9.1 Introduction

The first infrared predissociation (IRPD) spectra of Cl^- solvated by methane were obtained by Bieske and co-workers.[1] Methane is an intriguing solvating ligand because CH_4•••CH_4 non-covalent interactions are relatively weak, ~1 – 2 kJ/mol [2,3], thus direct ion•••CH_4 electrostatic interactions can be probed without significant interference from CH_4•••CH_4 interactions or hydrogen bonding.

In $X^-(CH_4)_n$, X=F, Cl, and Br, clusters, ion•••CH_4 interaction strengths are dependent on ion size and charge density, and trend as $F^- > Cl^- > Br^-$.[1,4-7] Methane molecules were reported to bind via a single X^-•••H-C ionic hydrogen bond (IHB), or η_1 configuration, which lowers methane's tetrahedral symmetry to C_{3v} symmetry. Spectroscopically, the IR inactive, totally symmetric, ν_1, mode was rendered infrared active and red shifted, with the ionic hydrogen bond supplying the principal intensity. The triply degenerate, ν_3, (perpendicular transition) mode, was split into a doubly degenerate and single mode of *e* and a_1 symmetries, respectively. Both of these modes were red shifted. Furthermore, MP2 level calculations indicated that methane molecules attract charge density and asymmetrically solvate the ion.[1]

Asymmetric, or surface, solvation is common in Cl^- containing clusters and has been thoroughly studied experimentally and computationally for several solvating ligands.[8-16] When the solvating ligands are polar, asymmetric solvation can result in

ligand•••ligand interaction. In the case of $Cl^-(H_2O)_2$, each water molecule donates a hydrogen to Cl^- forming two ionic hydrogen bonds while an O-H•••O-H hydrogen bond forms between the two waters.[9] Furthermore, experimental and calculated results of $Cl^-(H_2O)_3$ clusters indicate that a cyclic water trimer motif is preferred wherein three water molecules each form an ionic hydrogen bond with the remaining O-H oscillators forming a hydrogen bonded ring structure.[8,13,15-17]

It is noteworthy to mention the extensive work by Johnson and co-workers on the $Cl^-(H_2O)_1$ complex [18-23] wherein the ionic hydrogen bond appears at 3130 cm^{-1}, displaying a shift to lower frequency of over -500 cm^{-1}. When CCl_4 molecules are added to the cluster, this perturbation is significantly reduced by about 80-100 cm^{-1}/CCl_4 molecule.[24]

In chapter 7 of this Thesis, we reported the effects that occur when methane is included in hydrated alkali metal ion clusters. Since eloquent work has been reported on the solvation of Cl^- by methane and by water in separate studies, a natural next step is to extend the investigation to include the solvation of Cl^- by methane and water simultaneously.

9.2 Experimental Methods

Infrared predissociation (IRPD) spectra were obtained using a triple quadrupole apparatus and tunable infrared laser. Details of our experimental apparatus are reported in chapter 2 of this Thesis and elsewhere. [25-27] First, ~0.5% CH_4 and ~2% H_2O gases are seeded in argon gas and introduced into a source chamber through a 30°, 180 μm conical nozzle. Upon exiting the nozzle, neutral clusters are formed via supersonic expansion.

About 100 nozzle diameters downstream from the nozzle exit, ions, ejected by thermionic emission from a homemade filament coated with a chloride paste, perpendicularly intersect and collide with neutral clusters forming hot, unstable clusters. Cluster ions stabilize by evaporative cooling [28] until the lifetime of the clusters exceed the time required to transverse the apparatus. Quasi-stable clusters pass through a R.F. only octopole ion guide leading to the detector chamber which houses three quadrupoles. The cluster of interest is mass selected in the first quadrupole and allowed to pass into a second, r.f. only, quadrupole. Here the cluster can interact with the output of a counter-propagating pulsed, tunable infrared laser (Laservision OPO/OPA pumped by a 1064 nm output of a Surelite II 10 Hz Continuum Nd:YAG laser). If on resonance with a vibrational mode of the cluster ion, absorption of a photon can occur. Imparted photon energy can cause one, or more, ligands to fragment from the cluster ion. The third quadrupole is strategically tuned to mass select of the fragment ion which is allowed to pass and is detected by a conversion dynode and channeltron electron multiplier.

Spectra are obtained by scanning in 3 cm^{-1} increments and reporting the photodissociation cross section (correct for laser fluence) versus laser frequency. Absolute frequency calibration is achieved by simultaneously recording a photoacoustic spectrum of atmospheric water for O-H stretching region data and obtaining a reference spectrum of HCl for C-H stretching region data. Spectral features were fitted using Origin 7.5 [29] software to obtain peak frequencies.

9.3 Computational Methods

Calculations were carried out at the MP2/aug-cc-pVDZ level. Briefly, initial structures were generated using SPARTAN 02 [30] and geometries were allowed to optimize using GAUSSIAN 03 [31] to obtain structures and vibrational frequencies. Simulated spectra were generated using SWizard [32] software and O-H, C-H, and O-D vibrational frequencies were scaled by 0.9577, 0.9471, and 0.9695 to match neutral H_2O, CH_4, and D_2O values respectively.

9.4 Results and Discussion

The IRPD and calculated spectra of $Cl^-(H_2O)_1(CH_4)_1$ are shown in Figure 9.1. The calculated spectrum (MP2/aug-cc-pVDZ level) agrees well with the experiment. Peak assignments for all bands are listed in Table 9.1 along with previously reported experimental vibrational frequencies of $Cl^-(CH_4)_1$ [1] and $Cl^-(H_2O)_1Ar_3$. [18] The $Cl^-(H_2O)_1(CH_4)_1$ spectrum is dominated by a Cl^-•••H-O ionic hydrogen bond (IHB) at 3165 cm^{-1} while the bend overtone (B) and IHB+IW (ion•••H_2O intermolecular stretch) combination band borrow intensity from the IHB. Most notably, the presence of the CH_4 molecule has modestly weakened Cl^-•••H_2O electrostatic interaction as evident by the shift to higher frequencies of each band compared to the $Cl^-(H_2O)_1Ar_3$ values given in Table 9.1. The effect is not as dramatic as reported for $Cl^-(H_2O)_1(CCl_4)_1$ where the IHB overlaps with the bend overtone.[24]

In the C-H stretching region, the CH_4 ν_1 (IHB) and ν_3(e) bands are shifted 14 cm^{-1} and 13 cm^{-1} higher in frequency relative to the Cl^-•••CH_4 dimer frequencies reported by

Bieske and co-workers [1] (see Table 9.1), confirming the presence of H_2O weakens the Cl^-•••CH_4 electrostatic interaction.

Deuteration was necessary to circumvent the problem of overlapping masses of clusters upon the addition of CH_4. Therefore, D_2O complexes will be discussed for the reminder of this chapter. Unfortunately, O-D stretching modes in some clusters can appear below our minimum laser frequency, ~2600 cm^{-1} and were not detected.

An IRPD spectrum of $Cl^-(D_2O)_1(CH_4)_1$ is shown in the middle of Figure 9.2. The CH_4 ν_1 (IHB) and ν_3(e) bands appear at essentially the same frequencies, 2892 cm^{-1} and 2997 cm^{-1} respectively, mentioned earlier for $Cl^-(H_2O)_1(CH_4)_1$. The weak feature at 2739 cm^{-1} corresponds to a free O-D stretching mode which is near the value reported previously for $Cl^-(D_2O)_1$, 2737cm^{-1}.[21] A simulated spectrum of the $Cl^-(D_2O)_1(CH_4)_1$ complex is shown at the bottom of Figure 9.2 and agrees with the IRPD spectrum and confirms our assignments. The intense peak near 2400 cm^{-1} corresponds to the O-H IHB and is out of our laser frequency range.

An IRPD spectrum for $Cl^-(D_2O)_1(CH_4)_3$ is shown at the top of Figure 9.2. The free O-D feature is unshifted compared to n=1. This is consistent with reports by Johnson and co-workers who suggest that free O-D (and free O-H) stretching modes are insensitive to their environment when the D_2O (or H_2O) is involved in an ionic hydrogen bond.[21] The C-H stretching features are also unshifted from the n=1 to n=3 spectrum. This is counter intuitive as one might expect a gradual shift to higher frequencies as more CH_4 molecules are added which should weaken the ion•••CH_4 interaction. However, Bieske and coworkers reported a gradual blue shift of the ν_1 band for $Cl^-(CH_4)_n$, n=2-10, relative to the n=1 spectrum, as CH_4 molecules are systematically added until an

asymptotic frequency limit is reached at 2888 cm^{-1} for $Cl^-(CH_4)_{10}$, [1] which is similar to the CH_4 ν_1 frequency, 2892 cm^{-1}, for $Cl^-(D_2O)_1(CH_4)_1$. This implies that the Cl^-•••CH_4 electrostatic interaction is comparable in $Cl^-(CH_4)_{10}$ and $Cl^-(D_2O)_1(CH_4)_1$ clusters.

An IRPD spectrum for $Cl^-(D_2O)_2(CH_4)_1$ is shown in Figure 9.3 (see appendix A.12 for full $Cl^-(D_2O)_2(CH_4)_n$ IRPD spectra summary in the O-D stretching region). Two bands in the O-D stretching region appear at 2695 cm^{-1} and 2731 cm^{-1} while features above 2800 cm^{-1} arise from C-H stretching modes. The calculated spectrum for $Cl^-(D_2O)_2(CH_4)_1$ is shown in the bottom of Figure 9.3 and agrees with the experimental spectrum in the frequency range where experimental data was obtained. According to the optimized MP2/aug-cc-pVDZ level structure (see Figure 9.3), both D_2O molecules donate a single proton to form ionic hydrogen bonds while an O-D•••O hydrogen bond is present between the two waters. This structure is consistent with prior reports of $Cl^-(H_2O)_2$ structures. [9,15,16] The CH_4 molecule is located on the same side, as the three ligands asymmetrically solvate the ion. Thus we assign the bands at 2695 cm^{-1} and 2731 cm^{-1} to the intermolecular O-D•••O hydrogen bond (labeled a in Figure 9.3) and the free O-D stretching mode of the single proton acceptor-single proton donor D_2O molecule (labeled b in Figure 9.3) respectively. The two calculated bands below 2600 cm^{-1} correspond to the ionic hydrogen bonded stretching modes of the single proton acceptor-single proton donor and double proton donor D_2O molecules. Addition of more CH_4 molecules does not cause any shifts of the O-D bands shown in Figure 9.3 (see appendix A.12). The ionic hydrogen bonds appear below our minimum laser frequency.

Finally we report the IRPD spectrum of $Cl^-(D_2O)_3(CH_4)_1$ clusters in Figure 9.4. Most notably, there are no free O-D stretching features near 2700 cm^{-1} while an intense,

single band appears at 2663 cm^{-1}. C-H stretching modes are responsible for features above 2800 cm^{-1}. The simulated spectrum calculated MP2/aug-cc-pVDZ level is shown at the bottom of Figure 9.4 and agrees with the experimental spectrum in the frequency range where experimental data was obtained. In the optimized MP2/aug-cc-pVDZ structure (shown in Figure 9.4) three D_2O molecules form a pyramidal C_3 structure akin to $X^-(H_2O)_3$ structures previously reported.[8,15,16] Therefore we assign the band at 2663 cm^{-1} to the hydrogen bonding O-D modes of the pyramidal structure. Furthermore, the single hydrogen bonded O-D stretching mode remains the dominant feature in spectra of clusters with up to five CH_4 molecules indicating the presence of CH_4 does not affect the $Cl^-(D_2O)_3$ pyramidal structure (see appendix A.13)

9.5 Conclusions

IRPD spectra for $Cl^-(Water)_{1-3}(CH_4)_n$ clusters are reported along with supporting MP2/aug-cc-pVDZ simulated spectra and structures. Overall we find that vibrational frequencies and structures are unaffected when methane is systematically added to $Cl^-(D_2O)_{1-3}$ clusters. Thus CH4 acts as a non-perturbing tagging ligand. Also we showed that the presence of a water molecule significantly weakens the electrostatic interaction between Cl^-•••CH_4 in $Cl^-(H_2O)_1(CH_4)_1$ clusters based on the smaller C-H frequency shifts in this work compared to previous $Cl^-(CH_4)_n$ studies.

9.6 Figures and Tables

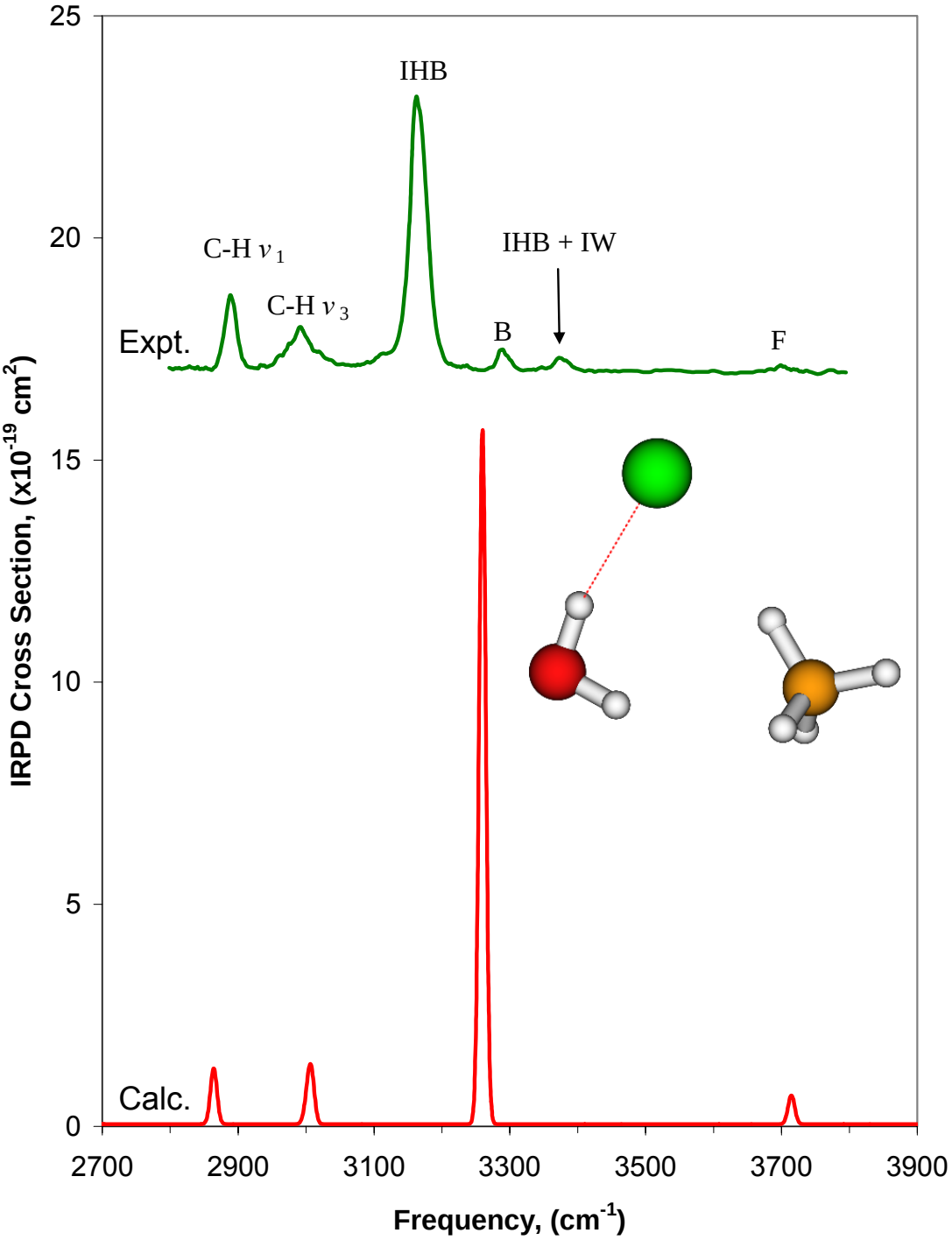

Figure 9.1: IRPD and simulated (MP2/aug-cc-pVDZ) spectra of $Cl^-(H_2O)_1(CH_4)_1$ along with the optimized calculated structure.

Table 9.1 Experimental vibrational frequencies for $Cl^-(CH_4)_1$, $Cl^-(H_2O)_1Ar_3$, and $Cl^-(H_2O)_1(CH_4)_1$

	[a]$Cl^-(CH_4)_1$	[b]$Cl^-(H_2O)_1Ar_3$	[c]$Cl^-(H_2O)_1(CH_4)_1$
CH_4 ν_1	2875	–	2889
CH_4 ν_3(e)	2980	–	2993
IHB	–	3130	3165
B	–	3283	3290
IHB + IW	–	3340	3375
Free O-D	–	3690	3700

IHB, B, and IW correspond to ionic hydrogen bond, bend overtone, and ion•••water intermolecular modes respectively.
[a]from Ref [1]
[b]from Ref [18]
[c]from this work

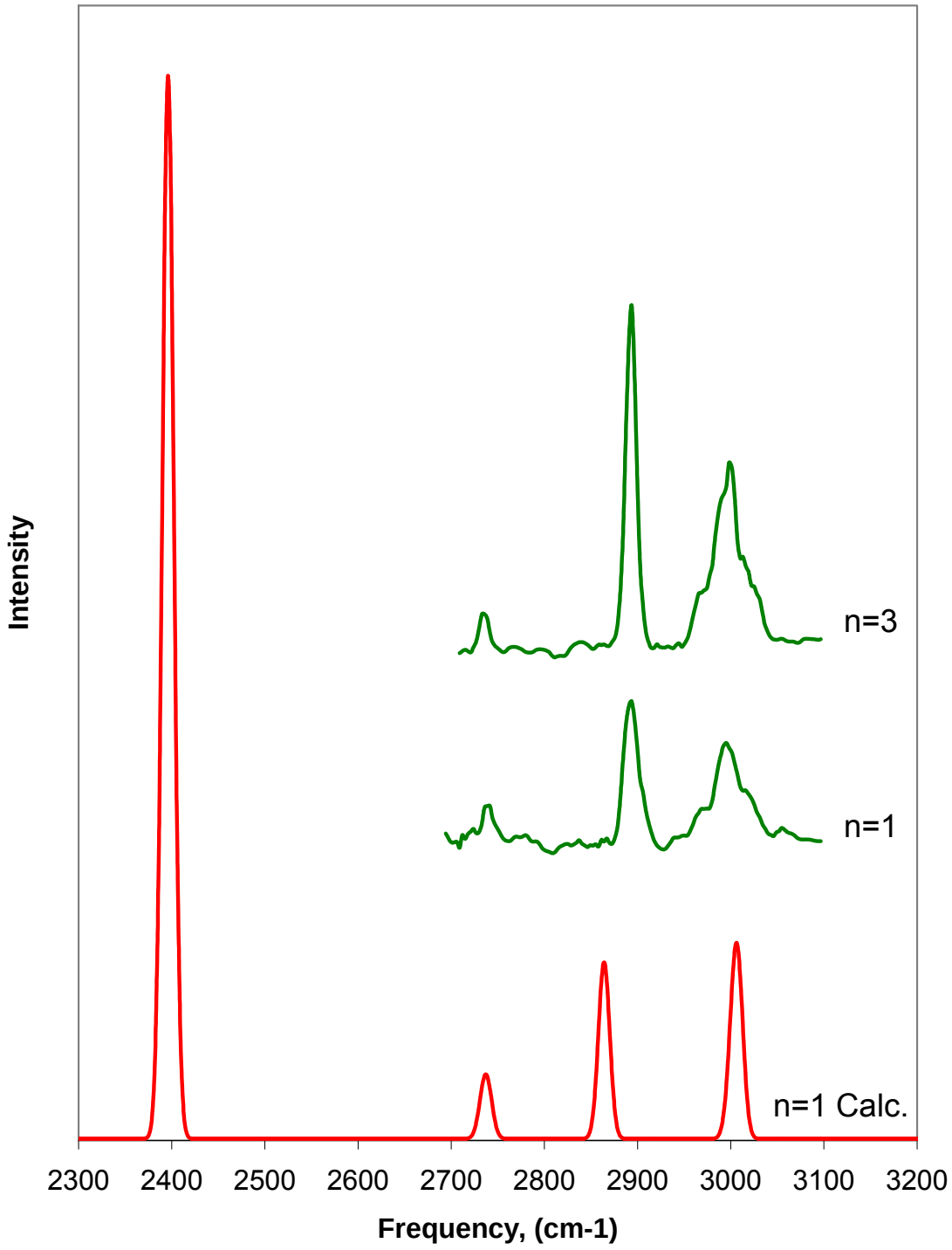

Figure 9.2: IRPD and simulated (MP2/aug-cc-pVDZ) spectra of selected $Cl^-(D_2O)_1(CH_4)_n$ clusters.

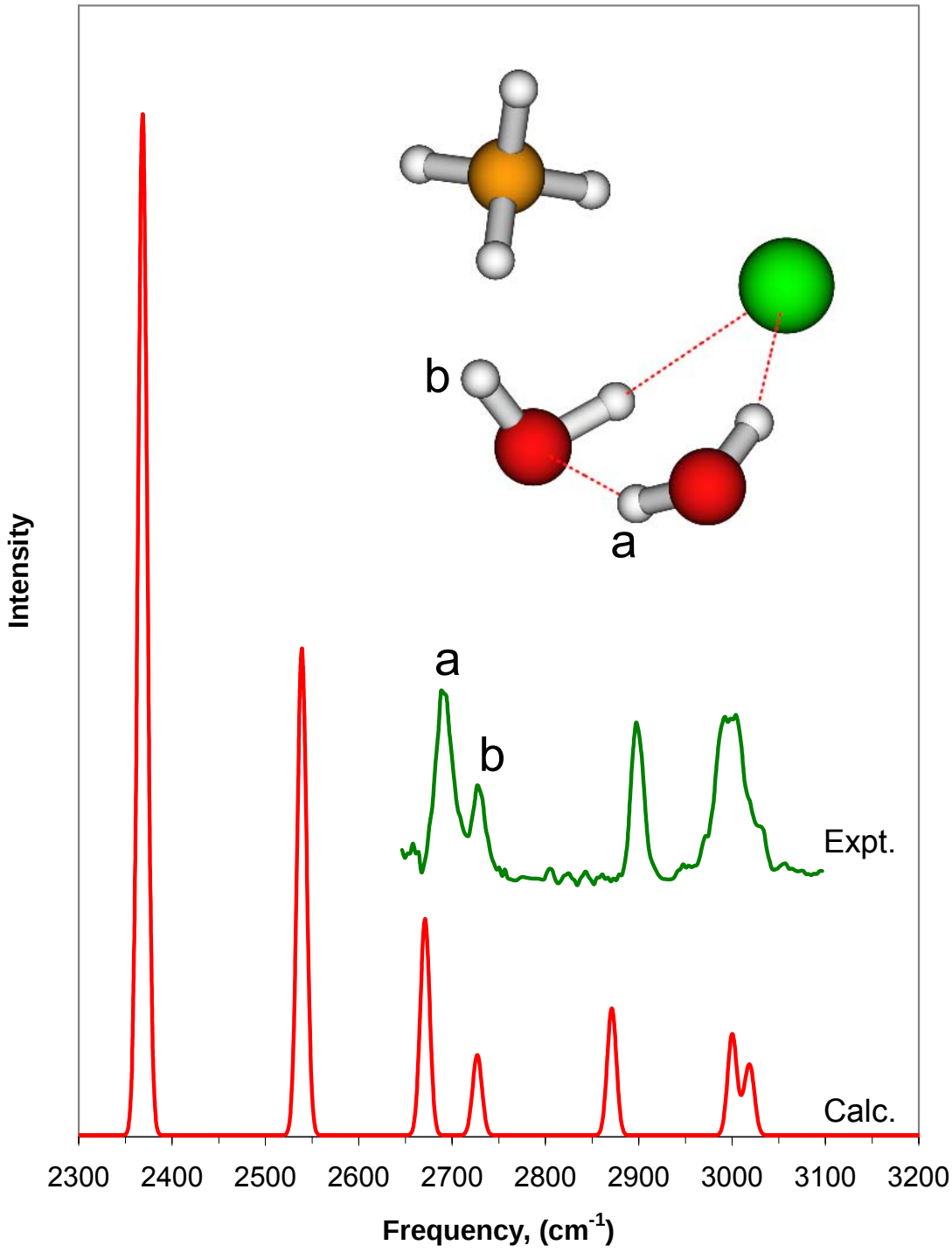

Figure 9.3: IRPD and simulated (MP2/aug-cc-pVDZ) spectra of $Cl^-(D_2O)_2(CH_4)_1$ clusters and optimized calculated structure.

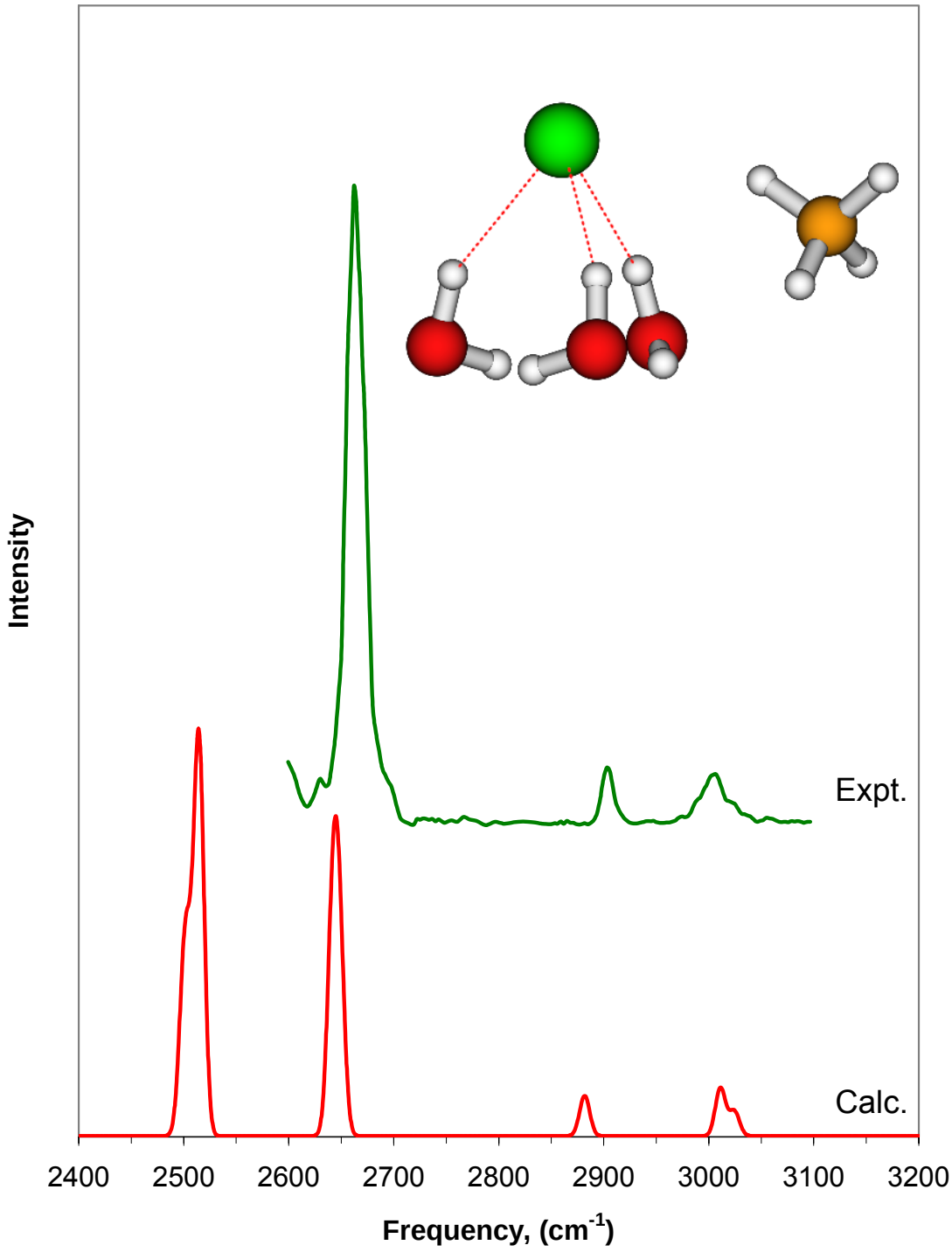

Figure 9.4: IRPD and simulated (MP2/aug-cc-pVDZ) spectra of $Cl^-(D_2O)_3(CH_4)_1$ and the optimized calculated structure.

9.7 References

[1] Z. M. Loh, R. L. Wilson, D. A. Wild, E. J. Bieske, M. S. Gordon. *J. Phys. Chem. A* 109 (2005) 8481.
[2] L. Ferrighi, G. K. H. Madsen, B. Hammer. *Chem. Phys. Lett.* 492 (2010) 183.
[3] J. B. L. Martins, J. R. S. Politi, E. Garcia, A. F. A. Vilela, R. Gargano. *J. Phys. Chem. A* 113 (2009) 14818.
[4] Z. M. Loh, R. L. Wilson, D. A. Wild, E. J. Bieske, M. S. Gordon. *Aust. J. Chem.* 57 (2004) 1157.
[5] Z. M. Loh, R. L. Wilson, D. A. Wild, E. J. Bieske, J. M. Lisy, B. Njegic, M. S. Gordon. *J. Phys. Chem. A* 110 (2006) 13736.
[6] D. A. Wild, Z. M. Loh, E. J. Bieske. *Int. J. Mass Spectrom.* 220 (2002) 273.
[7] D. A. Wild, Z. M. Loh, P. P. Wolynec, P. S. Weiser, E. J. Bieske. *Chem. Phys. Lett.* 332 (2000) 531.
[8] P. Ayotte, G. H. Weddle, M. A. Johnson. *J. Chem. Phys.* 110 (1999) 7129.
[9] P. Ayotte, G. H. Weddle, J. A. Kelley, M. A. Johnson, S. S. Xantheas. *J. Phys. Chem. A* 103 (1999) 10668.
[10] J. P. Beck, J. M. Lisy. *J. Phys. Chem. A* 114 (2010) 10011.
[11] O. M. Cabarcos, C. J. Weinheimer, T. J. Martinez, J. M. Lisy. *J. Chem. Phys.* 110 (1999) 9516.
[12] H. E. Dorsett, R. O. Watts, S. S. Xantheas. *J. Phys. Chem. A* 103 (1999) 3351.
[13] J. E. Combariza, N. R. Kestner, J. Jortner. *J. Chem. Phys.* 100 (1994) 2851.
[14] S. Lin, P. C. Jordan. *J. Chem. Phys.* 89 (1988) 7492.
[15] W. H. Robertson, M. A. Johnson. *Annu. Rev. Phys. Chem.* 54 (2003) 173.
[16] S. S. Xantheas. *J. Phys. Chem.* 100 (1996) 9703.
[17] J.-H. Choi, K. T. Kuwata, Y.-B. Cao, M. Okumura. *J. Phys. Chem. A* 102 (1998) 503.
[18] P. Ayotte, G. H. Weddie, J. Kim, M. A. Johnson. *J. Am. Chem. Soc.* 120 (1998) 12361.
[19] S. A. Corcelli, J. A. Kelley, J. C. Tully, M. A. Johnson. *J. Phys. Chem. A* 106 (2002) 4872.
[20] E. G. Diken, J. M. Headrick, J. R. Roscioli, J. C. Bopp, M. A. Johnson, A. B. McCoy, X. Huang, S. Carter, J. M. Bowman. *J. Phys. Chem. A* 109 (2005) 571.
[21] S. Horvath, A. B. McCoy, B. M. Elliott, G. H. Weddle, J. R. Roscioli, M. A. Johnson. *J. Phys. Chem. A* 114 (2010) 1556.
[22] J. A. Kelley, J. M. Weber, K. M. Lisle, W. H. Robertson, P. Ayotte, M. A. Johnson. *Chem. Phys. Lett.* 327 (2000) 1.
[23] J. R. Roscioli, E. G. Diken, M. A. Johnson, S. Horvath, A. B. McCoy. *J. Phys. Chem. A* 110 (2006) 4943.
[24] W. H. Robertson, G. H. Weddle, J. A. Kelley, M. A. Johnson. *J. Phys. Chem. A* 106 (2002) 1205.
[25] J. M. Lisy. *Int. Rev. Phys. Chem.* 16 (1997) 267.
[26] D. J. Miller, J. M. Lisy. *J. Am. Chem. Soc.* 130 (2008) 15393.
[27] D. J. Miller, J. M. Lisy. *J. Am. Chem. Soc.* 130 (2008) 15381.
[28] C. E. Klots. *J. Chem. Phys.* 83 (1985) 5854.
[29] Origin (OriginLab, Northampton, MA), 2003.

[30] J. Kong, C. A. White, A. I. Krylov, C. D. Sherrill, R. D. Adamson, T. R. Furlani, M. S. Lee, A. M. Lee, S. R. Gwaltney, T. R. Adams et al., SPARTAN'02, Wavefunction, Inc., Irvine CA, 2002.
[31] M. J. Frisch, G. W. Trucks, H. B. Schlegel, G. E. Scuseria, M. A. Robb, J. R. Cheeseman, J. A. Montgomery Jr., T. Vreven, K. N. Kudin, J. C. Burant et al., Gaussian 03, Revision B.04, Gaussian, Inc., Pittsburgh, PA, 2003.
[32] S. I. Gorelsky, *SWizard program*, 4.1, University of Ottawa, Canada, 2005.

Chapter 10

Conclusions

The results from this Thesis help explain the electrostatic interactions in ion•••hydrocarbon and ion•••water•••hydrocarbon cluster ions including a thorough analysis of the solvation of alkali metal ions by methane. Moreover, significant insights of ion solvation were uncovered from an experimental and computational analysis of trapped high energy conformers which reveal new information on the ion solvation process. This Thesis consisted of three parts. First, an analysis of alkali metal ion solvation by methane was discussed in order to characterize ion•••hydrocarbon interactions with the simplest hydrocarbon. Next, an extended investigation of previously reported $Li^+(H_2O)_{3\text{-}4}Ar_1$ clusters was carried out before proceeding into a three chapter series detailing the electrostatic interactions present in ion-water-alkane clusters.

The methanation of the alkali metal ions was discussed in Chapters 3-5. Two structurally different conformers were reported for $Li^+(CH_4)_1Ar_6$. In one conformer, +11 kJ/mol higher in energy than the global minimum energy conformer, the CH_4 molecule was found to reside in the second shell of an octahedral Li^+Ar_6 first shell core. More importantly, this conformer was found to fragment in two different ways following photon absorption indicating that important photodissociation dynamics can be associated with trapped high energy conformers.

It was shown in Chapter 6 that rare gas tagging can be utilized to probe high energy $Li^+(H_2O)_{3\text{-}4}Ar_1$ conformers. These previously unreported conformers contain water O-H hydrogen bonded motifs and are up to 44 kJ/mol higher in energy than the

global minimum energy conformer. For some trapped high energy $Li^+(H_2O)_4Ar_1$ conformers, the stored energy was shown to be essential to induce unique [Ar + H_2O] fragmentation. This is another example of taking advantage of the unique photodissocation dynamics in order to help identify other stable structural conformers which are higher in energy relative to the global minimum energy conformer.

In an effort to study the effect of hydrocarbons on hydrated clusters, methane (Chapter 7) and cyclohexane (Chapter 8) molecules were added $Li^+(H_2O)_{1-4}$ clusters. It was established from IRPD specra and calculations that an O-H•••hydrocarbon hydrogen bond exists wherein the alkane acts as a proton acceptor. More interestingly, results for $Li^+(H_2O)_{3-4}(Alkane)_n$ clusters indicated that trapped high energy conformers containing extensive H_2O hydrogen bonding were present in the cluster ion beam. This suggested that both CH_4 and C_6H_{12}, in addition to Ar, can effectively trap high energy conformers which are up to 30 kJ/mol higher in energy than their respective global minimum energy conformers.

The combined experimental and computational results in this Thesis indicate the importance of high energy conformer trapping in probing different structural conformers. The trapped energy stored in these clusters can also impact the photodissociation dynamics leading to unique fragmentation channels which may be utilized to selectively obtain IRPD spectra in some cases. Furthermore, these results have shed a new light on the subject of Li^+ hydration where it is thought that Li^+ will strongly coordinated water molecules. However, it has been shown in Chapters 6-8 that other stable structural water O-H bonding motifs can exist in the presence of other components, i.e. argon, methane, and cyclohexane. The new O-H hydrogen bonded motifs identified in Chapters 6-8 can

be the foundation for a more thorough computational study to find the energetic barrier heights to rearrangement and mapping out the potential energy surface in order to more fully understand ion solvation.

Appendix

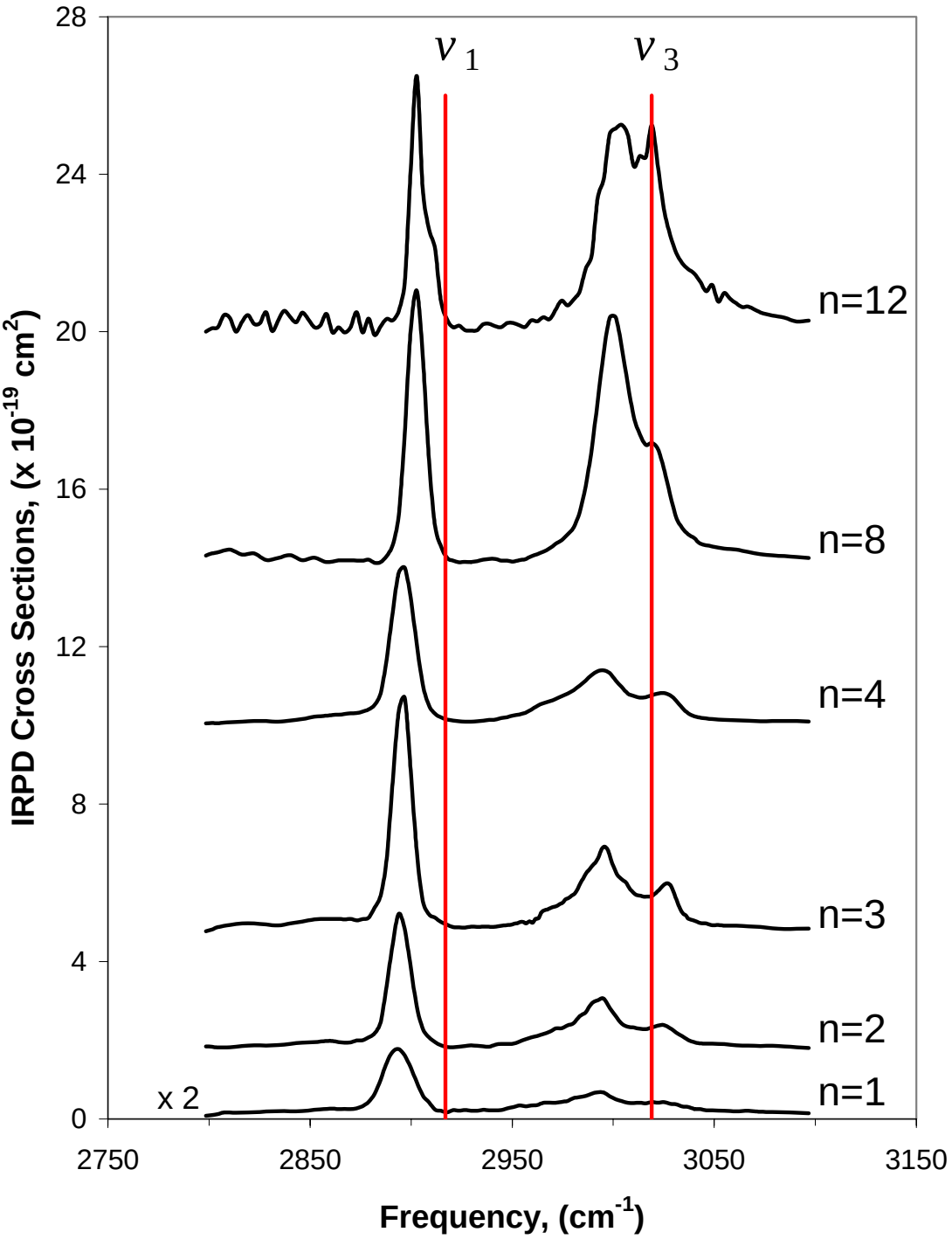

A.1: IRPD spectra of $K^+(CH_4)_n$ clusters. Neutral CH_4 ν_1 and ν_3 values are shown in red vertical lines.

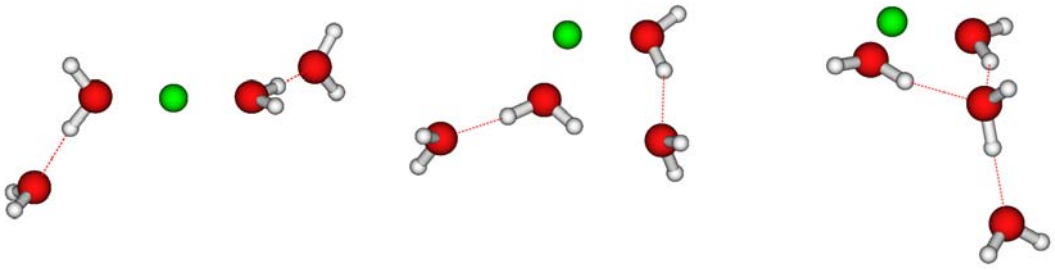

4c

+44 kJ/mol

4d

+50 kJ/mol

4e

+51 kJ/mol

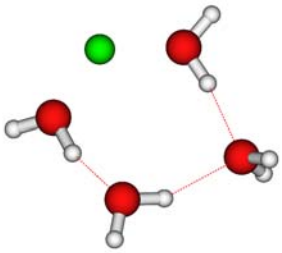

4f

+51 kJ/mol

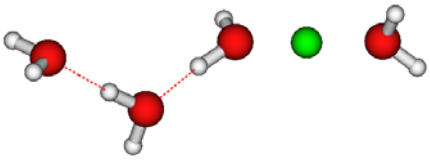

4g

+57 kJ/mol

A.2: Stable structures of non-argonated $Li^+(H_2O)_4$ clusters calculated at the MP2/aug-cc-pVDZ level. Relative energies are corrected for zero-point energy.

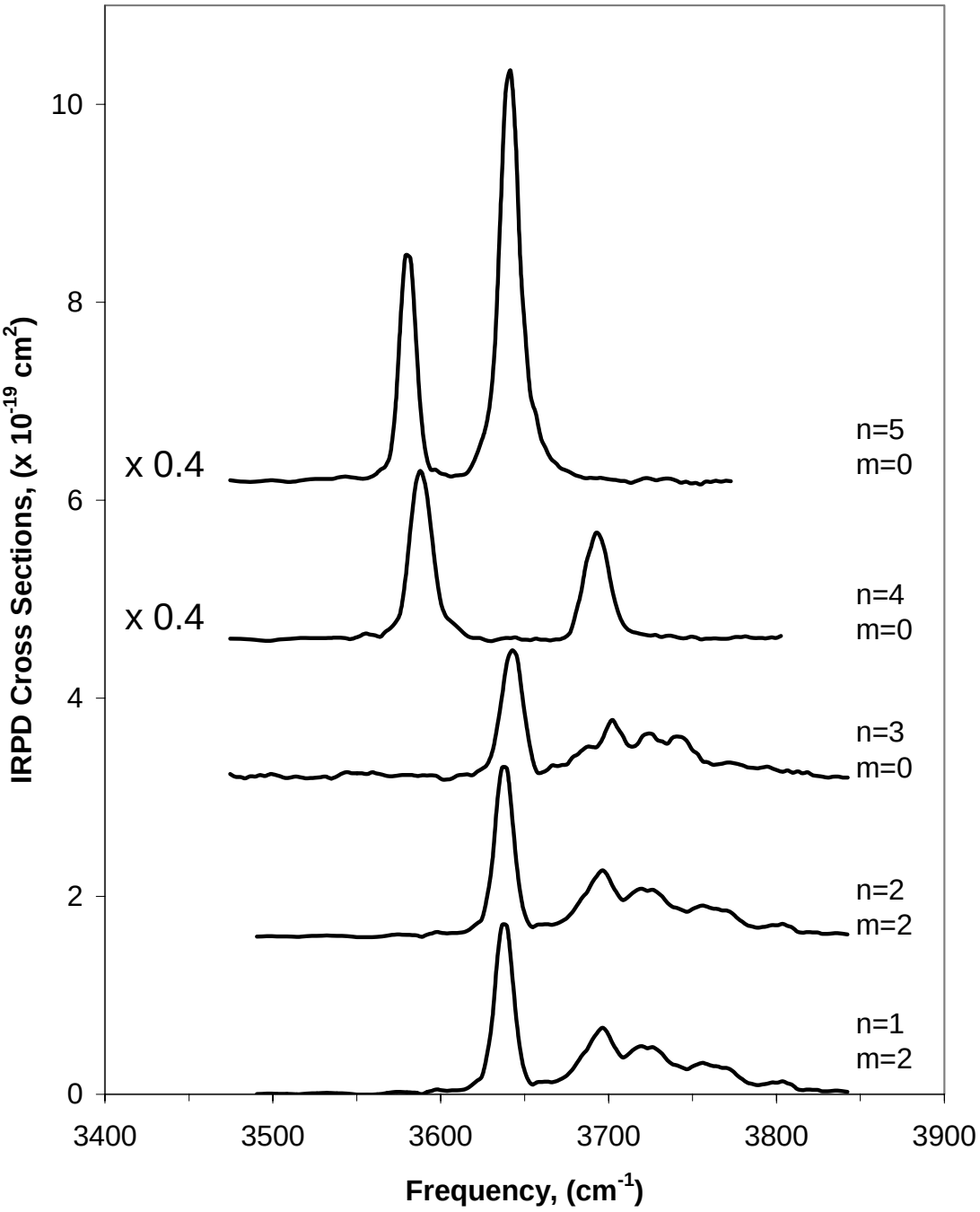

A.3: IRPD spectra in the O-H stretching region of $Li^+(H_2O)_1(CH_4)_nAr_m$.

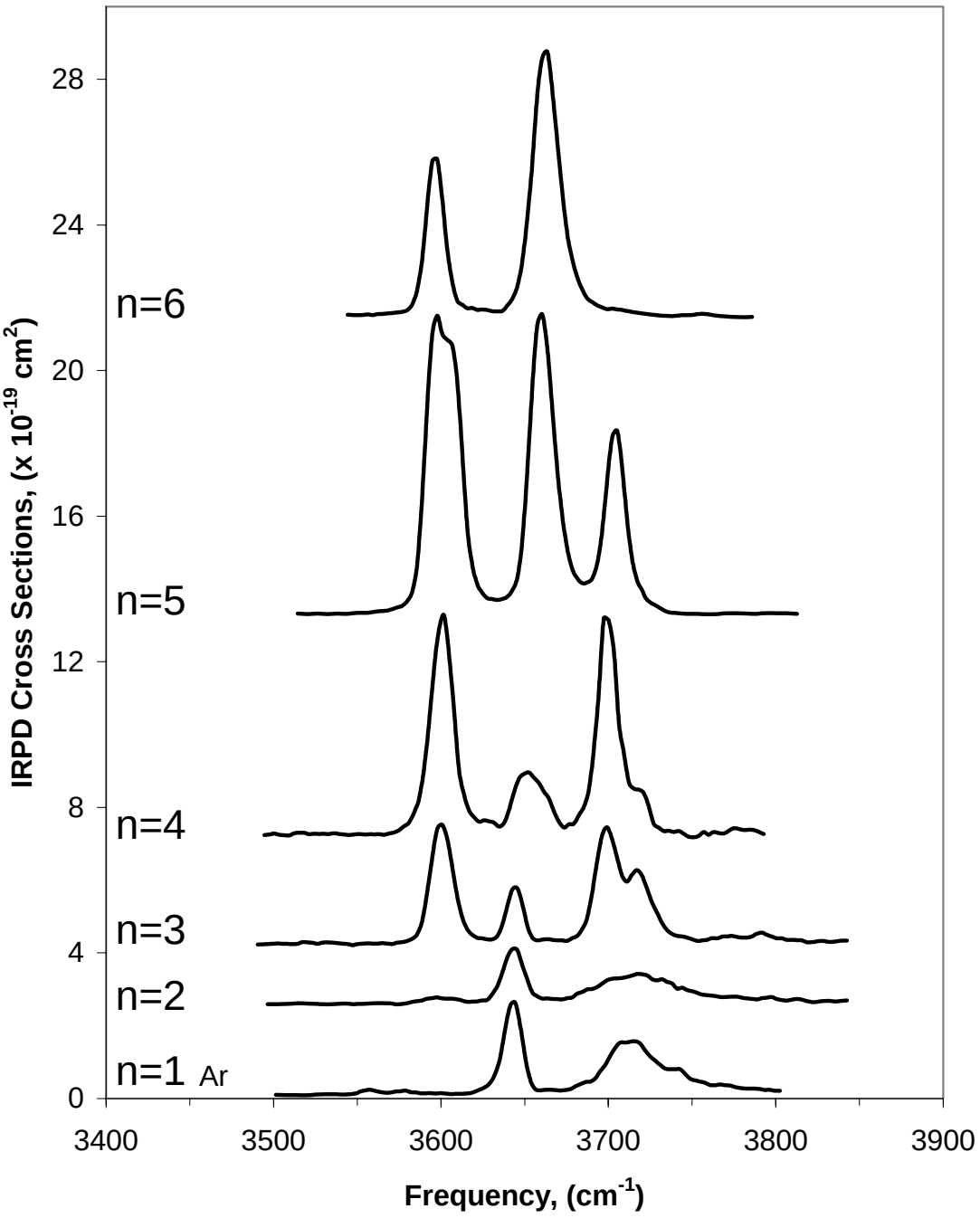

A.4: IRPD spectra in the O-H stretching region of $Li^+(H_2O)_2(CH_4)_n$.

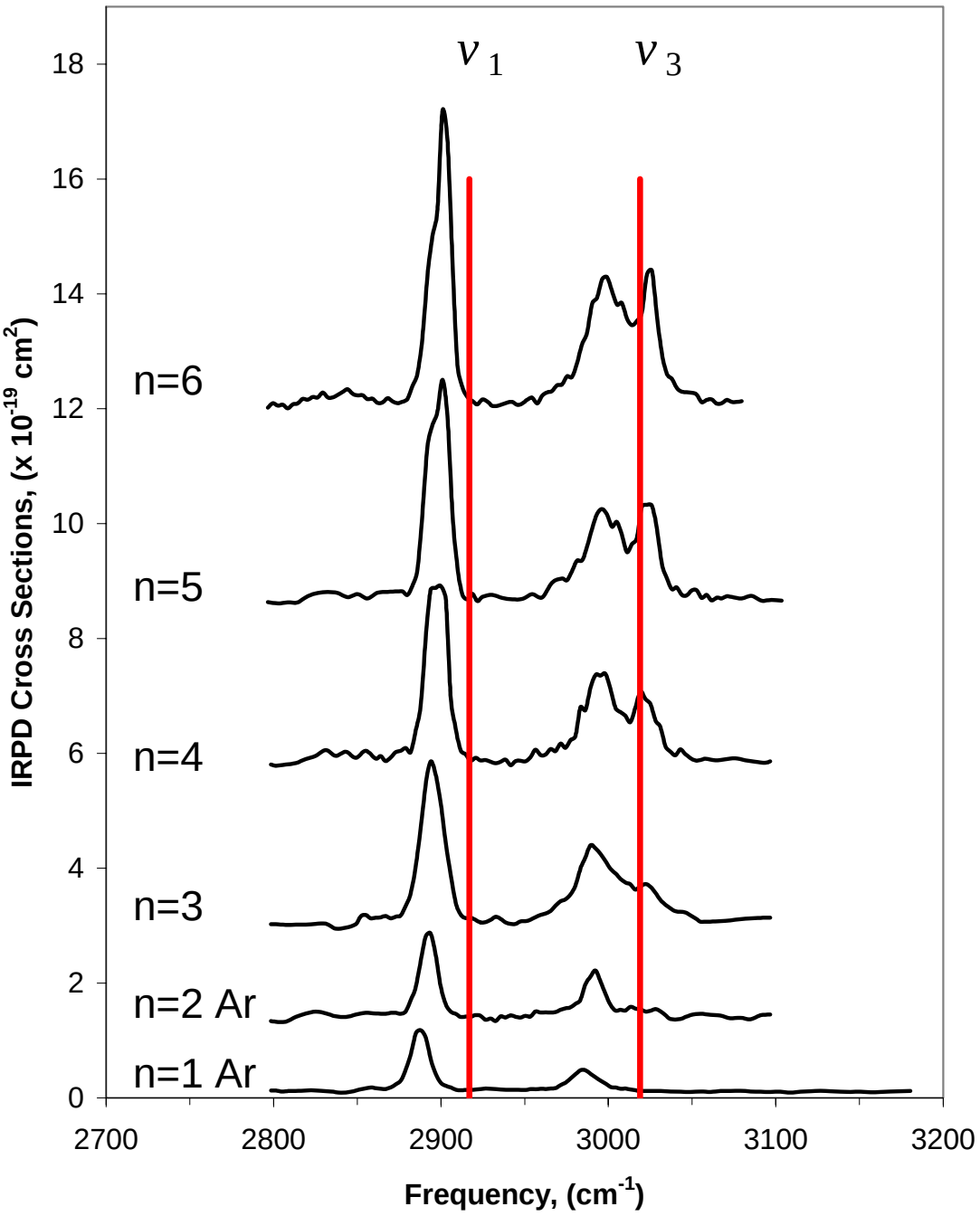

A.5: IRPD spectra in the C-H stretching region of $Li^+(H_2O)_2(CH_4)_n$.

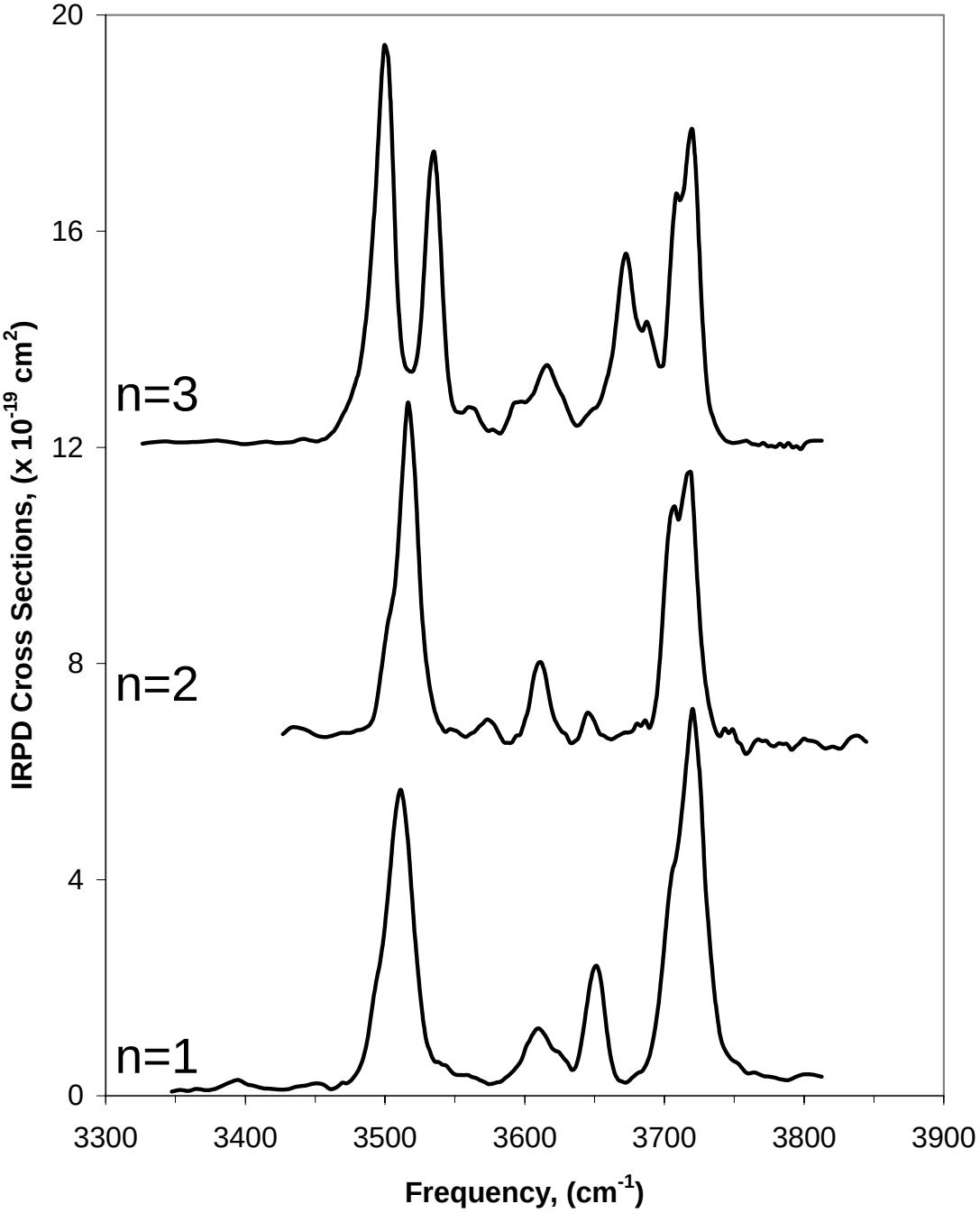

A.6: IRPD spectra in the O-H stretching region of $Li^+(H_2O)_3(CH_4)_n$.

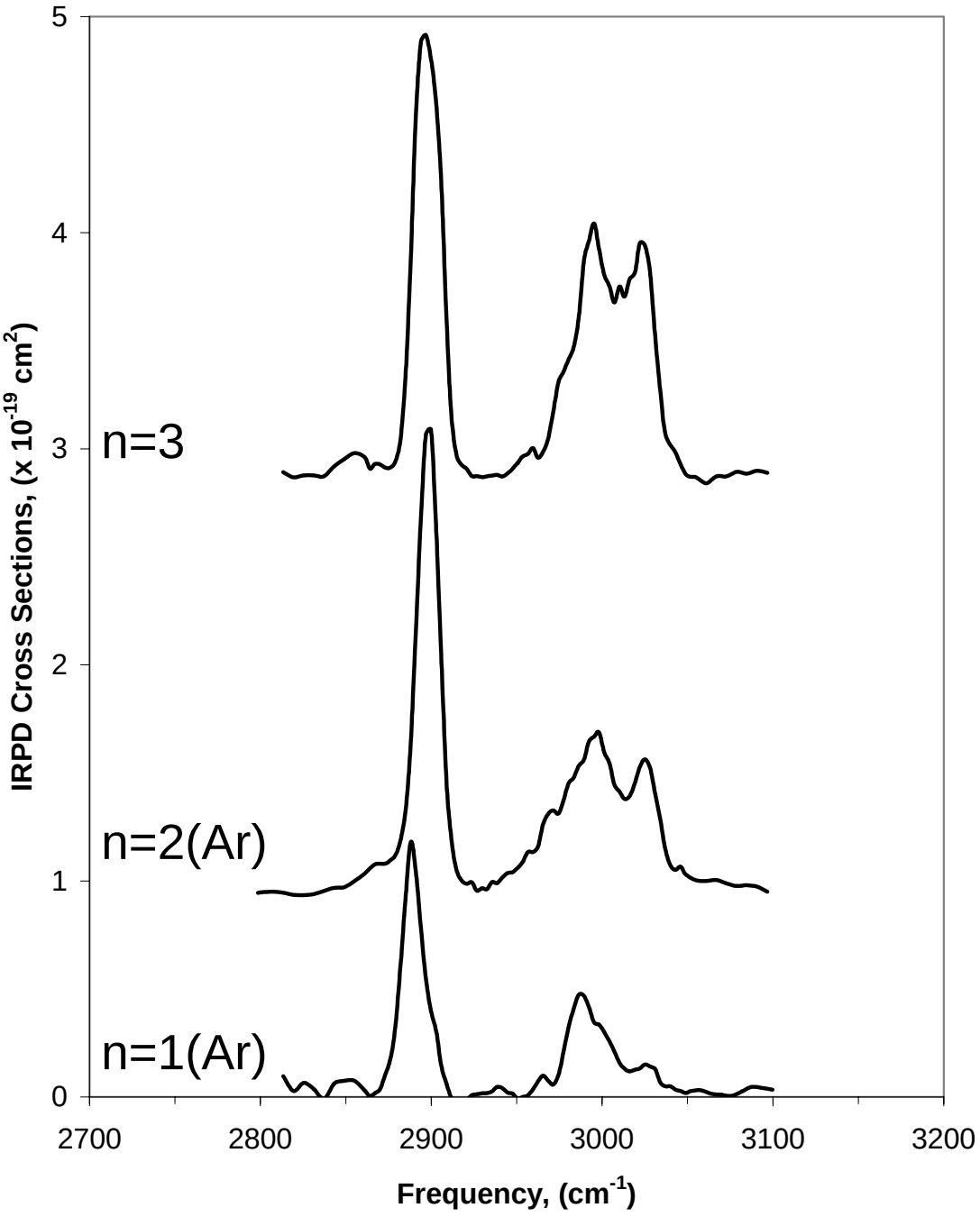

A.7: IRPD spectra in the C-H stretching region of $Li^+(H_2O)_3(CH_4)_n$.

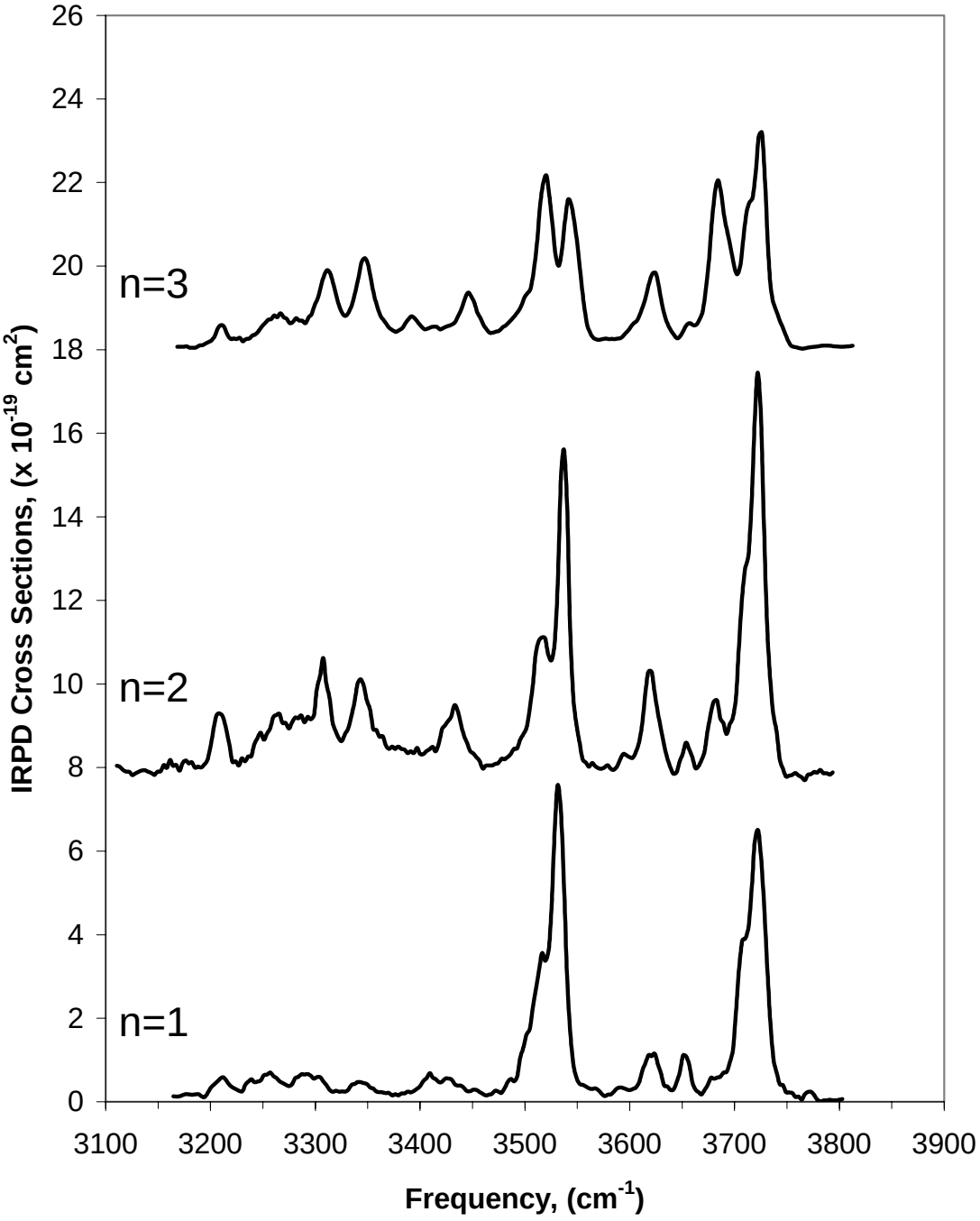

A.8: IRPD spectra in the O-H stretching region of $Li^+(H_2O)_3(CH_4)_n$.

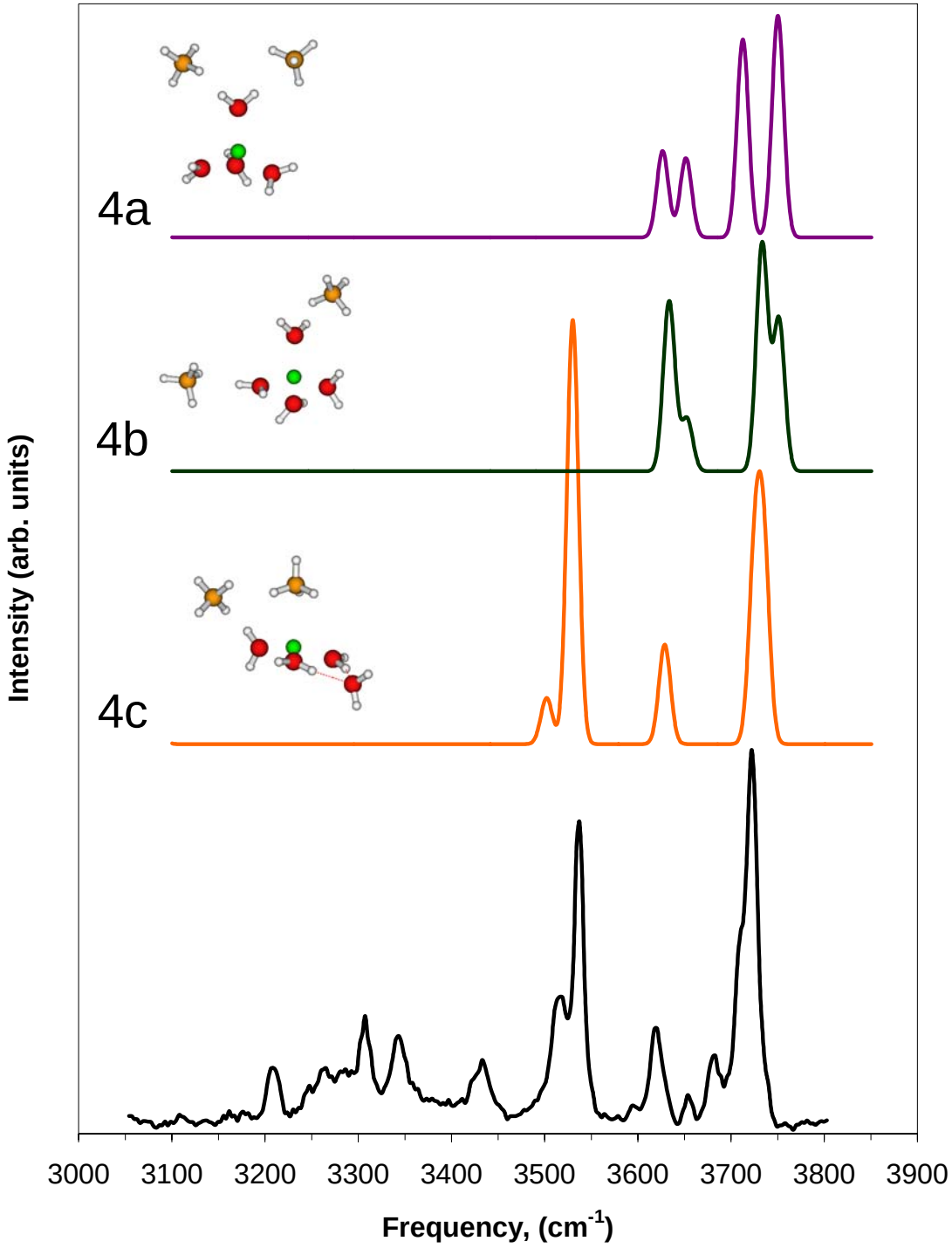

A.9: IRPD spectrum in the O-H stretching region for $Li^+(H_2O)_4(CH_4)_2$. Seven stable conformers were calculated. The simulated spectra for the three lowest energy conformers, 4a-4c, are shown.

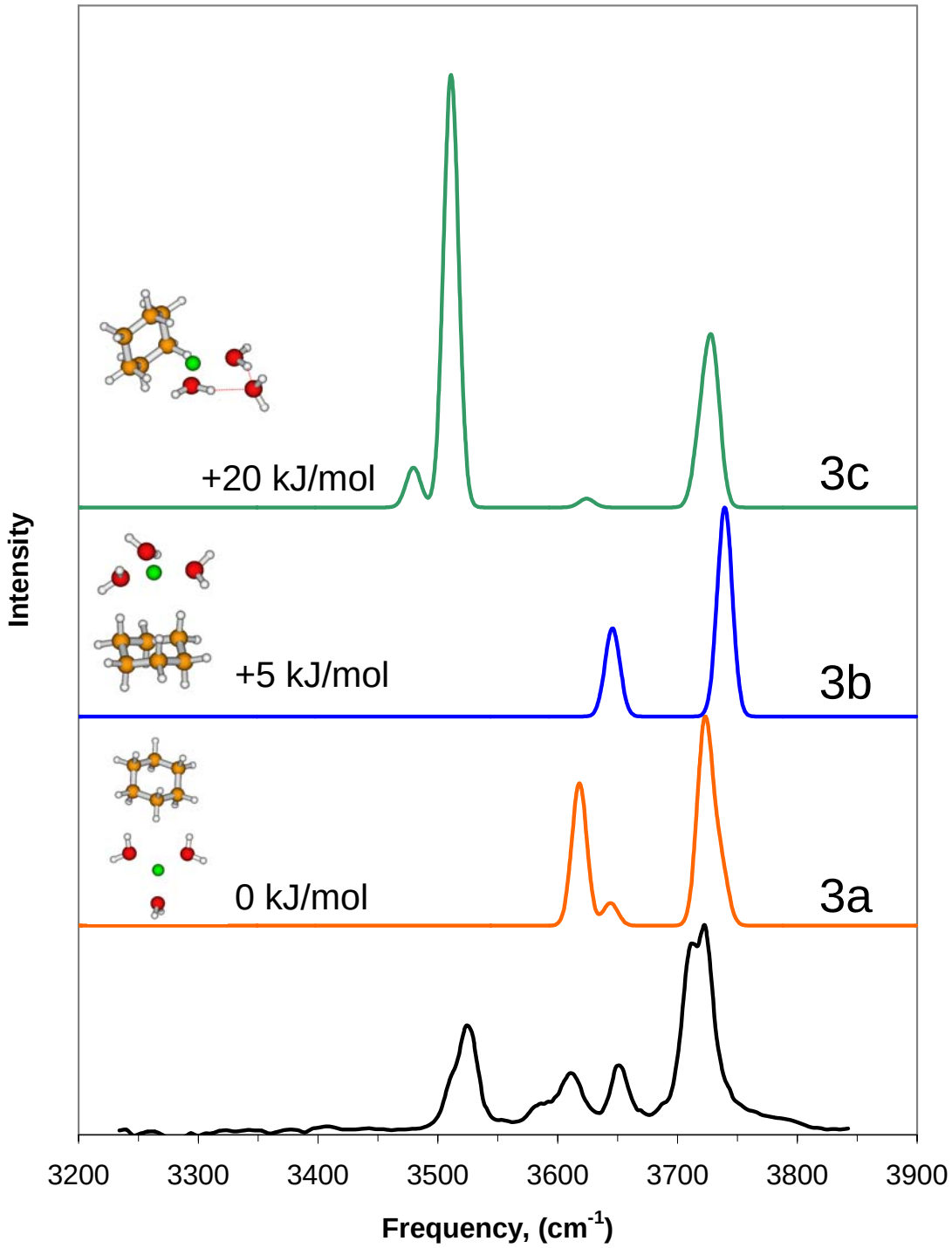

A.10: IRPD spectrum and optimized structures and simulated spectra for $Li^+(H_2O)_3(C_6H_{12})_1$. Relative energies are corrected for zero-point energy.

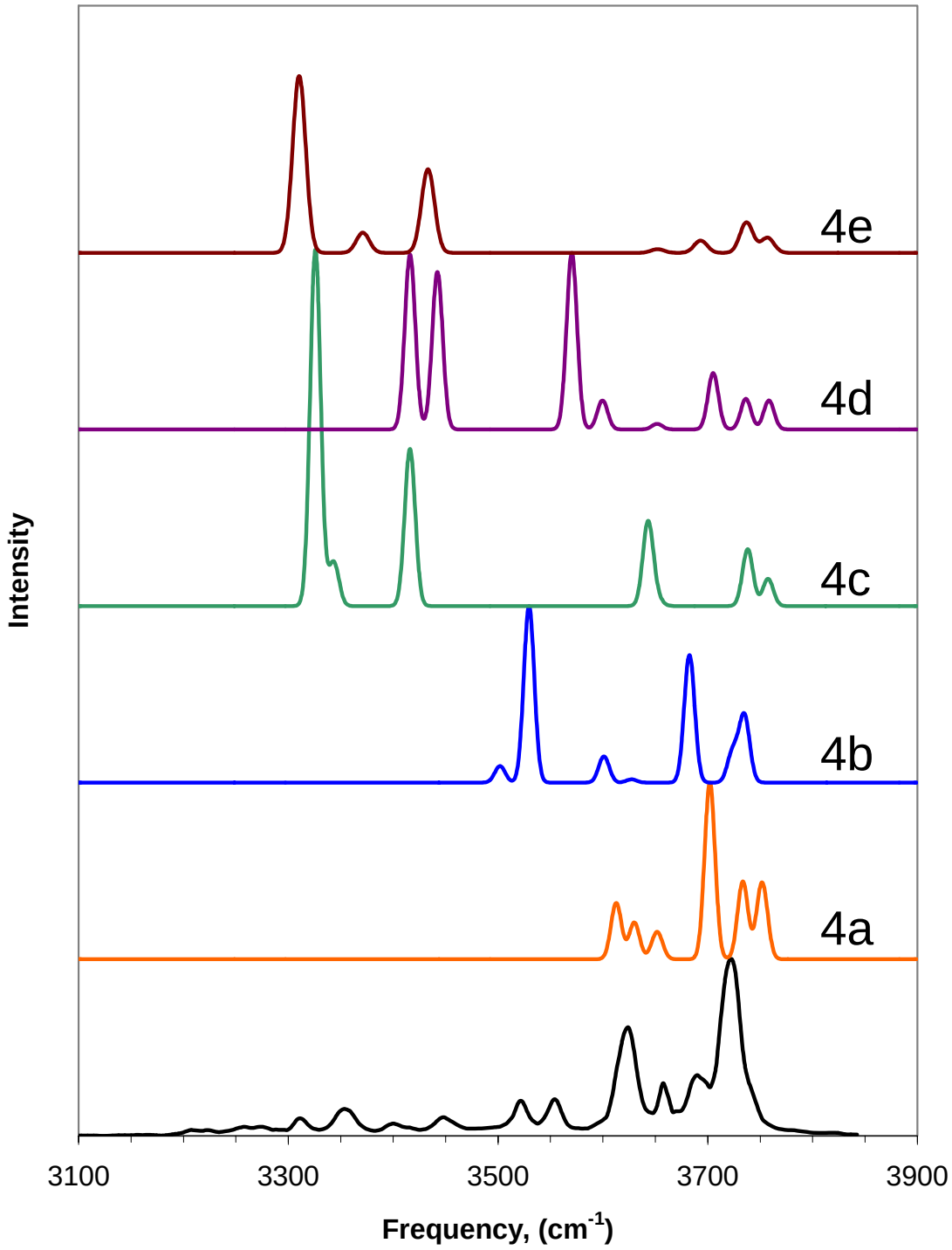

A.11: IRPD spectrum and simulated spectra for $Li^{+}(H_2O)_4(C_6H_{12})_2$.

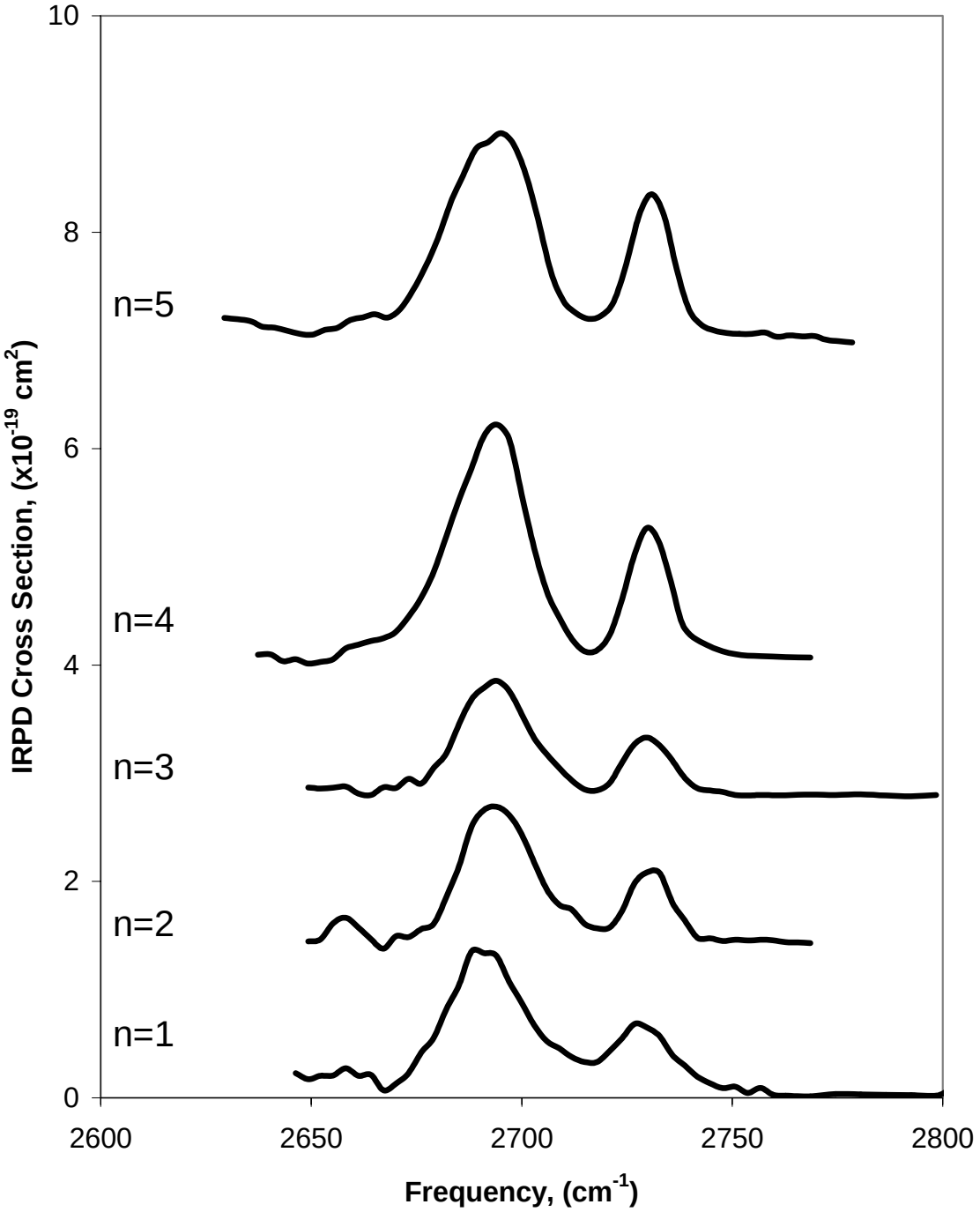

A.12: IRPD spectra of $Cl^-(D_2O)_2(CH_4)_n$.

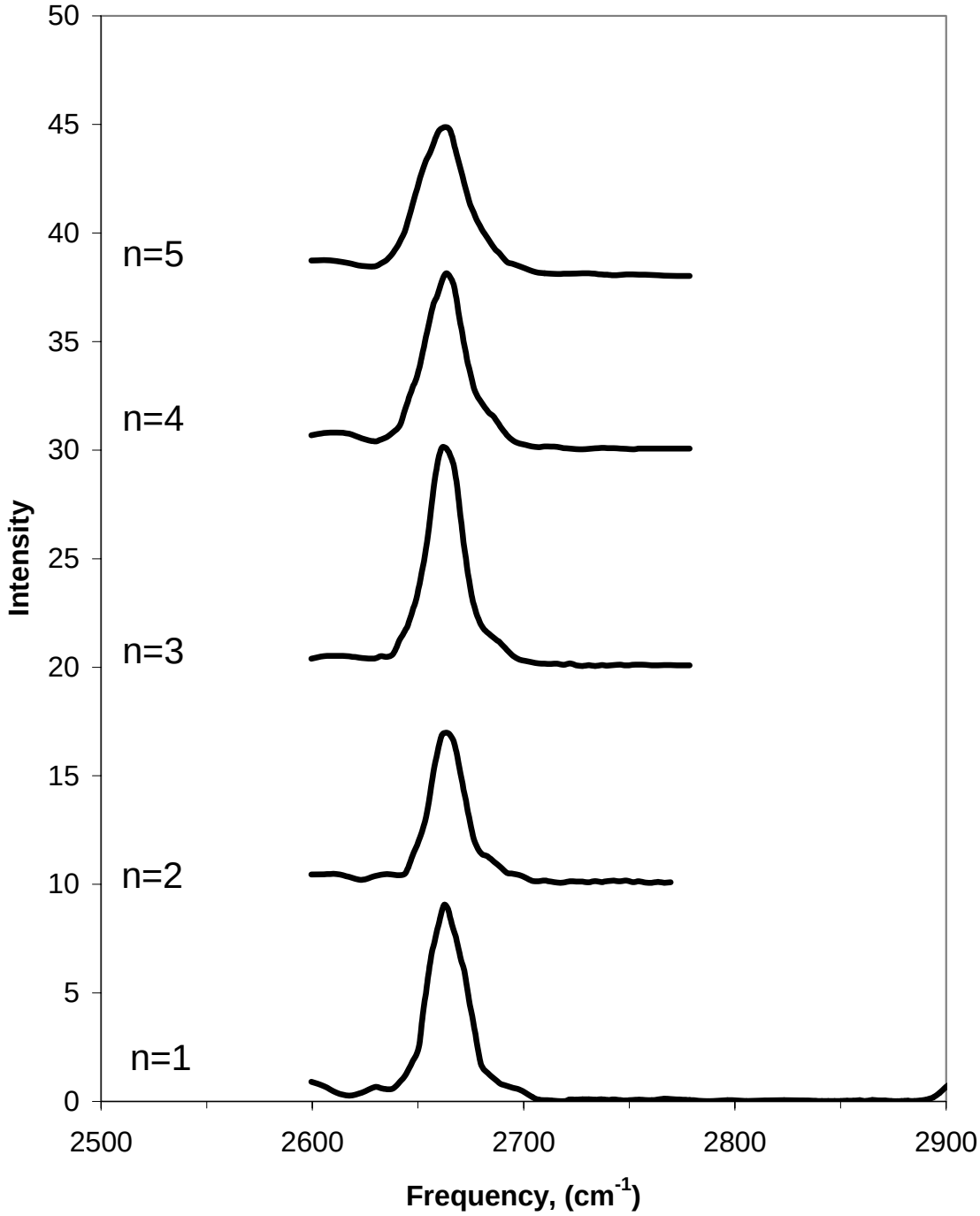

A.13: IRPD spectra of $Cl^-(D_2O)_3(CH_4)_n$.

Author's Biography

Oscar Rodriguez Jr. was born May 15th 1981 in Edinburg, TX and the first of two children born to Oscar and Gilda H. Rodriguez. He graduated from Pharr-San Juan-Alamo North High School in May of 1999 and proceeded to attend The University of Texas-Pan American in Edinburg, TX. There, Oscar received his Bachelors of Science degree in Chemistry with a minor in Biology in May of 2003. Immediately completing university studies, Oscar began working at the La Joya Water Supply Corporation where he served at the Water/Wastewater development chemist and manager, then as Billing and Meter Reading Supervisor. During this time, Oscar wed Lorena Lozano on February 12th 2005. After a successful tenure at the La Joya Water Supply Corporation, Oscar enrolled at the University of Illinois at Urbana-Champaign to pursue a doctoral degree in Chemistry under the supervision of Professor James M. Lisy. On June 21st 2009, Oscar and Lorena welcomed their first child, Nicolás Rodriguez.